Abstract

Imaging Electrons in Semiconductor Nanostructures

by

Ania Claire Bleszynski

Doctor of Philosophy in Physics, 2006

Harvard University

Advisor: Professor Robert M. Westervelt

Scanning probe microscopy (SPM) is a powerful tool that allows us to probe and manipulate electrons at the nanoscale. We have used a liquid helium cooled SPM with a conducting tip to image electrons in three types of semiconducting nanostructures: two-dimensional electron gases (2DEG's), quantum dots, and nanowires. Our images are obtained by scanning a charged tip over the sample and recording changes in device conductance as a function of tip position. We have directly imaged coherent electron wave flow from a quantum point contact (QPC) defined in a GaAs/AlGaAs 2DEG. The phase coherence of electron waves makes it possible to form an imaging electron interferometer. We have used our cooled SPM to image a one-electron GaAs quantum dot formed in a 2DEG by surface gates. Few electron quantum dots are promising candidates for single electronics, spintronics, and quantum information processing. Imaging and manipulating electrons in quantum dots promises to be useful in understanding and building circuits for these purposes. I present images of electron

motion through InAs nanowires with diameters of ~50nm, grown catalytically from Au nanoparticles. Semiconducting nanowires, assembled in a bottom-up approach, have recently seen an immense amount of research activity. Our images provide a detailed understanding of where the electrons are in the wire and how they flow through it. Heterostructure InAs/InP nanowires can be used to make an InAs quantum dot defined by two InP barriers. I demonstrate the ability of the cooled SPM tip to locate the InAs dot and tune the number of electrons down to one, and then zero, in a spatially dependent way.

Table of Contents

Acknowledgements

I would first and foremost like to thank my advisor Bob Westervelt who has been a wonderful advisor, scientifically and personally. I am very glad to have worked in his group throughout my six years at Harvard. I also want to thank the other two members of my committee: Rick Heller and Federico Capasso. It has always been a pleasure discussing physics with them, especially ideas for new projects.

Throughout the course of this project, I have also had the privilege to work closely with Leo Kouwenhoven's group in Delft and Lars Samuelson's group in Lund. I learned an immense amount of new physics in both collaborations and I am grateful to them and their groups for their hospitality while I worked there. Thank you Floris Zwanenburg, Linus Froberg, Jorden van Dam, Silvano De Franceschi, and Mikael Bjork!

I would like to thank all the imaging members of the Westervelt group with whom it has been a pleasure to work with, learn from, and teach. Thanks to Mark Topinka, Brian LeRoy, Kathy Aidala, Parisa Fallahi, and the newbies: Halvar Trodahl, Erin Boyd, and Melaku Muluneh. It has also been a pleasure to work with Tom Hunt and Jonathan Aguilar on the AFM – dielectrophoresis project. Also, many thanks to the other members of the group: Hak-ho Lee, Dave Issadore, Andy Vidan, Ian Chan, and Chungsok Lee and to our administrative assistant, Naomi Brave who makes everything run smoothly.

A big thank you to the clean room staff here at Harvard, especially Steve Shepard, who provided us with state-of-the-art and (working!) equipment.

And of course, my family and friends. You know who you are…

Imaging Electrons in Semiconductor Nanostructures

A thesis presented

by

Ania Claire Bleszynski

to

The Department of Physics
in partial fulfillment of the requirements
for the degree of
Doctor of Philosophy
in the subject of

Physics

Harvard University
Cambridge, Massachusetts

June, 2006

Chapter 1

Introduction

As physicists we are interested in research on the nanoscale because of the altogether new and different behavior that emerges when the size of the system under study approaches a length scale characteristic of a certain physical phenomenon. Relevant length scales include the Fermi wavelength of the electron, the electron's phase coherence length, and the exciton Bohr radius. At the nanoscale, many classical assumptions break down. Quantum mechanical effects become naturally important and quantum phenomena such as coherence, interference, and wave functions are observed. Electrons are no longer classical billiard balls that only take one path, for example. Rather electrons are waves that travel along multiple paths and those paths interfere with each other. In this research we are motivated to learn more about the phenomena of the quantum world both to broaden our understanding of physics and to learn how to use these phenomena to design and implement new kinds of technologies, such as spintronics devices and quantum computers. Our research will also be helpful to those who would like to use new technologies, such as semiconducting nanowires, to make faster and smaller devices for future nano-electronics, such as nanowire field effect transistors (FET's).

The motivation for imaging is simple: it gives us 'eyes' with which we can 'see' the tiny systems we study. In this thesis, I hope to convince the reader that imaging with a scanning probe microscope (SPM) is a powerful way to probe and manipulate the electronic properties of semiconducting nanostructures on a local scale. A new set of

eyes is necessary when studying electrons in nanoscale systems that are too small to be visualized with the more traditional optical microscopes and too small to be probed with standard voltage probes. New kinds of microscopy such as scanning electron microscopy (SEM) and transmission electron microscopy (TEM) have been a great boon to the progress of nanotechnology by allowing us to visualize the morphology of nanoscale systems.

The electrons we image are buried inside nanostructures so conventional surface probes cannot be used. In our research, we use a liquid helium cooled SPM (Topinka 2002) to visualize the electrical properties of semiconductor nanostructures on a *local* scale, namely where the electrons reside and how they flow through our devices. With current high precision lithographic techniques, we can make electrical contacts to very small devices and measure their conductance. Such measurements average over the whole device. As demonstrated in Figure 1.1 we can go one step further and use imaging to understand how the electrons flow between the source and drain contacts. Figure 1.1 displays the conductance of a 50nm diameter InAs nanowire as a function of position of a negatively charged SPM tip scanned at a fixed height over the wire. The locations of the nanowire (pink dotted line) and the source and drain contacts (black dotted lines) are schematically drawn in. These images will be discussed in more detail later, but for now I would like to point out a few things. The nanowire is very small, 50nm in diameter, and the distance between the contacts is only about 1 micron. And yet we are able to see many features in this conductance image along the nanowire; the image locates three quantum dots, at the centers of the concentric rings. Also, one electron is added to the nanowire in passing the tip over each ring. An image such as this one provides us with

valuable information about the local electrostatic fluctuations in the wire, information unattainable with standard transport measurements.

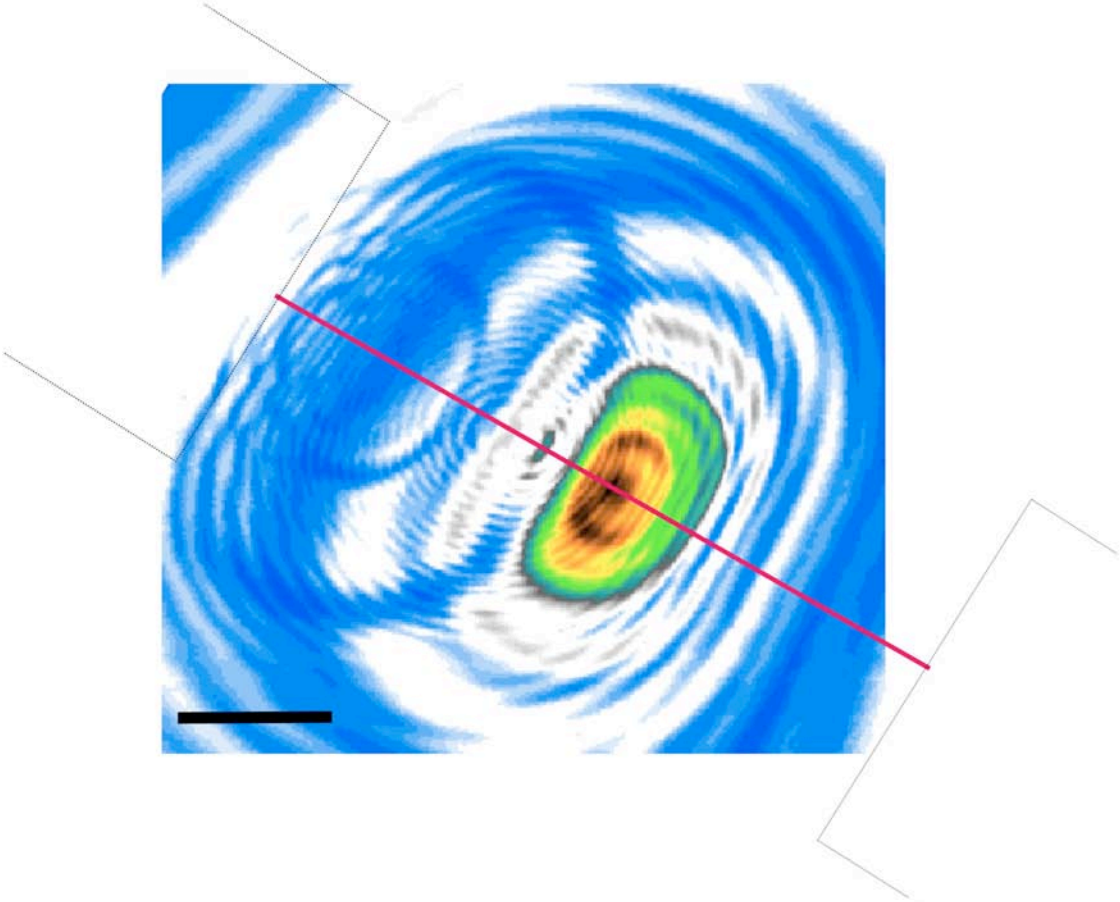

Figure 1.1 SPM image of an InAs nanowire. Scale bar is 200nm. Plotted is conductance of the nanowire as a function of position of a negatively charged tip scanned 100nm ove the wire.

Scanning probe microscopy is an important tool for mesoscopic systems (Topinka et al. 2003]. We use our scanning probe microscope to image electrons in four types of semiconductor nanostructures. Presented in this thesis are images of the motion of electon waves through GaAs/AlGaAs two-dimensional electron gases, lateral quantum

dots defined in a 2DEG, and quantum dots defined inside InAs/InP nanowire heterostructures.

Chapter 2 gives a brief description of the operation of the low temperature SPM.

Chapter 3 discusses the operation of an imaging interferometer for electrons. The interferometer was constructed inside a GaAs/AlGaAs heterostructure containing a two-dimensional electron gas (2DEG) 57nm below the surface. Two-dimensional electron gases have allowed for many exciting experiments and discoveries over the last twenty years [Beenakker and van Houten, 1991; Sohn et al. 1997]. They have permitted access to interesting new phenomena: both the quantum Hall effect [Von Klitzing et al 1980] and the fractional quantum Hall effect [Tsui et al 1982] were first observed in 2DEG's and both of these discoveries were awarded the Nobel prize. Some attractive qualities of 2DEG's are their long electron mean free paths and large electron Fermi wavelengths, ~17 μm and 40nm, respectively, in the 2DEG's used in our research. Additionally, at low enough temperatures, the quantum mechanical phase coherence of the electron can be maintained over distances of many microns. The long electron phase coherence length has been imaged in previous work in our group [Topinka et al. 2001] and it is what makes the construction of an imaging electron interferometer feasible.

We have used our scanning probe microscope to image electron flow in a 2DEG emanating from a quantum point contact (QPC). A QPC is the electronic analog of a single slit for photons [van Wees et al. 1988; Wharam et al 1988]. Images such as the one in Figure 1.2 show that electron flow paths emanating from a QPC are decorated by interference fringes spaced by half the Fermi wavelength, indicating the flow is coherent. We used the coherence of the electron waves to form an imaging interferomter. A small

reflecting gate is placed in front of one side of the QPC and energizing the reflector gate is seen to enhance the amplitude of the fringes at a similar distance from the QPC as the SPM tip. The interference fringes move with the position of the reflecting gate as controlled by its voltage as seen in Figure 1.3.

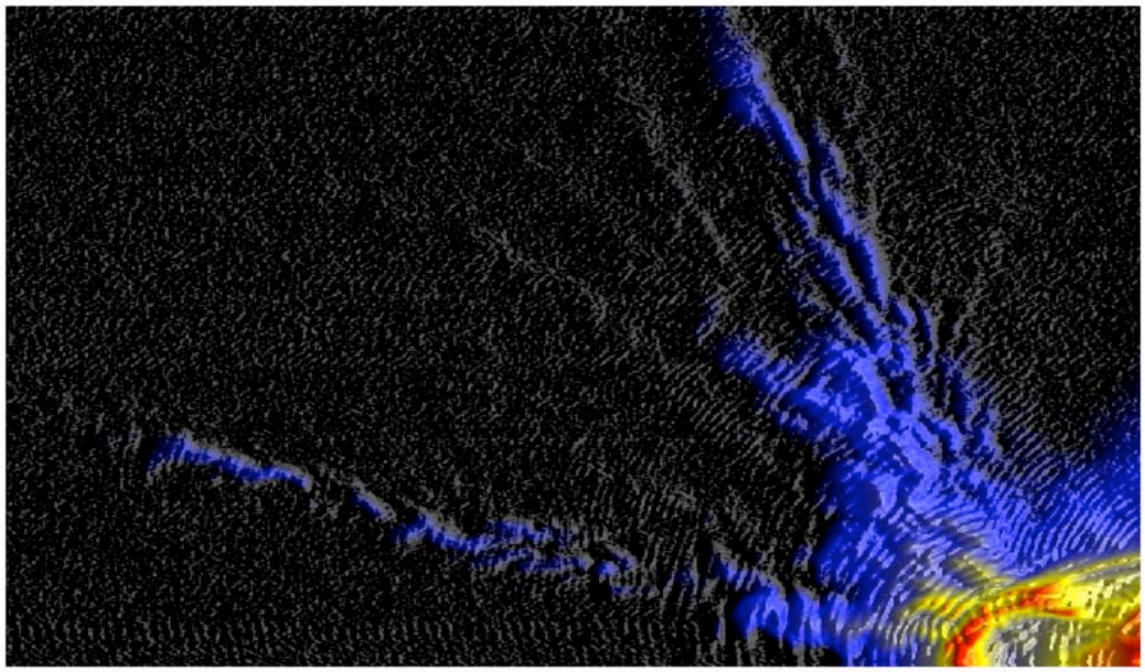

Figure 1.2 An image of coherent electron flow emanating from a quantum point contact, located to the bottom right of the figure. Fringes, spaced by half the Fermi wavelength, indicate the flow is coherent.

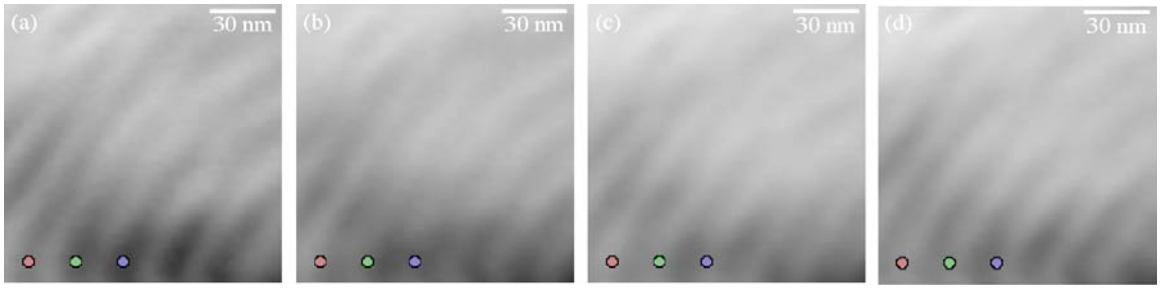

Figure 1.3 (a)-(d) Images of electron flow taken in a small area 1 μm from the QPC at different reflector gate voltages V_{refl}: (a) – 0.5 V, (b) – 0.52 V, (c) – 0.54 V, (d) – 0.56 V. The circles are guides to the eye showing how the fringes move as V_{refl} is changed.

It is possible to further confine electrons inside a 2DEG to zero dimensions, forming a quantum dot [Kastner et al. 1993]. In Chapter 4 we demonstrate a method to image electrons in quantum dots in the Coulomb blockade regime using scanning probe microscopy[14]. We evaporated metallic electrostatic gates on the surface of the GaAs/AlGaAs heterostructure and by applying a negative voltage to the gates, we formed a small puddle of electrons, the quantum dot. An SEM micrograph of the structure is shown in Figure 1.4(A).

Single-electron quantum dots have been recognized as prime candidates for spin qubits in quantum information processing [Loss and DiVincenzo 1998]. Applying the techniques of scanning probe microscopy to single-electron quantum dots can reveal a lot about the spatial properties of electrons on the dot. The knowledge acquired from the SPM images of few-electron quantum dots will be useful in the design and implementation of quantum dot systems for quantum information processing. Additionally the ability to manipulate electrons on quantum dots with an SPM tip acting as a movable gate has many potential applications in quantum dot circuits.

We present images of a one-electron quantum dot, obtained by recording the dot conductance as the charged tip is scanned above. A representative image is shown in Figure 1.4(B). The images display rings of peaked conductance that correspond to Coulomb blockade peaks of the dot at the ring's center. As indicated by the numbers on the figure, when the tip lies outside the ring, there is one electron on the dot and when the

tip lies inside the ring, there are zero electrons on the dot. These data show the tip can act as a movable gate, tuning the number of electrons on the dot by varying its position.

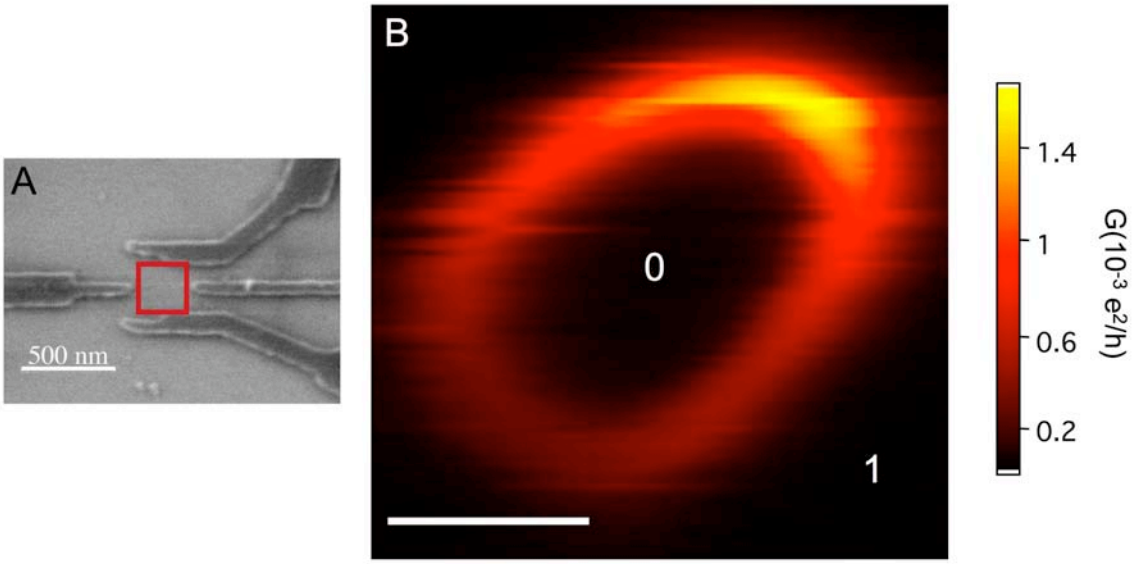

Figure 1.4 (A) SEM micrograph of the one electron quantum dot imaged in this research. (B) SPM image of the quantum dot taken in the area indicated by the red square in (A). Plotted is quantum dot conductance as a function of tip position for a negatively charged tip scanned above the surface of the dot. When the tip lies outside (inside) the ring of peaked conductance there is 1(0) electrons on the quantum dot.

The focus of Chapters 5 and 6 are semiconductor nanowires, grown in a bottom-up approach from gold catalyst particles. These quasi one-dimensional systems have recently enjoyed an immense amount of attention due to their potential applications across a broad spectrum of fields, including nanoelectronics, nanophotonics, quantum information processing, and biology [Lieber 2003; Yang 2005; Samuelson et al. 2004]. There is currently a large push to develop semiconducting nanowires as fast and small FET's. Due to the nanowires' small size, (diameters on the order of 50nm) and the relatively large Fermi wavelength of electrons in semiconductors, transport through these nanowires exhibits quantum mechanical effects. Thus, in addition to their technological

potential, they are interesting playgrounds in which to explore novel one-dimensional physics.

In Chapter 5, we study nominally open InAs nanowire devices fabricated in a field effect transistor (FET) geometry, with a source, a drain, and a gate that can tune the number of charge carriers in the nanowire channel. InAs is a particularly interesting system because of its large g-factor, large exciton Bohr radius, and its' electron affinity for the surface. Standard transport measurements of these nanowires reveal an intricate pattern of Coulomb blockade peaks. Through imaging we use our SPM tip as a movable gate to elucidate where the electrons are along the nanowire and how they flow through it. Figure 1.1 shows an SPM image that locates three seections along the nanowire that behave as quantum dots. The figure demonstrates how we can use the tip as a movable gate to individually tune the charge state of each of the quantum dots.

Chapter 6 shows images of InAs nanowire quantum dots formed between two InP barriers inside an InAs nanowire. The disc shaped dots are 18nm long and 50nm in diameter. The ability to grow tunable one-electron quantum dots in self-assembled nanowire heterostructures has been recently demonstrated [Bjork et al (2004)]. These structures offer a highly ideal system for studying single electron motion in the few electron regime. The bottom-up nature of their assembly results in atomically smooth surfaces and allows for precise control of shapes and sizes, making them attractive candidates for ultra-small electronics and quantum information processing. Figure 1.5(A) demonstrates the high quality of semiconductor nanowire growth. Shown is an InAs/InP nanowire heterostructure; the InAs dot (light) is sandwiched between two InP (dark)

barriers. Note the individual atomic planes along the growth direction, the uniformity of the nanowire diameter, and the sharp interfaces between InAs and InP.

We present experimental electrical conductance images of InAs/InP nanowire quantum dots in the few electron regime as well as simulations of the electronic wave functions in the quantum dot. In the images, such as the one in Figure 1.5, we record nanowire conductance as we scan a charged SPM tip at a fixed height above the nanowire. As the tip is moved, the induced charge on the dot, q_{ind}, varies as $q_{ind} = C_{tip\text{-}dot}(r) * V_{tip}$, where $C_{tip\text{-}dot}(r)$ is the position dependent capacitance between the tip and the dot. The discreteness of the electron charge results in Coulomb oscillations that, in the images, take the form of concentric rings of peaked conductance centered on the quantum dot. The images clearly show the where the dot is located. Using the tip voltage, we can completely empty the dot of electrons, or operate the dot in the one-electron regime that is important for quantum information processing.

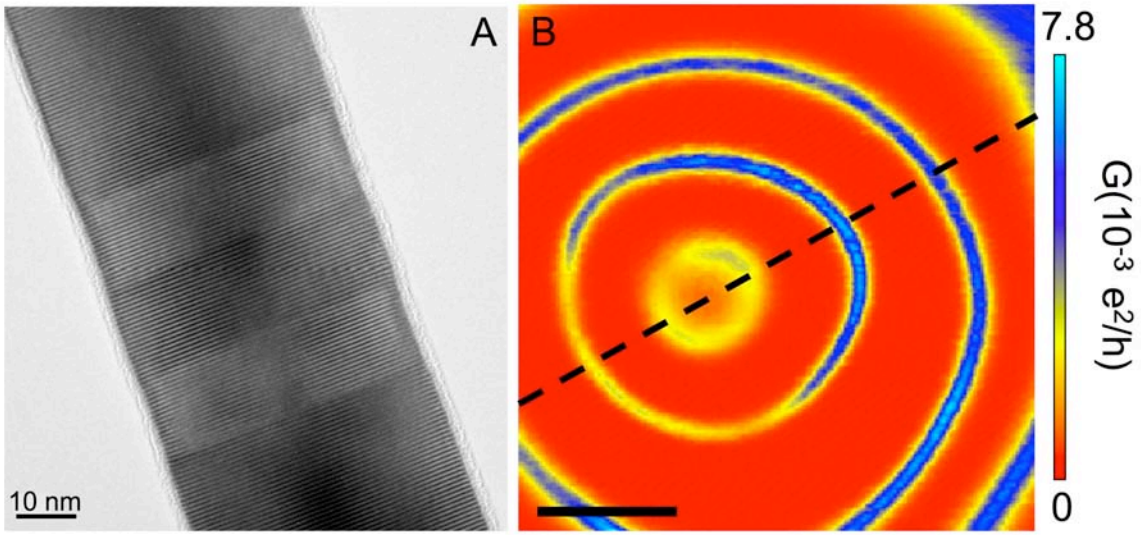

Figure 1.5 (A) TEM image of an InAs/InP nanowire heterostructure showing the individual atomic planes. SPM image of an InAs quantum dot defined inside an InAs/InP nanowire. The location of the wire is schematically indicated by the dashed

black line and the quantum dot lies at the center of the rings of peaked conductance. The image plots nanowire conductance as a function of lateral position of an SPM tip scanned 100 nm over the wire. The rings of peaked conductance correspond to Coulomb blockade peaks of the dot at the rings' center. An electron is added to the dot in passing the tip over each ring. The scale bar is 100nm.

We also present fully self-consistent quantum mechanical simulations of the electronic wave-functions which, together with the images, we use to gain information on where the electrons reside within the nanowire and how their spatial characteristics are affected by applied voltages on the back gate and tip. We demonstrate that we can significantly change the shape of the wave function through varying the tip voltage, back gate voltage, or tip position and we make an estimate of the size of the wave function by comparing experiment and simulation.

Chapter 2

Experimental Techniques

The dewar

The system I have used for all the measurements presented is an Infrared Laboratories dewar that operates at helium 4 temperatures. Details of its operation can be found in Brian LeRoy's thesis (2004) and Mark Topinka's thesis (2002). I will just give a very brief overview of its operation here.

The AFM sits in vacuum and is heat sunk to a He_4 cold plate. Normal operating temperature is 4.2K and we can use a rotary vane pump to pump on the whole helium bath to operate at 1.7K. A picture of the dewar is shown in Figure 2.1. The two fill ports on the top of the dewar are for liquid nitrogen and liquid helium. The liquid nitrogen bath is heat sunk to an outer radiation shield inside the dewar and the helium bath is heat sunk to an inner radiation shield and the cold plate inside the dewar. When cold, ~5 liters of liquid helium and liquid nitrogen need to be filled every 10-11 hours. If the dewar vacuum begins to go soft when the dewar is cold, it has been sufficient to hook up the turbo pump to the vacuum space and pump overnight while keeping the dewar cold.

There are four feedthroughs around the dewar, one mechanical and three electrical. The mechanical feed through is the coarse approach rod. By turning the knob on the outside of the dewar counterclockwise, the tip is brought closer to the sample.

Each turn of the rod brings the tip 1/80th of an inch closer to the sample. The first electrical feed through is a high voltage connector for the electrical leads going to the piezo tube. These lines can carry upwards of 500V each. Care should be taken to ensure all the voltages are down before connecting or disconnecting this connector. The next electrical feed through is for the sample leads. The blue box on the outside of the dewar has 24 BNC connectors but only 12 of them are wired up to go to the sample inside the dewar. The last feed through is used for electrical connections to the cantilever and its Wheatstone bridge, the thermometer, and the LED.

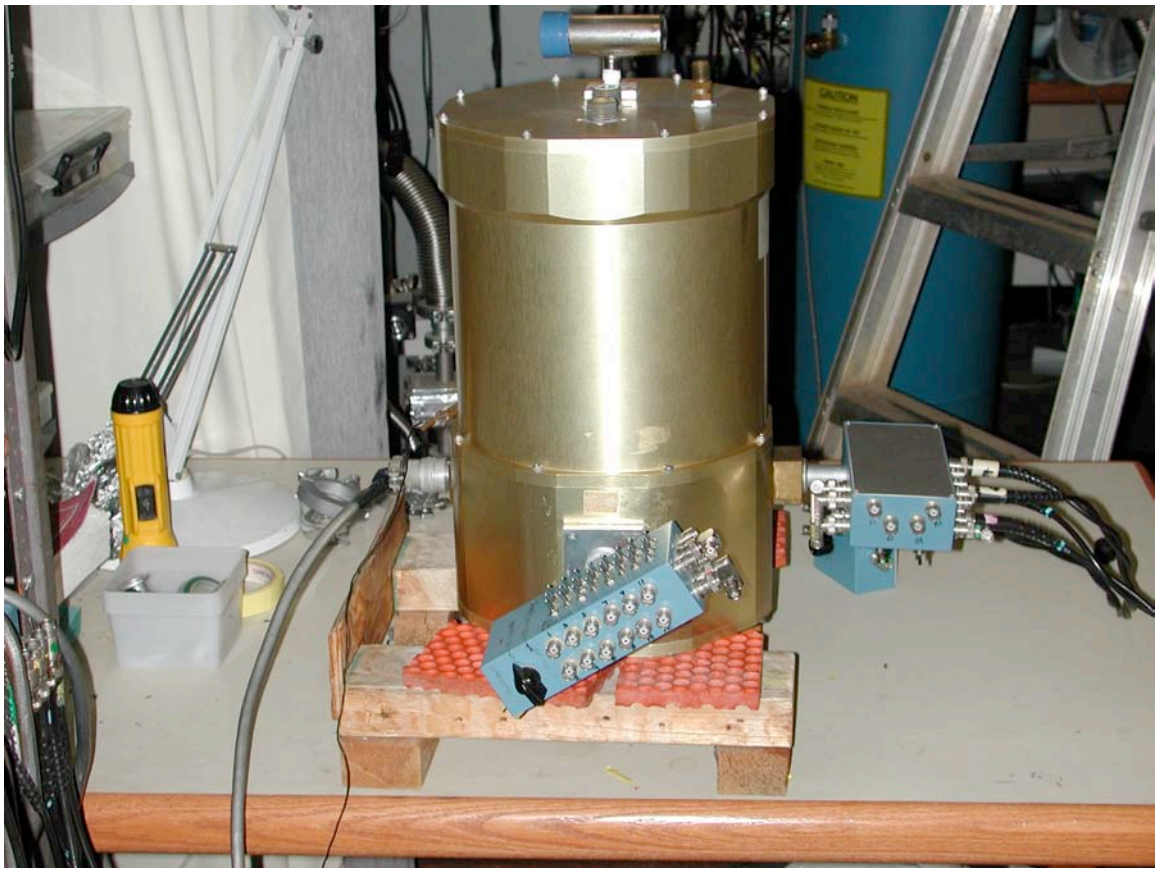

Figure 2.1 Helium 4 dewar used for the imaging experiments in this thesis. The two fill ports for liquid nitrogen and liquid helium are at the top. The mechanical feedthrough for the coarse approach rod is on the other side of the dewar and is not visible in this picture. The high voltage connector is attached to the dewar on the left side, the connector for the

cantilever, thermometer, and LED leads is attached on the right. The breakout box for the sample leads is attached on the front of the dewar.

Preparing the Samples for Imaging

I will only discuss nanowire sample preparation as fabricating structures in GaAs/AlGaAs two-dimensional electron gases has already been detailed in Brian LeRoy's and Mark Topinka's theses. The wires were grown at Philips Research Laboratories and Lund University and the devices were fabricated at DIMES in Delft University and at Lund. I spent a month at Delft and a few weeks at Lund fabricating the devices together with our collaborators there. Details of the device fabrication process can be found in the chapters on imaging InAs nanowires and InAs/InP nanowire quantum dots. Once the devices are at Harvard, they are stored in vacuum until they are ready to be cooled down. This is even more crucial for the nanowire samples than for the 2DEG samples as electrical transport through the nanowires is right near the surface as opposed to 50nm or so below the surface for 2DEG samples. It is imperative to protect the nanowire surfaces.

We mount the samples on sample holders that we make especially for our microscope setup, such as the one shown in Figure 2.2. The procedure for mounting the samples is the same as mounting the 2DEG samples, with the exception of contacting the back gate. The substrates the nanowire samples are deposited on are conducting and thus to make contact to the back gate, we mount the sample with conductive silver paint onto a conductive piece of Al foil and wire bond to the Al foil. I have used two types of sample holders for the nanowire imaging, one with a metal base and one with a base

made out of printed circuit board (shown in Figure 2.2). If the sample holder with a metal base is used, first a thin sheet of filter paper is glued down to the sample holder with insulating GE varnish and then baked for three hours to harden. Then I use conductive silver paint to glue down a small piece of aluminum foil, cut to such a size that when the sample is mounted on top of that, a piece of aluminum foil protrudes far enough beyond the sample that a wire bond can be made to the aluminum foil. The last step is to glue the sample down onto the aluminum foil with conductive silver paint. The filter paper layer is meant to isolate substrate from the grounded sample holder and thus care should be taken that no silver paint contacts the metallic sample holder. If it does, any voltage applied to the back gate will be sent directly to ground and gating the wire with back gate will be impossible. If the printed circuit board sample holders are used, the aluminum foil can be directly mounted onto the printed circuit board and the sample on top of that.

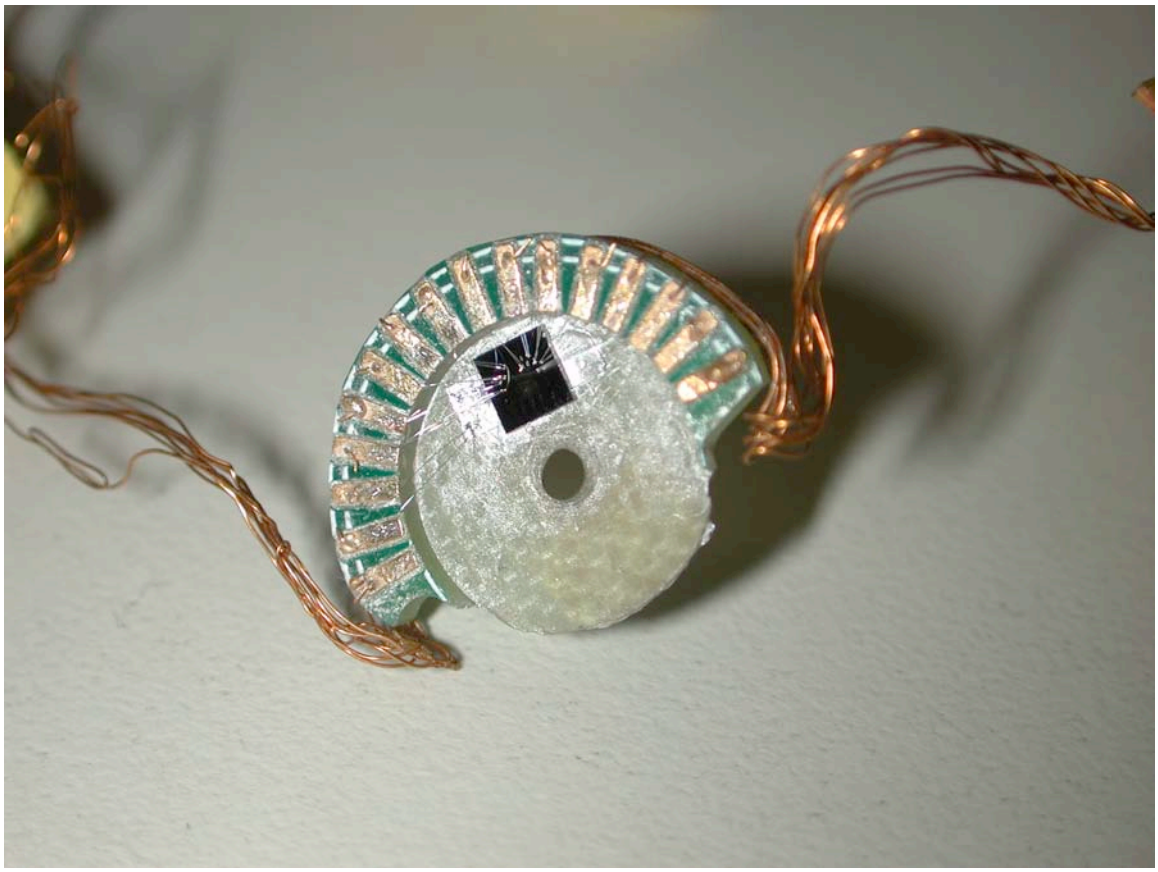

Figure 2.2 An example of a sample holder used in the helium 4 dewar. This sample holder is made out of printed circuit board. The sample is mounted with silver paint onto a small piece of aluminum foil, which protrudes to the left from under the sample as seen in the figure. To contact the back gate, a wirebond is made from a lead on the sample holder to the aluminum foil.

Once the sample is mounted on the sample holder, the sample holder is mounted on top of the piezo tube. The AFM head is then secured down with springs onto the AFM cage (making sure that the tip has plenty of clearance and will not crash into the sample). The tip is then optically aligned over the sample laterally and brought close to the sample. It is important that the silicon chip the cantilever sits on is parallel to the sample. At this point the AFM can be taken to the dewar for precise lateral alignment before cooling down. Topographically scanning the tip over alignment markers on the sample is used to locate the tip with respect to the device of interest. The alignment

markers form a grid of lithographically defined numbers spaced 10 microns apart. Once the tip is positioned at the proper distance from the device of interest (taking into account the drift of the piezo tube from room temperature to cold temperature), the dewar is ready to be sealed up and cooled down.

The liquid nitrogen and liquid helium shields are screwed on for radiation shielding, the dewar top is screwed on tightly forming a good vacuum seal, and the dewar is flipped over so that the fill ports are on the top. One should scan again to make sure the tip has not drifted in lateral position, and then come TWO FULL TURNS off the surface. If this is not done, the tip will crash into the surface of the sample due to varying thermal expansion coefficients of the various materials in the dewar. The next step is to pump out the vacuum space with a turbo pump for at least 3 hours, or until the pressure reaches down into the 10^{-6} mTorr range. Sometimes, it is good to pump for many days or even a week when cooling down a nanowire sample. I have noticed an improvement in device characteristics after pumping for long periods of time on the sample. After pumping, both ports are filled with liquid nitrogen. After an hour and a half, the liquid nitrogen from the inner port is blown out and liquid helium is transferred to the inner port. The sample should be cold in about two hours. You will know when the sample is cold by either monitoring the thermometer, or the cantilever signal, whose resistance is very sensitive to temperature. Once the cantilever signal stops drifting, the system is at 4.2K. All of this should be done while the handler is grounded as, like the 2DEG samples, the nanowire samples are sensitive to electric shocks.

Imaging the Nanowires

When the sample is cold, the first thing to do is check the lateral position of the tip with respect to the sample. It is advisable to scan slowly and pay attention to the topography in case the tip landed right over the device. Scanning over the device in contact mode will almost certainly damage the device. If you are within striking distance of the device (i.e. if the tip position is within 20 microns of the device), the next step is to electrically test the device. If the device is working, you are ready to electrically image. First find the tilt of the sample and use this as the z-guide (see Brian's thesis for the description of the z-guide). In short, the z-guide outputs a z-voltage to the piezo tube for every x and y position of the tip. In this way, the tip follows the plane of the sample and flies at a fixed height above the sample when performing electrical imaging scans. With the z-guide on, bring the tip a comfortable height off the surface and scan in an area near the expected wire location while measuring its conductance. The image will show the largest changes in conductance when the tip is over the wire. In this way, it is possible to find the exact location of the wire.

I would like to make two suggestions that will make scanning over the wire safer. Firstly, it is a good idea to fit the plane for the z-guide as close to the wire as possible. The reason for this is that the plane might be a little different depending on the x-y position of the tube. For example, if the tube is extended far in the x-direction, it may have a slightly different microns/Volt characteristic than when it has close to its equilibrium state. Secondly, when performing electrical scans you will want to use the limited feedback option on the z-axis of the piezotube. In short, the limited feedback allows the tube to push the sample out towards the tip a limited amount (the amount can

be set by an external voltage), while retaining its full range of pull back if the tip hits something and is deflected. If the feedback were fully on, the tip would stay in contact with the sample – not what you want!

Chapter 3

The Imaging Electron Interferometer

3.1 An Introduction to 2DEG's and Quantum Point Contacts

In this chapter, I present work that was done together with Brian LeRoy. I will give a brief overview of the experimental results and details of the experiment can be found elsewhere [LeRoy et al. 2005, LeRoy 2003].

Through highly controlled growth of semiconducting heterostructures it is now possible to confine electrons to flow in two dimensions, forming a two-dimensional electron gas (2DEG) [Davies 1998]. These structures have revolutionized semiconductor physics [Beenakker and van Houten, (1991); Sohn et al. (1997)]. From a basic physics standpoint, 2DEG's have permitted access to interesting new phenomena: both the quantum Hall effect [Von Klitzing et al. 1980] and the fractional quantum Hall effect [Tsui et al 1982] were first observed in 2DEG's. In a more applied vein, 2DEG's are ubiquitous in electronics applications: for example, cell phones and satellite receivers employ high-density 2DEG's in the form of high electron mobility transistors (HEMT's).

Figure 3.1 schematically shows the structure that produces the 2DEG we have used for the imaging interferometer. The two-dimensional electron gas is formed at the interface of GaAs and $Al_{0.3}Ga_{0.7}As$ [Davies 1988]. Electrons are constrained to flow parallel to this interface due to a combination of the conduction band offset between the two layers and the electric field induced by the ionized silicon donor layer. The conduction band of the relevant part of the structure is shown in Figure 3.1 showing the

triangular well that constrains electrons to flow parallel to the GaAs/AlGaAs interface. For a planar system with no electron-electron interactions, the Hamiltonian separates into two parts - a two-dimensional Hamiltonian for motion in the plane, and a one-dimensional Hamiltonian for motion perpendicular to the plane. The electrons are attracted to the donor ions left behind in the barrier, and skate across the interface between the GaAs and AlGaAs layers. If the system is doped so that only the lowest energy state in the one-dimensional Hamiltonian is occupied, then the two-dimensional electron gas is quantum mechanically two dimensional.

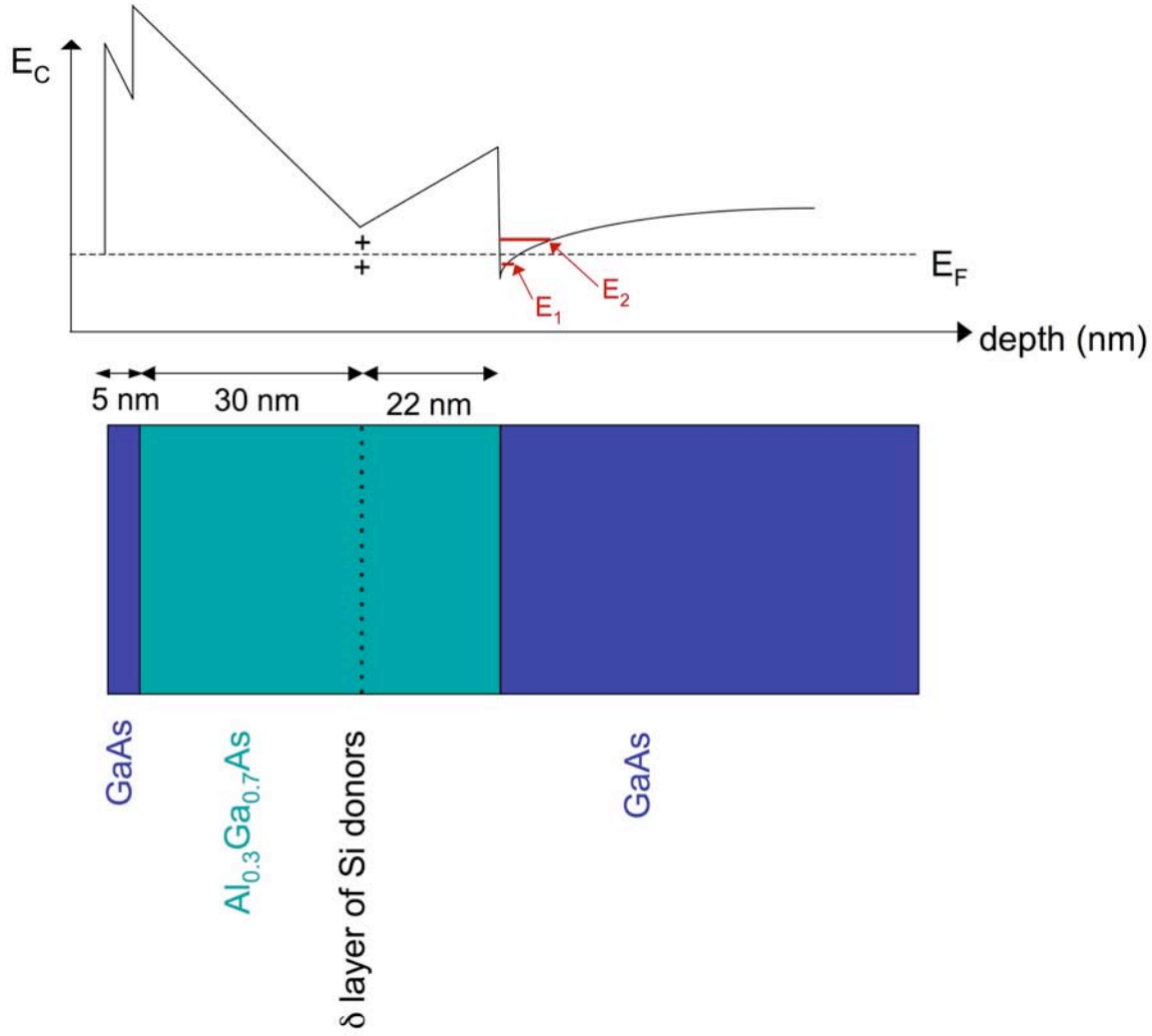

Figure 3.1 GaAs/AlGaAs heterostructure schematic showing the epitaxial layers of GaAs, AlGaAs, and a delta layer of Si donors (bottom half of the drawing). The resulting conduction band energy profile is shown in the upper half of the figure. Electrons are confined to flow at the interface of the GaAs and AlGaAs, 57nm below the surface of the heterostructure (surface is at the left of the figure). The electrons in the 2DEG come from the ionized silicon donors 22 nm away. At 4.2K, the electrons in the 2DEG only occupy the lowest energy state, E_1, of the triangular well.

By depositing metal gates on the surface of the heterostructure and applying a negative voltage to them, we can locally modify the 2DEG's electron density through the capacitive coupling of the gate to the 2DEG. We can form a quantum point contact (QPC), the electronic analog of a single slit for photons, by evaporating two metal gates facing each other as shown at the very right of Figure 3.2(B) and applying enough negative voltage to deplete the electron gas below the gates. The electron gas between the two QPC gates is not depleted, leaving a small aperture through which electrons can flow under an applied bias across the QPC. The width of the aperture can be adjusted through a voltage applied to the QPC gates V_g; the aperture decreases in size with more negative V_g. As V_g is made more negative, conductance falls in steps of $2e^2/h$ every time the width of the QPC decreases by $\lambda_F/2$ where λ_F is the Fermi wavelength of the 2DEG electrons. This conductance quantization was first observed in 1988 [van Wees et al. 1988; Wharam et al. 1988] and spatial images of the electron flow emanating from a QPC were first obtained in our lab [Topinka et al. 2000; Topinka et al. 2001] using our SPM. These images display the modal pattern of the electron flow whose number of lobes and angular spread both increase with increasing QPC width.

Coherent interference fringes were observed in the original images of electron flow from a QPC and the coherence persisted over a distance of many microns. The fringe spacing is half the Fermi wavelength and can be changed with a voltage applied to a back gate in accord with a simple capacitor model (LeRoy et al. 2002].

3.2 The Imaging Interferometer

SPM images of electron flow, such as the one shown in Figure 3.2(C) show the flow is coherent. This coherence motivates the construction of an interferometer for electrons shown in Figure 3.2 (B). Electron waves emitted from the QPC return to the QPC along two paths: reflection from a concave mirror formed by a reflector gate and backscattering off the depleted divot formed in the 2DEG underneath the negatively charged SPM tip. When the reflector gate is energized, interference fringes are produced in SPM images recorded by the tip. By varying the reflector gate voltage, and consequently the distance between the QPC and the mirror, the phase of the reflected electron waves is changed; the fringes in the SPM image move a corresponding amount.

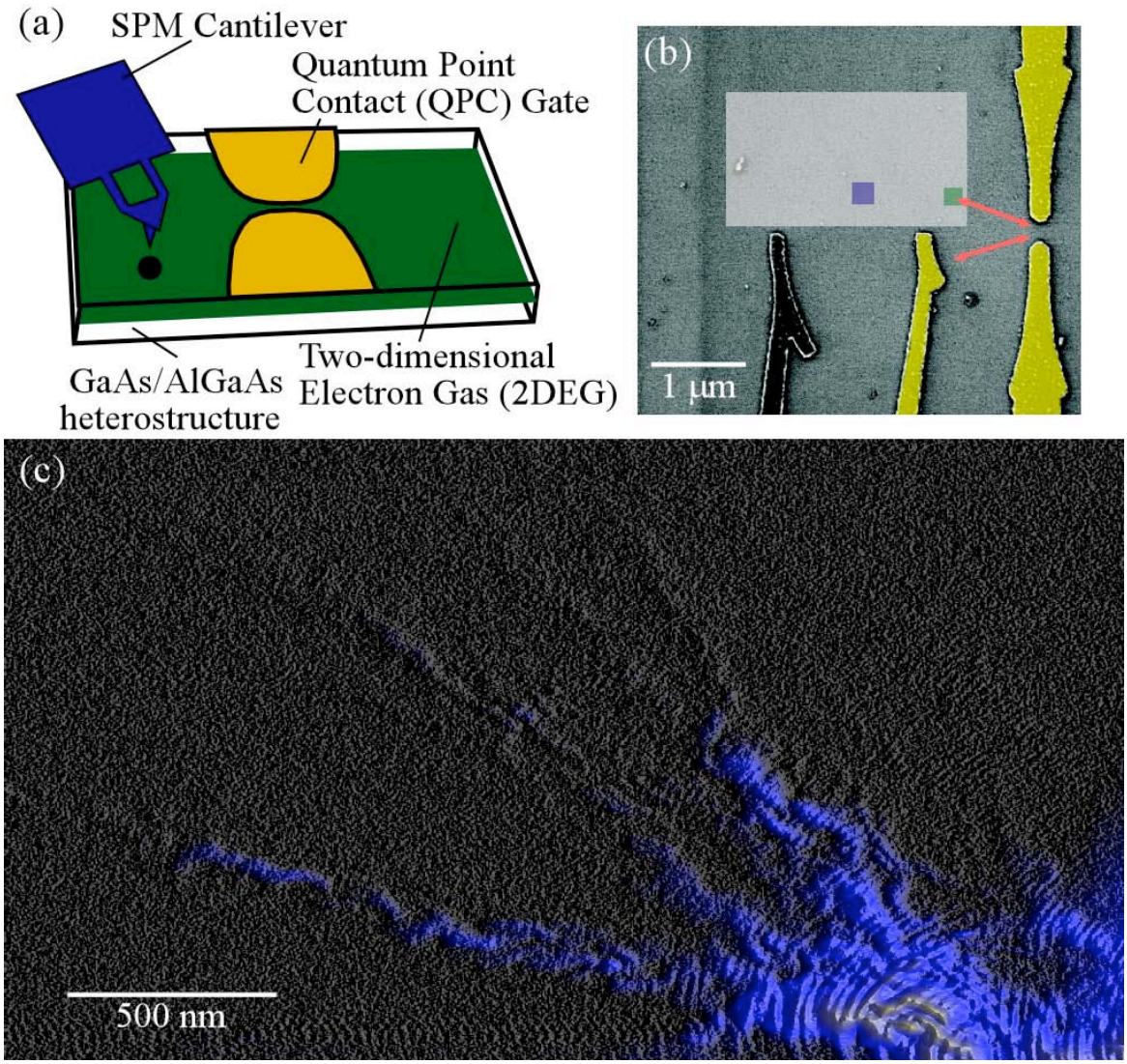

Figure. 3.2 (a) Schematic diagram showing the technique used to image electron flow through a 2DEG. A negatively biased tip causes backscattering through the QPC. The conductance as a function of tip position is measured to produce an image of electron flow. (b) Scanning electron microscope image of the device used to probe the interference fringes, with three areas indicated where images of electron flow are acquired. The QPC and reflector gate are shown in yellow. (c) Image of electron flow taken in the area indicated by the large gray box in (b).

Figure 3.2(A) illustrates the technique used to image electron flow [Topinka et al. 2000; Topinka et al. 2001]. An SPM tip was scanned at a fixed height above the surface of a GaAs/AlGaAs heterostructure. Two surface electrostatic gates formed a QPC, a

narrow constriction in the 2DEG. A negative voltage was applied to the tip, producing a small, depleted disc in the 2DEG directly below the tip. This depleted area served to backscatter electrons arriving from the QPC, reducing its conductance. Images of electron flow, such as the one in Figure 3.2(C), were obtained by recording the change in QPC conductance as a function of tip position.

An imaging electron interferometer was made by adding a circular reflector gate that forms an electron mirror when it is energized. Figure 3.2(B) is a scanning electron micrograph of this device that contains two reflector gates at distances of 1 μm and 2.5 μm away from the QPC. In the images presented below, only the gate 1 μm away from the QPC was energized. The GaAs/AlGaAs heterostructures contained a 2DEG 57nm below the surface with measured density 4.2×10^{11} cm^{-2} and mobility 1.0×10^{6} $cm^2/Vsec$. The heterostructure was grown by molecular beam epitaxy on an n–type GaAs substrate with the following layers: smoothing superlattice, 1000 nm GaAs, 22 nm $Al_{0.3}Ga_{0.7}As$, δ-layer of Si donors, 30 nm $Al_{0.3}Ga_{0.7}As$ and a 5 nm GaAs cap.

Figure 3.3 shows a series of SPM images taken with the interferometer that show how the interference fringes move as the reflector gate voltage is changed. The scan area for Figures 3.3(A)-(D) indicated by the blue box in Figure 3.2(B) is at the same distance (1 μm) from the QPC as the reflector gate. The scan area for Figures 3.3(E)-(H) in the green box is at twice the distance (2 μm) from the QPC. As the reflector gate is moved via its gate voltage, the fringes in Figures 3.3(A)-(D) move the same distance as the electron mirror, at an average rate of 100 nm/V, while the fringes in Figures 3.3(E)-(H) move twice as far, at an average rate of 230 nm/V.

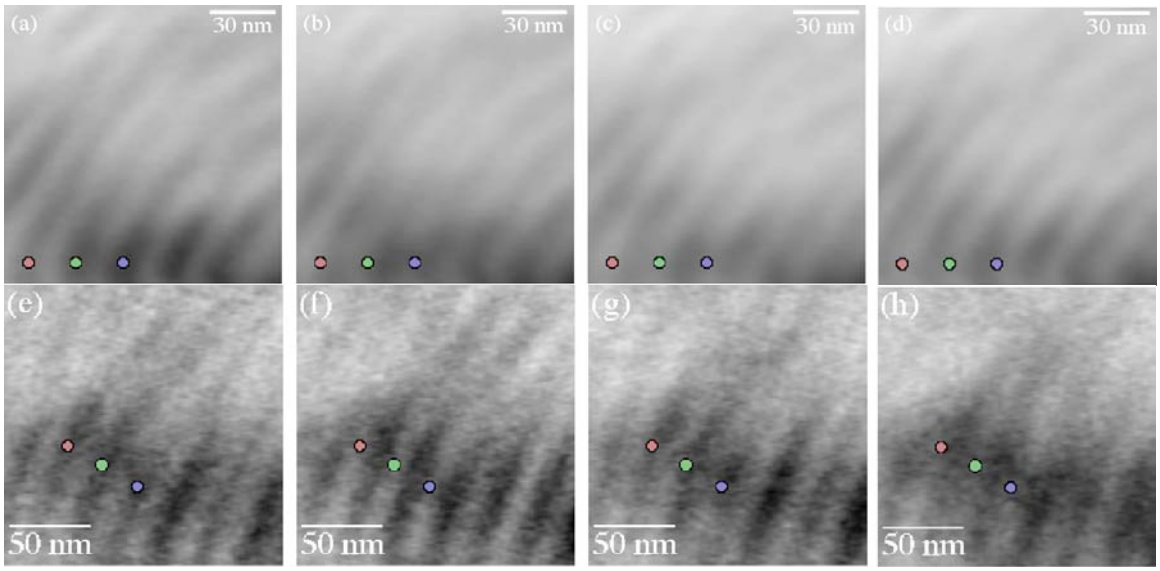

Figure 3.3 (A)-(D) Images of electron flow taken in the area denoted by the green square in Fig. 1B at different reflector gate voltages V_{refl}: (A) – 0.5 V, (B) – 0.52 V, (C) – 0.54 V, (D) – 0.56 V. The circles are guides to the eye showing how the fringes move as V_{refl} is changed. (E)-(H) Images of electron flow taken twice as far away from the QPC, in the location indicated by the blue square in Fig 1B for the same series of reflector gate voltages. The fringes move twice as far as those in A-D.

A simple thermal argument explains this factor of two speed-up in the lower series of images [Shaw et al. 2001; Shaw et al. 2002]. A thermal average over the range of electron wavelengths tends to wash out interference fringes at distances longer than the ballistic thermal length $\ell_T = \hbar v_F / \pi k_B T$ where v_F is the Fermi velocity and T is the temperature; $\ell_T \cong 170$ nm at $T = 4.2$K for this sample. The effects of coherence in the interference signal can thus be lost, even though the coherence of individual electrons is maintained. Interference fringes are observed when the interfering path lengths are the same length, within the thermal length ℓ_T. A single bounce path between the QPC and the mirror satisfies this requirement for the upper series of images in Figures 3.3(A)-(D), whereas a double bounce between the QPC and mirror is needed to match the QPC-tip

roundtrip path length in the lower series in Figures 3.3(E)-(H). Consequently, the fringes move twice as far as the mirror when the tip is positioned twice as far from the QPC.

Figure 3.4 plots the position of the interference peaks seen in Figure 3.3 as a function of reflector gate voltage. From the slopes of the lines in this figure, it is clearly seen that the fringes move 100nm/V_{refl} when scanning the tip in an area comparable to the reflector gate – QPC distance and 230nm/V_{refl} when scanning twice as far from the QPC as shown in Figure 3.3. These values agree very well with the expected movement of the depletion region of the reflecting gate calculated using SETE, Mike Stopa's fully self-consistent quantum mechanical program [Stopa 1996]. The proper 2DEG parameters (density, 2DEG depth, temperature) were input as well as the SEM picture of Figure 3.1(B) to specify the proper geometry. The results of the simulation are shown in Figure 3.4. The point of back scattering for electrons moves inwards towards the QPC at a rate of 104 nm/V_{refl}, in very good agreement with the experimentally determined 100nm/V_{refl}.

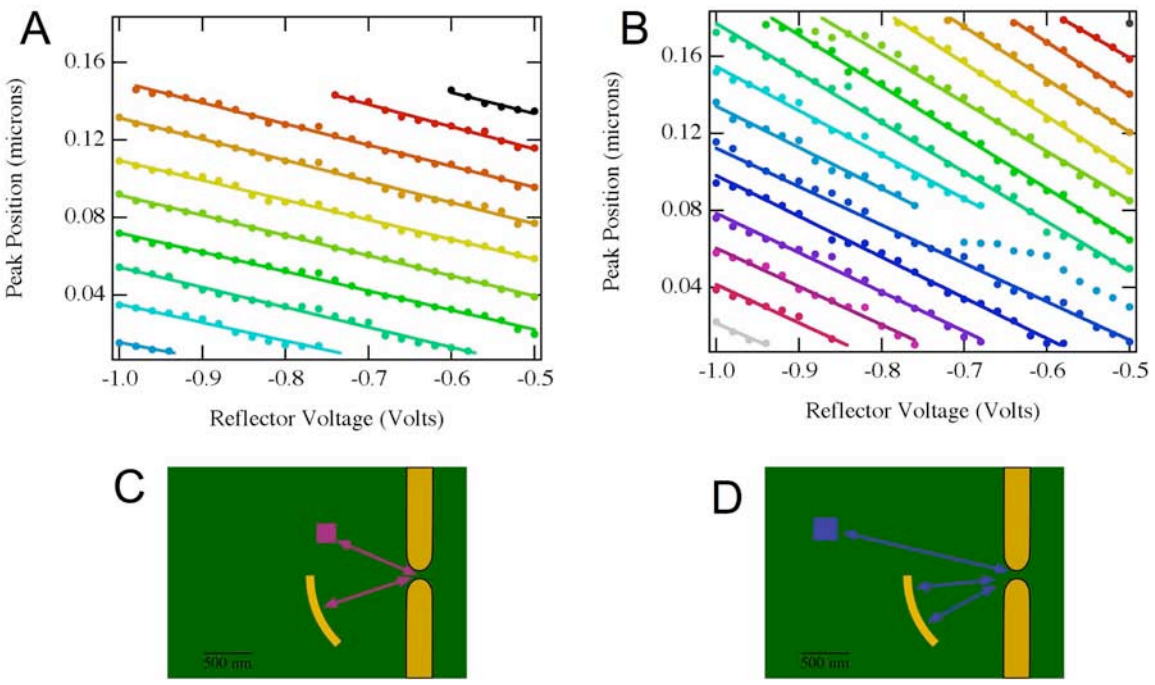

Figure 3.4 (A)-(B) Movement of interference fringes at the location of the tip with changing reflector gate voltage. In (A) the tip is scanned at a distance from the QPC comparable to the distance between the reflecting gate and the QPC. The fringes arise from interference of the two paths shown in pink in (C). As the voltage on the reflector gate is changed, so is the path length of the lower pink path, thus shifting the location of the fringes at the tip. By looking at the slope of the lines in (A), we see that the fringes move at an average rate of 100nm/V_{refl}. In (B) the tip is scanned at a distance twice as far from the QPC as the reflector gate and the fringes are seen to move twice as quickly with reflector voltage.

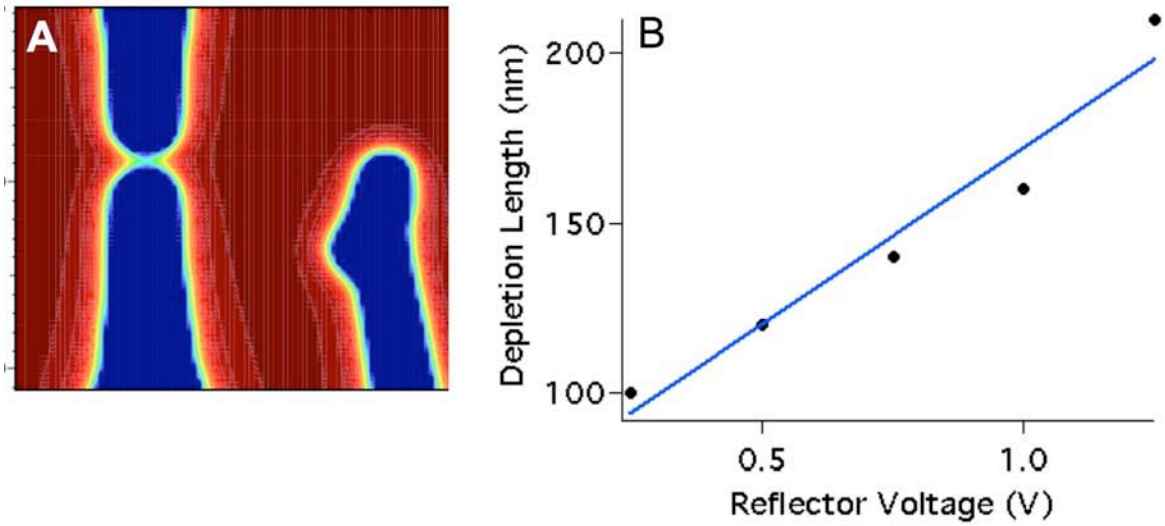

Figure 3.5 (A) Simulation of the potential inside the 2DEG for the gate geometry of the interferometer device. The potential directly below the QPC gates and reflector gate is negative enough such that the electrons are depleted below the gates and a small distance outwards from the gates. This distance, the depletion length, depends on the voltage applied to the gates. (B) shows the calculated depletion length inside the 2DEG as a function of voltage applied to the reflector gate. The slope of a best fit line is 104nm/V_{refl}.

In conclusion, an imaging electron interferometer was constructed in a 2DEG - electron waves traveling from a QPC are backscattered by a circular mirror and by the depleted divot beneath a SPM tip, and interfere when they return to the QPC. Strong fringes are produced in images of electron flow when the electron paths have

commensurate lengths, within the ballistic thermal length ℓ_T. Warmer experiments above 4.2 K are certainly desirable. Of course, incoherent electron-electron scattering [Giuliani and Quinn 1982; Zheng and S. Das Sarma 1996] will eventually become dominant. Before that, however, even better time and spatial resolution will emerge.

Chapter 4

Imaging a One-Electron Quantum Dot Formed in a GaAs 2DEG

4.1 Introduction to Quantum Dots and the Coulomb Blockade

Images of a one-electron quantum dot were obtained in the Coulomb blockade regime at liquid He temperatures using a cooled scanning probe microscope (SPM). The charged SPM tip shifts the lowest energy level in the dot and creates a ring in the image corresponding to a peak in the Coulomb-blockade conductance. Fits to the lineshape of the ring determine the tip-induced shift of the electron energy state in the dot. SPM manipulation of electrons in quantum dots promises to be useful in understanding, building and manipulating circuits for quantum information processing.

Semiconducting quantum dots, often referred to as artificial atoms, are islands of charge housed inside a small chunk of a semiconductor whose dimensions range from a few nanometers to microns [Kastner 1993]. Like atoms, they have discrete energy levels and they hold a discrete number of electrons, anywhere from one to many hundreds [Kouwenhoven et al. 1997; Kouwenhoven et al. 2001]. Unlike atoms, it is possible to vary the quantum dot's electron number through an applied voltage on an external gate capacitively coupled to the dot. It is also possible to wire up individual quantum dots because of their relatively large size as compared to real atoms. We exploit both of these properties to measure electrical transport through quantum dots in the few-electron

regime. Source and drain leads are tunnel coupled to the dot and dot conductance is measured as a function of source-drain voltage V_{sd} and external gate voltage V_g.

We perform spectroscopy on artificial atoms using the Coulomb-blockade phenomenon [Kouwenhoven et al 2001]. Coulomb blockade is observable at low temperatures, small dot sizes, and resistive tunnel barriers[1]. In this regime conductance through the quantum dot is blocked when the Fermi energy of the leads is less than the sum of the energy of the highest filled state in the dot plus the charging energy. The charging energy $E_C = \frac{e^2}{C}$, where C is the total capacitance of the dot to its environment, is the energy required to add another electron to a quantum dot and is analogous to the ionization energy of an atom. The electrostatic energy of the dot, and hence the energy levels in the dot, can be varied by applying a voltage V_g to a capacitively coupled gate (with capacitance C_g to the dot). The competition of the dot's electrostatic energy and its charging energy produces peaks in the dot's conductance, Coulomb-blockade peaks, as a function of gate voltage. On a Coulomb-blockade peak it is equally energetically favorable for the dot to hold either N or N+1 electrons, where N is an integer. Coulomb blockade diamond plots, such as the one shown in Figure 4.2, are obtained by measuring quantum dot conductance as a function of V_g and V_{sd}. These plots offer a wealth of information about the system. For example, we can extract values for C_g and C as well as the quantum dot's energy level structure.

Single-electron quantum dots are promising candidates for quantum information processing. Loss and DiVincenzo have proposed using a scheme for which the electron

[1] The conditions for Coulomb-blockade are $R_l >> h/e^2$ and $e^2/C >> k_BT$, where R_l is the leads' tunnel resistance, and C is the total capacitance of the dot.

spin is the qubit, and two qubits can be entangled using tunnel-coupled one-electron dots [Loss and DiVincenzo 1998]. To pursue these ideas, quantum dots that contain only one electron are being developed, as individual single-electron dots [Kouwenhoven et al. 2001; Tarucha et al. 1996; Ashoori 1996; Potok et al. 2003] and as tunnel-coupled single-electron dots [Elzerman et al. 2003; Chan et al. 2004]. A useful circuit for quantum information processing will consist of many coupled quantum dots. Scanning probe microscopy promises to be important for the development and understanding of quantum dots and dot circuits, by providing ways to image electrons and to probe individual dots using electromagnetic fields.

4.2 Imaging Mechanism

We have fabricated a single-electron quantum dot and used a scanning probe microscope to probe the spatial properties of the electrons inside in the Coulomb blockade regime. Our imaging technique is illustrated in Figure 4.1. A conducting SPM tip is scanned at a fixed height above the surface of a GaAs/AlGaAs heterostructure as shown in Figure 4.1(A). A voltage applied to the tip with respect to the 2DEG, perturbs the gate confining potential and shifts the energy levels in the dot, changing the dot conductance in the Coulomb blockade regime. Images were obtained by measuring the dot conductance as a function of tip position. In these images, the contrast was offered by Coulomb blockade peaks.

Figures 4.1(C)-(E) schematically show how electrons move through the dot for different tip positions. When the tip is far from the dot (Figure 4.1(C)), the dot conductance is blocked and the dot contains one electron. As the negatively charged tip

is brought closer (Fig. 4.1(D)), the energy of the electron on the dot shifts upwards, and the electron energy level comes into resonance with the Fermi energy of the leads, causing the dot conductance to peak. Bringing the tip even closer (Fig. 4.1(E)) pushes the single-electron off the dot and conductance is again blocked. Note the position of the tip for which the Coulomb blockade is lifted, indicated by the green circle in Figure 4.1(B), depends on the tip voltage and the gate voltage. The images presented in this chapter are taken in an area similar to the one indicated by the red square in Figure 4.1(B) and the dot conductance peaks when the tip lies within the image area, much closer to the center of the dot than indicated schematically by the green circle.

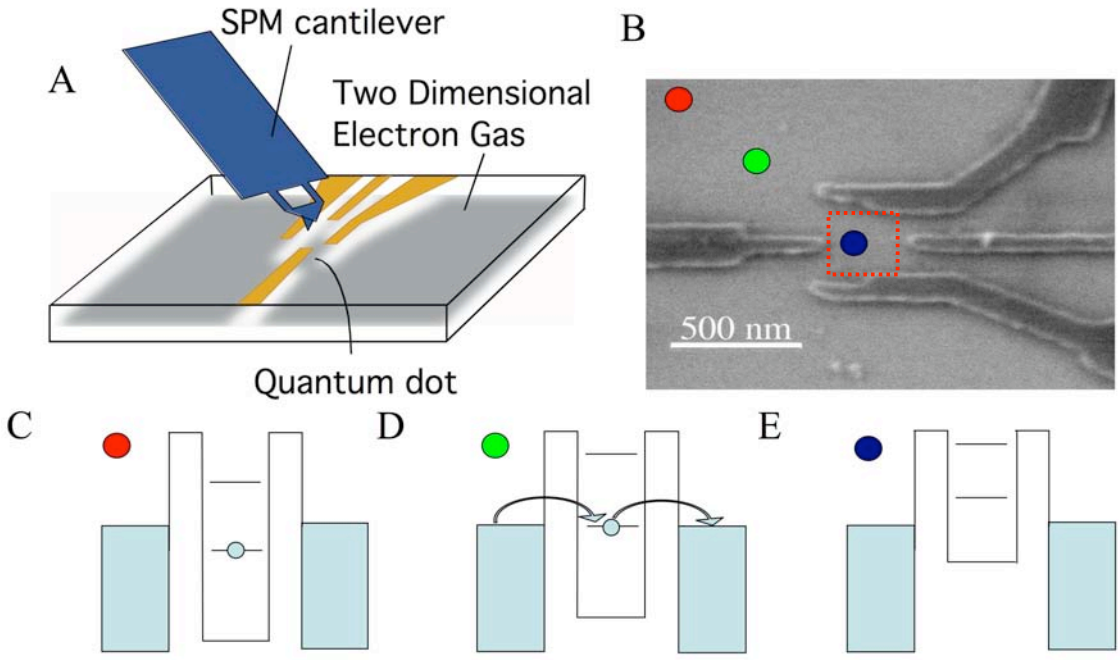

Figure 4.1 (A) Schematic diagram of the experimental setup used to image electrons in a one-electron quantum dot. The dot is formed in a 2DEG located 52nm below the surface of a GaAs/AlGaAs heterostructure. A charged SPM tip is scanned above the dot and the dot conductance is measured as a function of tip position. (B) A scanning electron micrograph of the device. The SPM tip induces a perturbation to the dot's gate confining potential, shifting the dot energy levels and altering the electron occupancy of the dot. (C)-(E) Schematics of the tip-induced shift in quantum dot energy level for different tip

positions. The dashed red square in (B) indicates the image area for the images shown in Figures 4.5(A)-(D).

Figure 4.1(B) is a scanning electron micrograph of the quantum dot studied here. The dot was fabricated in a GaAs/$Al_{0.3}Ga_{0.7}As$ heterostructure containing a 2DEG. The 2DEG was 52nm below the surface and had a measured density $n = 3.8\times10^{11}$ cm^{-2} and mobility $\mu = 470{,}000$ cm^{2}V^{-1}s^{-1}. The heterostructure was grown by molecular beam epitaxy with the following layers: 5 nm GaAs cap layer, 25 nm $Al_{0.3}Ga_{0.7}As$, Si delta-doping layer, 22 nm $Al_{0.3}Ga_{0.7}As$, 20 nm GaAs, 100 nm $Al_{0.3}Ga_{0.7}As$, a 200 period GaAs/$Al_{0.3}Ga_{0.7}As$ superlattice, 300 nm GaAs buffer and a semi-insulating GaAs substrate. The 2DEG was formed in the 20 nm wide GaAs square well sandwiched between two $Al_{0.3}Ga_{0.7}As$ barriers. The dot was defined using Cr surface gates fabricated using e-beam lithography.

4.3 Images of a One-Electron Quantum Dot

Without the tip present, the quantum dot could be tuned to contain 0 or 1 electrons in the Coulomb blockade regime. This is clearly shown in Figure 4.2(A), which plots the differential dot conductance dI/dV_{SD} vs. source-to-drain voltage V_{SD} and side gate voltage V_G at T = 1.7 K. The conductance peaks correspond to resonant tunneling through a single quantum state. Coulomb blockade diamond measurements reveal an appreciable amount of information: from Figure 4.2(A) we determine the one-electron charging energy E_C to be 4.2 meV and the ground-state to first-excited-state energy spacing ΔE to be 3.1 meV.

Figure 4.2(B) shows a Coulomb blockade diamond taken using the SPM tip as a movable gate. This is a plot of the differential conductance dI/dV_{sd} of the dot vs. V_{sd} and tip voltage V_{tip} ; the side gate voltage V_g was fixed, and the charged SPM tip was held at a height directly above the dot. The pattern of Coulomb blockade diamonds is similar to those obtained by varying V_G in Figure 4.2(A), demonstrating that the tip acts as a gate, and that the tip to dot coupling is similar to the coupling between the side-gate and the dot.

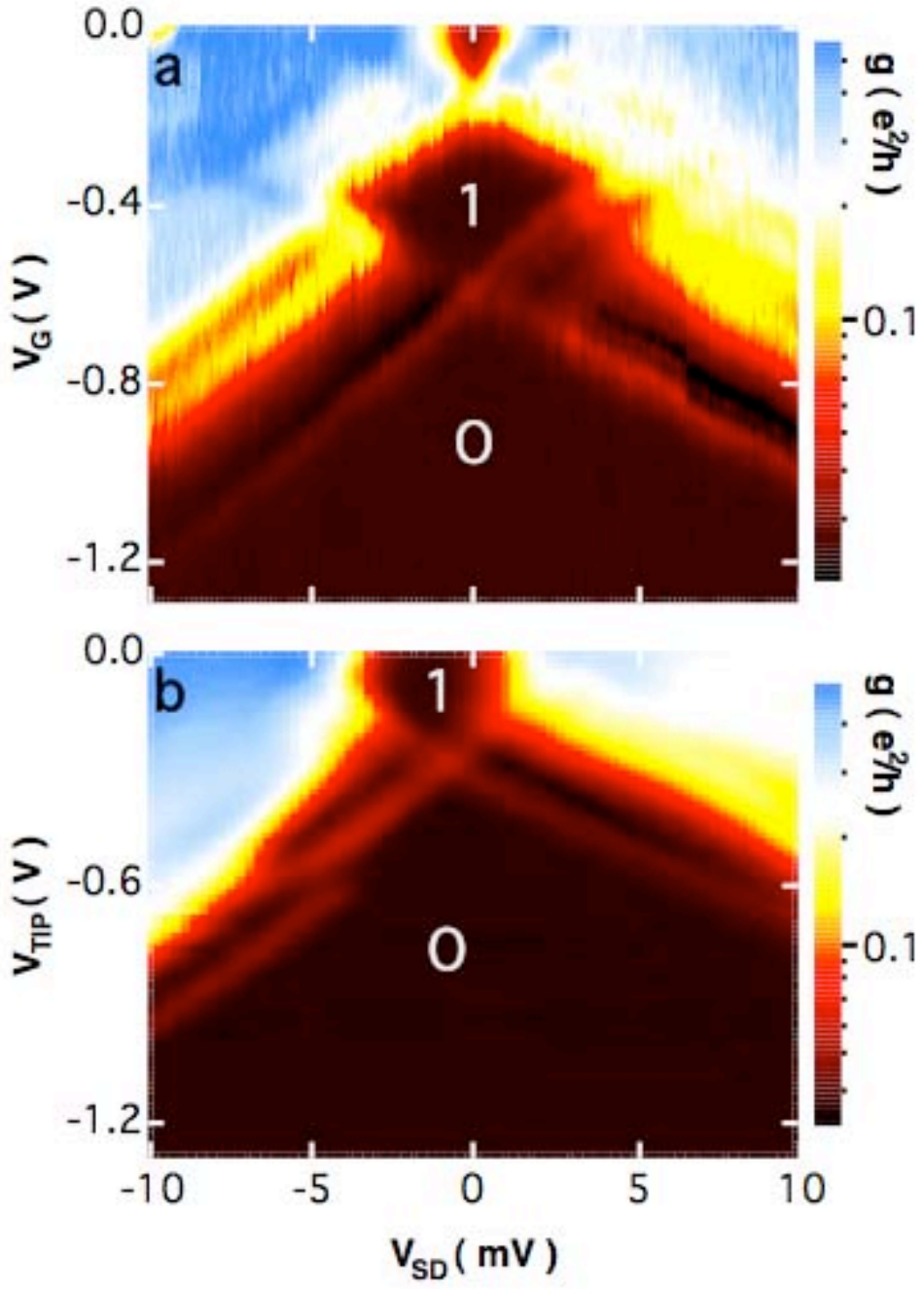

Figure 4.2. (a) Plot of differential conductance $g = dI/dV_{SD}$ as a function of side-gate voltage V_G and source-to-drain voltage V_{SD} at $T =$ 1.7 K, showing Coulomb blockade diamonds for 0 and 1 electrons, and resonant tunneling through the ground and first excited energy levels separated by 3.1 meV. (b) Plot of differential conductance $g = dI/dV_{SD}$ vs. SPM tip voltage V_{tip} and V_{SD} at $T = 1.7$ K for a fixed tip position, showing that the tip acts as a moveable gate.

Figures 4.3(A)-(C) show Coulomb blockade diamonds recorded at three different tip heights. The ratio of the tip-dot capacitance C_{td} to the total dot capacitance C_{Σ} ,are extracted from these plots are found to decrease from $C_{td} / C_{\Sigma} = 0.063$ for a tip height of 60nm above the dot to $C_{td} / C_{\Sigma} = 0.051$ for a tip height of 280 nm above the dot to $C_{td} / C_{\Sigma} = 0.046$ for a tip height of 400 nm above the dot. The SPM tip, acting as a movable gate, has the added benefit of mobility over a stationary side gate: the tip-dot capacitance can be varied by changing the tip's position over the dot. The SPM tip can also be used to direct electrons in a desired direction. These abilities promise to be very useful for the development of quantum dot circuits for quantum information processing.

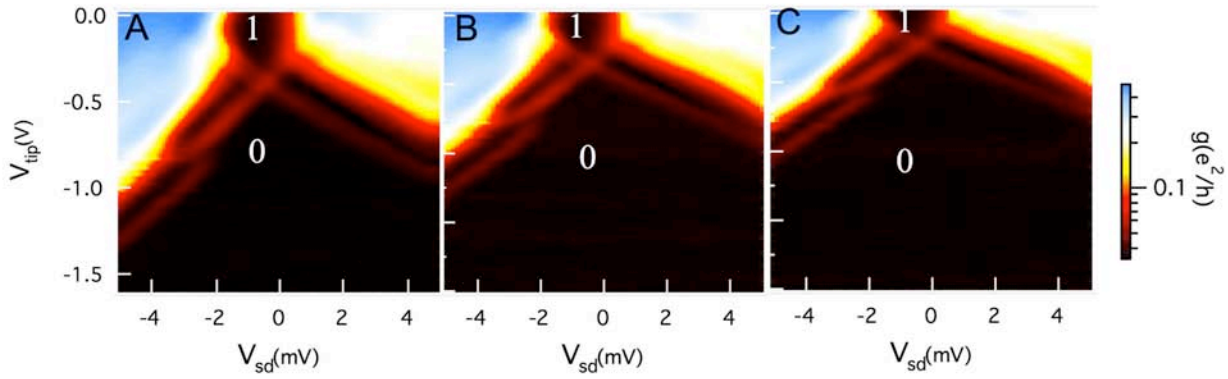

Figure 4.3: (A)-(C) Coulomb blockade diamonds obtained by showing the differential conductance dI/dV_{sd} of the dot vs. tip voltage V_{tip} and source-to-drain voltageV_{sd} for fixed side gate voltage, at 1.7 K. The measurements were taken at three different heights of the SPM tip above the surface: (A) 60 nm, (B) 280 nm, and (C) 400 nm with the tip positioned directly over the dot. The number of electrons on the dot is indicated. The diamonds qualitatively show that the tip-dot capacitance decreases for increased tip-dot separation.

Figures 4.4 (B)-(C) show Coulomb blockade images of the single-electron quantum dot; the scan area is indicated by the red square in Fig. 4A. The rings observed in these images are maxima in conductance, corresponding to the Coulomb blockade conductance peak between zero and one electron, or between one and two electrons on the dot as indicated. The rings follow contours of constant tip-dot coupling. The images were obtained by fixing the tip and side gate voltages and measuring the differential dot conductance dI/dV_{sd} as the tip was scanned in a small area above the dot shown in Fig. 4.4(A). When the negatively charged tip was moved outside the ring, the dot contained one electron and conductance was blocked. When the tip was brought inside the ring, the electron was pushed off, the dot was empty, and conductance was again blocked. The dot conductance peaks when the tip is positioned on the ring and it is equally energetically favorable for the dot to hold N or N+1 electrons.

As shown in Fig. 4.4(B)-(C), the size of the Coulomb blockade rings can be tuned by varying the side gate voltage V_g. When the side-gate voltage is made less negative (Fig. 4.4(C)) the ring between zero and one electron shrinks to a ridge-like feature in the center of the image. Additionally, an additional ring corresponding to a Coulomb blockade conductance peak between the one and two-electron states becomes visible.

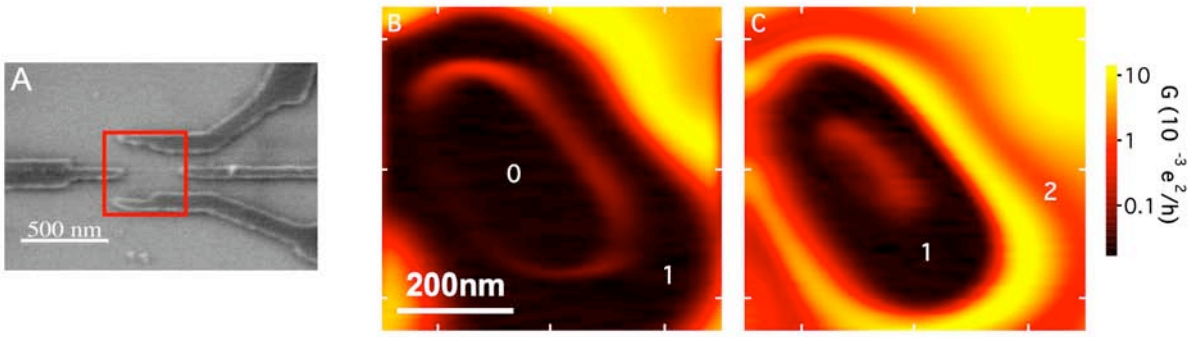

Figure 4.4 (A) SEM micrograph of the quantum dot indicating the scan area for SPM images in (B) and (C). (B)-(C) SPM images of Coulomb blockade conductance of a single-electron quantum dot vs. tip position for side gate voltages V_g (B) – 0.97 V and (C) – 0.83 V. The tip voltage is held at – 0.3 V for both scans. The ring of peaked conductance in (B) corresponds to resonant tunneling through the lowest energy state of the quantum dot. As the side gate voltage decreases, this ring shrinks to the ridge-like feature in the center of (C), and a second ring appears as a second electron is added to the dot. The number of electrons on the dot is indicated in each image.

A series of images of the single-electron quantum dot are shown in Figures 4.5 (A)-(D) for tip voltages 40mV, 50mV, 60mV and 80mV respectively. The field of view covers an area within the gates of the quantum dot (see red square drawn on Figure 4.1 (B)). In each image, as in Figure 4.4, a ring-shaped feature is observed, centered on the middle of the dot. The dot contains one electron when the tip is outside the ring and zero electrons when the tip is inside the ring. To confirm that the dot is empty inside the ring, we moved V_G to more-negative voltages and verified that no additional conductance peaks appeared.

The strength of the interaction between the SPM tip and the dot can be adjusted by changing the tip voltage V_{tip} as shown in Figures 4.5(A)-(D). In Figure 4.5(A) the tip pushes the electron off the dot when the tip is about 100 nm to the side of the center. As V_{tip} is increased in a series of steps from Figures 4.5(A)-(D), the radius of the ring shrinks to a small value. As discussed below, the lineshape of the ring provides a window through which one can extract information about the dot. The probing window can be moved to any desired location with respect to the dot by changing the ring radius.

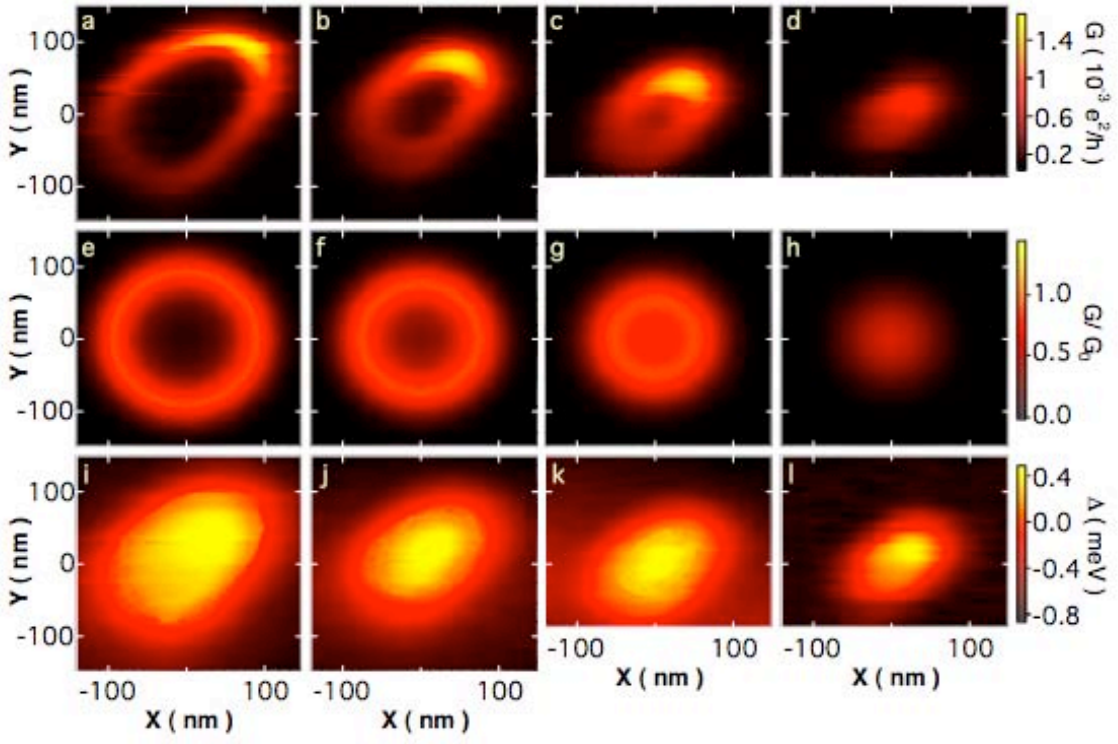

Figure 4.5 (a-d) Coulomb blockade images of a single-electron quantum dot at T = 1.7 K, showing the dot conductance G vs. tip position. The ring of high conductance around the center of the dot is formed by the Coulomb blockade peak between 0 and 1 electron in the dot. The tip voltages V_{tip} for A-D are 40 mV, 50 mV, 60 mV and 80 mV respectively. (e-h) Theoretical simulations of the images in a-d for a dot formed by a parabolic potential with energy spacing 3.1 meV (energy of first excited state from Figure 2a) for the same tip voltages as a-d. (i-l) Experimental maps of the energy shift Δ of electrons in the dot vs. tip position, extracted from the measured lineshape of the Coulomb blockade conductance peak forming the rings in images a-d.

The spatial resolution in Figures 4.5(A)-(D) is quite good, finer than the width of the tip electrostatic potential $\Phi_{tip}(\vec{r},\vec{r}_e)$ at the point $\vec{r}_e$ in the 2DEG for tip position $\vec{r}$; this width is determined in part by the height of the tip above the surface. The resolution is enhanced by the strong dependence of the Coulomb blockade conductance G on the change Δ_{tip} in electron energy, where Δ_{tip} is the shift in energy of the electron state in

the dot induced by the presence of the tip at position $\vec{r}$. However, the images in Figure 4.5 do not determine the shape of wave function amplitude $\left|\psi(\vec{r}_e)\right|^2$, because it is much narrower than $\Phi_{tip}(\vec{r},\vec{r}_e)$ for this case.

Simulated images of the single-electron quantum dot are shown in Figures 4.5(E)-(H). These images show the calculated dot conductance as a function of lateral tip position using parameters from the experiment, including the tip voltage and height. In these calculations the dot was assumed to have a parabolic confining potential with an energy level spacing $\Delta E = 3.1$ meV matching the measured value for the first excited state from Figure 4.2 (A). The ground state energy of the dot in the presence of the tip was obtained by solving Schrödinger's equation for this system. The dot conductance was calculated in the resonant tunneling regime, involving only a single energy level in the dot [Beenakker 1991]. The simulations in Figures 4.5(E)-(H) show rings of high dot conductance that are in good agreement with the experimental images (Figures 4.5(A)-(D)). Changes in ring diameter with changing tip voltage accurately match the experimental images.

Maps of the tip induced shift in energy level vs. tip position obtained from the lineshape of the Coulomb blockade rings in Figures 4.5(A)-(D) are shown in Figures 4.5(I)-(L). These maps were determined in the following way. For resonant tunneling, the lineshape is given by [Beenakker 1991]

$$G = G_{\max}\left[Cosh\left(\Delta/2k_BT\right)\right]^{-2}, \qquad (1)$$

where Δ is the energy difference between the lowest energy level in the dot and the Fermi energy in the leads. The energy difference is zero at resonance and deviates from zero as

the tip shifts the energy level upwards or downwards. The dot conductance at resonance is [Beenakker 1991]:

$$G_{\max}(\vec{r}) = \left(e^2/4k_BT\right)\Gamma(\vec{r}). \qquad (2)$$

The tunneling rate $\Gamma(\vec{r})$ alters as the tip is scanned above the dot, due to changes in the coupling between the tip and the point contacts, resulting in variations in G_{max} along the ring as seen in Figures 4.5(A)-(D). The values of $G_{\max}(\vec{r})$ in Eq. 2 used to compute the maps were obtained from a smooth two-dimensional polynomial function that was fit to the measured values of G_{max} along the crest of the ring. The strong dependence of the Coulomb blockade conductance on Δ allows us to measure the energy shift accurately.

If the SPM tip is sufficiently close to the 2DEG, at distances less that the width of the electron wavefunction $|\psi(\vec{r}_e)|^2$, it is theoretically possible to extract the shape of the wavefunction inside the dot from SPM images. The wavefunction $|\psi(\vec{r}_e)|^2$ can be extracted from a map of the dot energy level shift $\Delta(\vec{r})$, where $\Delta(\vec{r})$ equals $\Delta_{tip}(\vec{r})$ plus a constant determined by the side-gate voltage V_G. The tip voltage V_{tip} is adjusted to produce only a weak tip perturbation $\Phi_{tip}(\vec{r},\vec{r}_e)$, the change in electrostatic potential due to the tip in the plane of the 2DEG. From first-order perturbation theory, $\Delta_{tip}(\vec{r})$ is the convolution of the wave function of the electron in the dot and the tip potential:

$$\Delta_{tip}(\vec{r}) = \langle\psi|\Phi_{tip}(\vec{r},\vec{r}_e)|\psi\rangle = conv\left(|\psi(\vec{r}_e)|^2, \Phi_{tip}(\vec{r},\vec{r}_e)\right). \qquad (3)$$

Knowing the shape of $\Phi_{tip}(\vec{r},\vec{r}_e)$, one can deconvolve measurements of $\Delta_{tip}(\vec{r})$ using Eq. 3 to extract the shape of the unperturbed wavefunction amplitude $|\psi(\vec{r}_e)|^2$. For the images presented in this paper, the tip perturbation was wider than the wavefunction, and

this method is not applicable. In future experiments we hope to extract the shape of the wavefunction using a relatively narrow tip perturbation.

4.4 Simulations of the Wave Function

As mentioned in the previous section, we hope to use our SPM images to extract the shape of the wave function of the electron on the quantum dot. Though we have not achieved the resolution necessary for this task yet, we have worked together with Mike Stopa to attack this problem from another angle, with simulations. He has written a program to simulate the quantum dot's electrostatic confining potential and resulting electronic wave functions for a particular gate geometry, heterostructure, and temperature [Stopa 1996]. His program, SETE, uses a density functional approach that is fully self-consistent and quantum mechanical and includes exchange and correlation effects. The exact gate geometry can be inputted in the form of an SEM image as well as the parameters of the GaAs/AlGaAs heterostructure, including 2DEG density, 2DEG depth, setback layer, and quantum well depth. Additionally, Mike has recently added an SPM tip to the simulation. This is particularly useful to us as it is important to know how much the wave function is perturbed by the presence of a charged tip at a certain position. The results of the SETE program run on our quantum dot are shown in Figure 4.6 and 4.7.

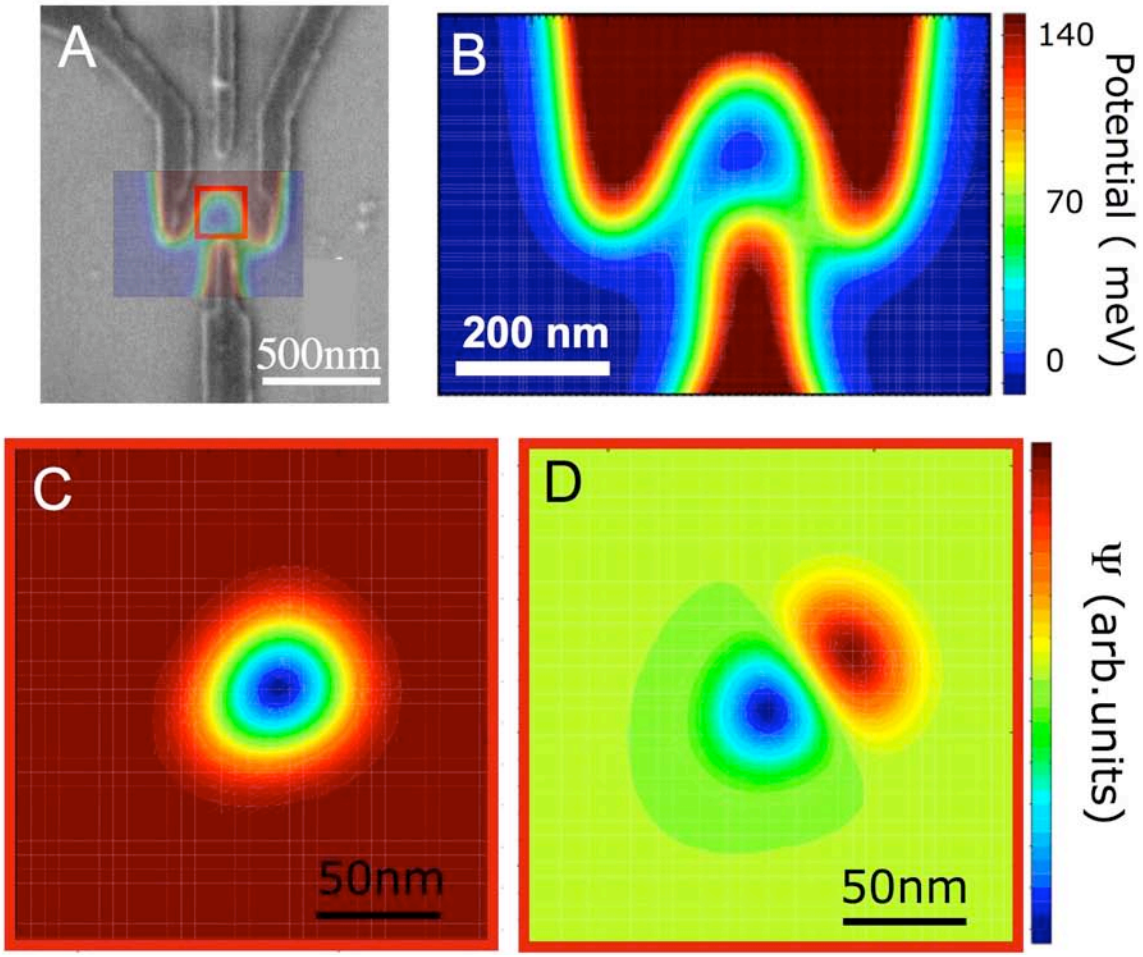

Figure 4.6 (B) Simulated electrostatic potential inside a quantum dot with gate geometry of the dot used in our experiment. The potential simulation is overlayed with an SEM of the device in (A) to indicate the area of the simulation. The voltages on the 4 gates starting from the rightmost gate and moving clockwise are -0.75 V, -0.75 V, -0.7 V, -1.09 V. There is no tip present in this simulation. (C) and (D) are simulations of the single particle wave functions plotted in an area indicated by the red square in (A). (C) plots the ground state and (D) plots the first excited state.

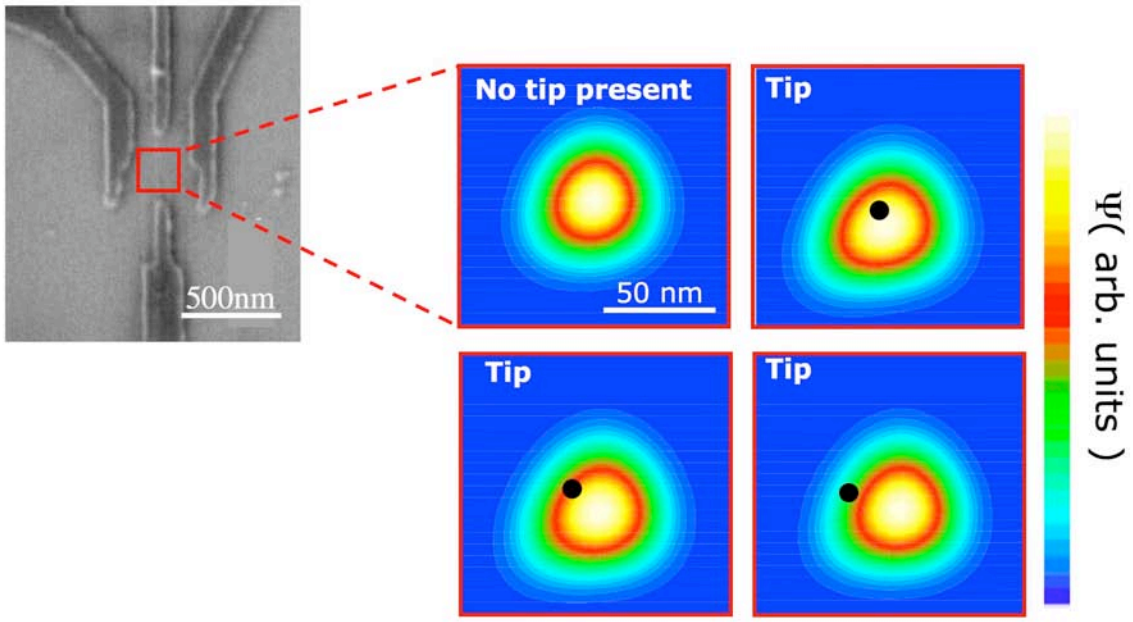

Figure 4.7 Simulations of the wave function in the quantum dot in the presence of a charged tip placed 100nm above the surface of the sample at a location indicated by the black dot. The wave function is plotted in an area indicated by the red square superimposed on the SEM image.

Two approaches we would like to use to image the wave function are as follows. The first approach is to study the shape of the rings. The shape of a ring corresponding to the addition of an electron to the ground state and a ring corresponding to the addition of an electron to the first excited state should be qualitatively different. We could either study the rings for the addition of the 1st electron at low V_{sd} and 3rd electron at low V_{sd}, or we can study the rings for the addition of the 1st electron at small V_{sd} and the 1st electron at high V_{sd} when transport occurs through an excited state. The second approach seems more promising because in both cases, there is only one electron on the dot and electron-electron interactions do not have to be reckoned with.

Another approach would entail sweeping a back gate voltage for different positions of the SPM tip. The idea here is that if we position the tip directly over a node in the wave function, the position of the Coulomb blockade peak in back gate voltage

would not shift much. However, if the tip is placed over an area where the wave function has a large amplitude, the wave function will be perturbed more and the Coulomb blockade peaks will shift more. A back gate would be better than a side gate as a back gate should change the shape of the confining potential less than a side gate. The wafer we used for this experiment did not have a back gate, but back gated samples are routine.

Of course, the largest stumbling block to imaging the wave function is the size of the perturbing potential relative to the size of the wave function. Effort needs to be put into minimizing the size of the perturbing potential. An easy fix include scanning closer to the surface of the heterostructure. However, that is not enough. 2DEG's closer to surface, or even 2DEG's at the surface would increase our resolution. InAs 2DEG's at the surface are known to exist though gating them is notoriously hard. If the 2DEG can be brought closer to the surface, a tip with a higher aspect ratio would increase the resolution. Attaching small diameter carbon nanotubes to the end of an AFM tip has been done before and could be a viable option. However, this is not an easy task. One more option is making the dot larger. The disadvantage of this approach is that one needs to go to lower temperatures to be able to resolve energy levels in a large dot.

Chapter 7 in this thesis discusses imaging quantum dots in InAs/InP nanowires. This system offers much promise as the electrons sit right at the surface of the InAs. Additionaly, these structures are very small, yielding large energy level spacings, and thus can be operated at relatively high temperatures.

Chapter 5

Imaging Electrical Conduction Through InAs Nanowires

5.1 Introduction to Nanowires and their Applications

We use a scanning probe microscope (SPM) to investigate nominally open InAs nanowire FETs with source and drain contacts and a back gate, showing how the SPM can be used to understand the physics of nanowire devices. SPM images of nanowire conductance *vs*. tip position spatially map the conductance of InAs nanowires at liquid He temperatures. Plots of conductance *vs*. back gate voltage without the tip present show complex patterns of Coulomb-blockade peaks. Images of nanowire conductance identify multiple quantum dots located along the nanowire - each dot is surrounded by a series of concentric rings corresponding to Coulomb blockade peaks. An image locates the dots and provides information about their size. The rings around individual dots interfere with each other like Coulomb blockade peaks of multiple quantum dots in series. In this way, the SPM tip can probe complex multidot systems by tuning the charge state of individual dots.

Semiconducting nanowires, gown in a bottom up approach, have seen an explosion of research activity in the past decade [Lieber 2003; Yang 2005; Samuelson et al. 2004]. The ability to control the dimensions and composition of nanowire devices shows great promise for future spintronics, nanoelectronics, nanophotonics, and quantum information processing. Quantum effects are naturally important due to the small size, opening new possibilities for quantum devices. Several important feats have recently

been accomplished in the field of semiconducting nanowires. These include single electron control [De Franceschi et al. 2003, Bjork et al. 2004; Yang et al. 2005; Zhong et al. 2005], high performance field effect transistors [Xiang et al. 2006], proximity-induced superconductivity [Doh et al. 2005; Jarillo-Herrero et al. 2006], electrically and optically pumped lasing [Huang et al. 2001; Duan et al. 2003], ultra-small LED's [Duan et al. 2001], and high resolution biological/chemical sensing [Cui et al. 2001].

The attention that both semiconducting nanowires and carbon nanotubes have recently enjoyed is in large part due to the fact that they offer an alternate way to make very small transistors and switches [Lieber 2003]. In order to keep up with the pace set by the International Technology Roadmap for Semiconductors (ITRS), feature sizes must be 45nm by 2010 and 5-10 nm by 2025 [ITRS 2005]. This is expected to be very difficult with current CMOS technology and many researchers are looking towards nanowires and nanotubes assembled in a bottom-up approach. Although both systems offer many exciting properties, semiconducting nanowires have some distinct advantages over nanotubes, the primary one being controlled versatility. The electronic properties of carbon nanotubes are highly sensitive to their diameter and crystal structure, which are not well controlled during growth. In nanowire growth, there is good control over nanowire diameter and length as well as a vast library of semiconducting materials to choose from, including Si, Ge, InAs, and InP, and. Additionally, it is possible to vary the material within the nanowire, producing radial or axial heterostructures [Lauhon et al. 2002; Lauhon et al. 2004; Bjork et al 2001]. Using a heterostructure growth technique, for example, quantum dots and p-n junctions have been grown into a nanowire [Bjork et

al. 2004; Yang et al. 2005]. Quantum dots in nanowires will be discussed in more detail in Chapter 7.

In order to make a high performance transistor it is important to have good ohmic contacts at the source and drain, uniform flow of electrons through the nanowire, and good fast control of the electron flow with a nonleaking gate. An understanding of where the electrons are along the nanowire and how they flow through it will aid in the development of nano electronic devices such as nanowire transistors. Standard transport measurements have yielded much information about the electrical properties of the wires, but averaged over the whole length of the wire [Doh et al. 2005; De Franceschi et al. 2003; Bjork et al. 2004]. SPM imaging allows one to locally probe the motion of electrons along the wire and modify the potential profile to locally allow or block electron transport with high spatial resolution. Nanowire imaging techniques are just being developed [Ahn et al. 2005; Gu et al. 2005] and this imaging work represents one of the first electrical imaging measurements on semiconducting nanowires.

InAs nanowires are a particularly attractive system to study for several reasons. InAs has a large g-factor, making it useful for spintronics and quantum information processing (QIP) applications [Awschalom et al. 2002]. Furthermore, it has been shown recently [Bjork et al. 2005] that the g-factor of an InAs nanowire quantum dot can be varied from 2 to its bulk value of 14, through varying the size of an InAs nanowire quantum dot, an exciting prospect for QIP. Another property of InAs that makes it interesting to study is its large bulk exciton Bohr radius, a_B = 34nm. Quantum confinement occurs when one of the dimensions of the semiconducting structure approaches a_B. The InAs nanowires we study here have radii of ~25nm which is

comparable to a_B, producing quantum confinement and thus making the wave-like properties of the electrons important. In fact the large variation of g-factors observed in InAs nanowire quantum dots is largely a consequence of quantum confinement. A simple explanation for this effect is that in III-V semiconducting compounds, the g-factor has a strong dependence on the energy gap E_g and quantum confinement causes E_g to decrease from its bulk value [Kiselev et al. 1998; Hermann and Weisbuch 1977]. Lastly, whereas some semiconductors are known to have a surface depletion layer, the surface of InAs is known to have a charge accumulation layer [Olsson et al. 1996]. This potentially allows for very small radius nanowires that are not depleted of electrons as well as Schottky-barrier-free contact to metallic leads.

5.2 Nanowire Growth, Sample Preparation, and Sample Storage

The InAs nanowires I have imaged were grown by Erik Bakkers and Arnoud Roest at Philips Research Laboratories in Eindhoven, the Netherlands. The InAs nanowires were grown in a catalytic process from small gold seed particles using laser ablation of an undoped InAs target (Wagner and Ellis 1964; Doh et al. 2005; Bakkers et al. 2004]. The nanowires have diameters of ~80 nm and lengths of ~3 μm. They are unintentionally doped but exhibit n-type characteristics, either because of carbon impurities in the growth chamber or due to Fermi-level pinning above the conduction band at the surface of InAs. After growth the InAs nanowires are transferred onto a conducting p+ silicon substrate capped with a 250nm thick SiO_2 insulating layer. The silicon substrate acts as a back gate that can tune the number of charge carriers in the wire through an applied voltage. Electron beam lithography is used to define electrodes

~2 μm apart and 110 nm of Ti/Al is subsequently deposited to form the contacts. Figure 5.1(A) shows an SEM picture of a contacted InAs wire.

I have noticed a severe degradation of the InAs nanowires' electrical characteristics after exposure to ambient atmosphere for more than a few days. I have also noticed that keeping the sample in a vacuum inside the dewar for a long time (upwards of a week) directly before cooling can improve the sample's electrical characteristics. Electron transport in InAs is known to be very sensitive to the exact nature of the surface. Oxide and adsorbed junk can dramatically change the nanowire's properties and thus great care should be taken to keep the nanowires in a clean and inert environment. I have purchased both a nitrogen dry box (from Terra Universal) and a dry pump (a Scroll pump from Varian) for sample storage. The nanowire group at Lund University advocates storage in a vacuum chamber evacuated by a dry vacuum pump.

5.3 SPM Images of InAs Nanowires

Scanned probe microscopy (SPM) images of InAs nanowire FET's are presented in this section. These images show how a cooled SPM can be a powerful diagnostic tool for nanowire devices. They allow us to understand how electrons move through the nanowires and show us what needs to be done to produce a high quality nanowire FET. Simple plots of conductance G vs. backgate voltage V_G without the tip present show complex patterns of Coulomb blockade peaks with uneven spacings and heights. The spatial pattern of electron flow can be imaged and understood by using the SPM tip as a movable gate. The tip voltage V_{tip} partially depletes or enhances the electron density below. By displaying the conductance *vs.* tip position as the tip is scanned above the

nanowire, an image of electron flow is obtained. Using images of these InAs nanowires, we find a number of quantum dots formed at locations along the wire. Each dot is located at the center of a series of concentric rings that correspond to Coulomb blockade conductance peaks that occur as electrons are added to that dot. The rings from nearby dots overlap. By using the tip as a movable gate, we can tune the charge state of each dot individually. The spacing and intensity of the rings provide information about dot size and tunneling rate, and the interference between overlapping rings gives information about the interdot coupling.

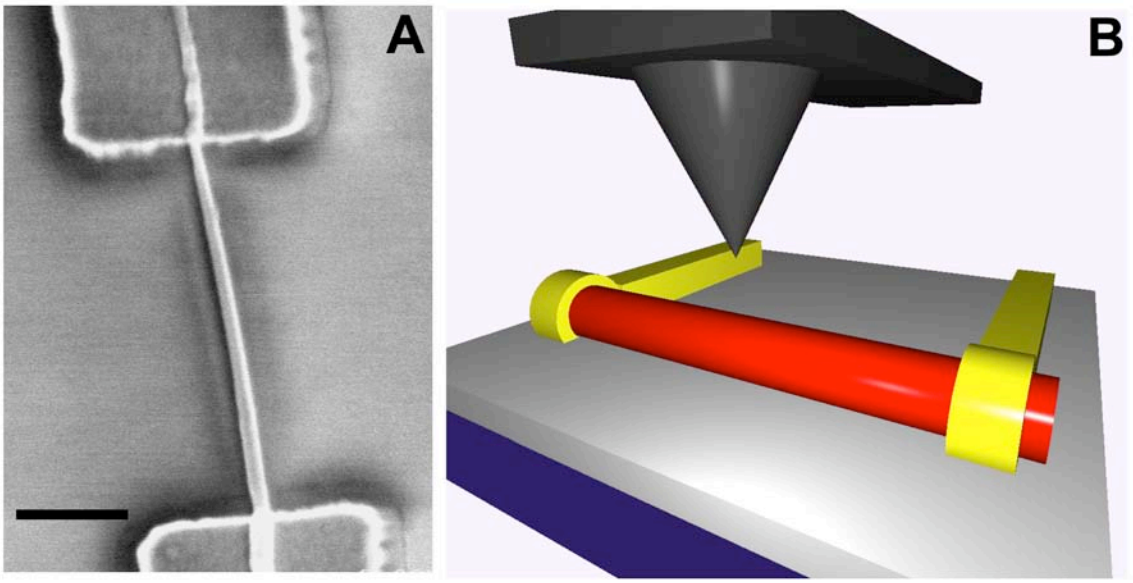

Figure 5.1 (A) SEM photo of an InAs nanowire (Device D1) contacted with Ti/Au electrodes. (The slight kink in the wire at the top contact, due to AFM tip crash, occurred after the data presented in this paper was obtained). The scale bar is 500 nm. (B) Imaging schematic. A charged AFM tip is scanned ~100nm above the contacted InAs nanowire. Nanowire conductance as a function of lateral tip position is recorded to form the image. The wire lies atop a conducting substrate with a 250nm thick SiO2 capping layer

We use a home-built liquid helium temperature scanning probe microscope (SPM) [Topinka 2002] to image electrical conduction through the nanowires. As schematically shown in Figure 5.1(B), we laterally scan a charged SPM tip over the nanowire at a fixed height above the substrate. With fixed tip and back gate voltages, an image of electron motion through the nanowire can be obtained by displaying the nanowire conductance as a function of tip position. Figure 5.2 (C) and (D) are examples of images obtained with this imaging technique. The images display rings of peaked conductance centered on quantum dots in the nanowire. These rings are similar in appearance to those observed in images of a one-electron quantum dot formed in a two-dimensional electron gas [Fallahi et al 2005] and of multi-electron quantum dots formed in carbon nanotubes [Woodside and McEuen 2002].

Figures 5.2 (A)-(B) show plots of nanowire conductance as a function of back gate voltage for two different InAs nanowire devices, D1, and D2. The corresponding SPM images in Figures 5.2 (C)-(D) show that multiple quantum dots were formed along the length of each nanowire. For the plots in Figures 5.2 (A)-(B), the wires exhibit irregular Coulomb blockade oscillations indicative of multiple dots in series [Ruzin et al. 1992; Waugh et al. 1995; Kouwenhoven et al. 1997]. For a single dot, one would expect to see regularly spaced Coulomb blockade peaks. For multiple dots in series with varying capacitances to the gate, "stochastic" Coulomb blockade peaks are expected [Ruzin et al. 1992]. "Stochastic" peaks are due to the interference between two or more dots in series with different spacings in gate voltage between peaks – the conductance only peaks for the series combination when all the dots peak individually. Additionally

with a small amount of inter-dot tunneling or inter-dot capacitance, splitting of the conductance peaks is expected [Ruzin et al. 1992].

It is impossible to say what along the wire is giving rise to these irregular Coulomb oscillations and therefore we have used imaging to spatially probe the wire on a local scale to elucidate the local electrostatic fluctuations that give rise to quantum dot behavior in the wire. The resulting SPM conductance images of devices D1 and D2 are shown in Figures 5.2 (C) and 5.2 (D) respectively. The contrast in these images is offered by rings of peaked conductance centered on quantum dots along the wire. As described by Fallahi et al (2005) and Woodside et al. (2002). each ring corresponds to a Coulomb oscillation of the quantum dot at the ring's center. The charge induced by the tip on a dot is given by

$$q(r_{t\text{-}d}, V_{t\text{-}d}) = C_{t\text{-}d}(r_{t\text{-}d}) * V_{t\text{-}d}. \qquad \text{Eq. (1)}$$

where $r_{t\text{-}d}$ is the distance between the tip and the dot, $C_{t\text{-}d}$ is the capacitance between the tip and the dot, and $V_{t\text{-}d}$ is the voltage difference between tip and dot. Therefore, the charge on a dot can be controlled with the tip voltage or the tip position. If one were to plot the dot conductance as a function of the tip's distance from the dot, there would be oscillations in conductance every time the charge state of the dot changes by one electron. In the images we show nanowire conductance vs. two-dimensional tip position and the conductance oscillations take the form of closed rings centered on the dot. If the tip is moved along a ring surrounding a dot, the capacitance of the tip to that dot remains constant, maintaining the charge state of that dot. The rings are thus contours of constant tip to dot coupling.

In Figure 5.2 (C), there are three sets of concentric rings, indicating the presence of three quantum dots at locations schematically indicated by the black dots superimposed on the image. The rings surrounding the middle dot in D1 are more closely spaced than those surrounding the other two dots in D1, indicating that the center dot is larger than the other two dots. In Figure 5.2 (D) there are two sets of concentric rings indicating the presence of two quantum dots, whose locations are again marked by black dots. In both images, the rings are elongated along an axis perpendicular to the wire due to slight screening of the tip by the contacts.

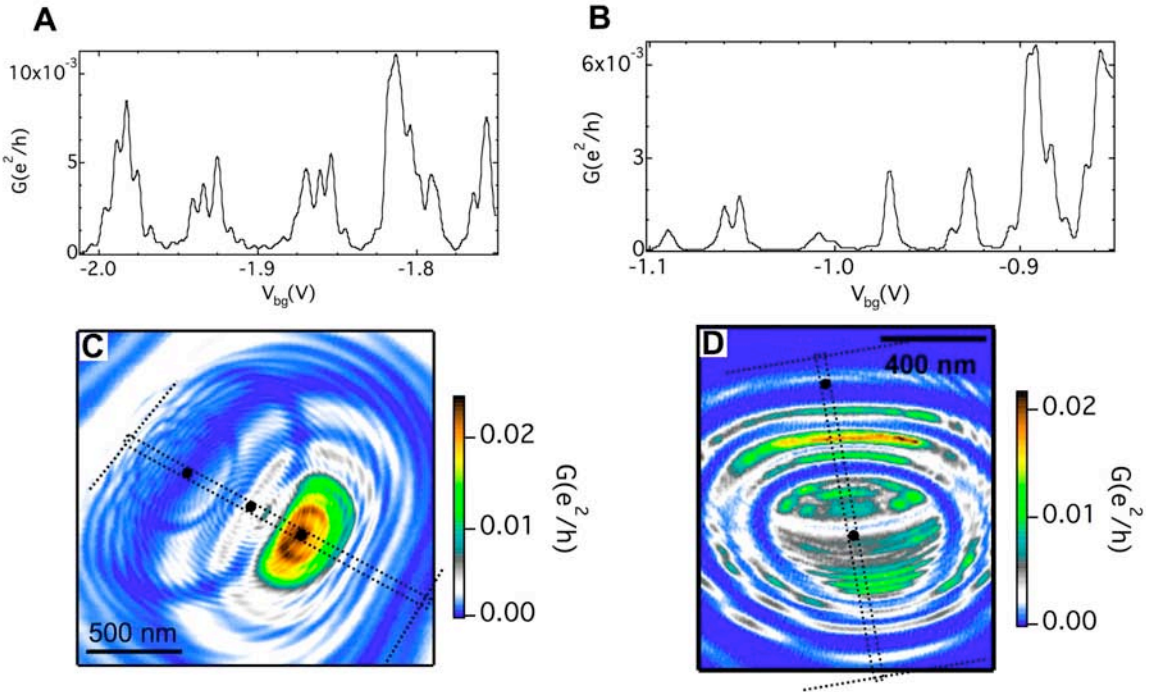

Figure 5.2 InAs nanowire electrical transport measurements and corresponding images that spatially illuminate the behavior seen in the transport measurements. (A-B) Nanowire conductance as a function of back gate voltage for devices D1 and D2. The plots show randomly spaced Coulomb blockade peaks characteristic of transport through multiple dots in series. (C-D) SPM images for D1 and D2 plotting nanowire conductance as a function of position of a charged SPM tip scanned 100nm above the nanowire. Rings of peaked conductance, corresponding to Coulomb blockade peaks, are centered on quantum dots in the nanowire, confirming the presence of multiple series dots. In (C), three sets of concentric rings identify three quantum dots whose positions are marked by black dots as guides to the eye. (D) reveals two quantum dots along the nanowire. Dotted lines denote the outline of the wire and the contacts for device D1 (C) and D2 (D).

Imaging allows us to detect the existence of one or more dots located along the length of the nanowire and provides information about their size. Once we have located the quantum dots, we can use the tip as a movable gate to individually control the charge on one dot in a nanowire that contains many dots, like the ones shown in Figure 5.2 (C)-(D). This movable tip gating technique has a great advantage over static gating techniques for two reasons. Firstly, in coupled dot systems with multiple static gates, the gates for each dot couple to neighboring dots, making it difficult to address only one dot without affecting a neighboring dot. Secondly, to address multiple dots with static gates, multiple gates need to be lithographically defined and aligned to the quantum dots. This is a difficult task when the dot locations are a priori unknown and/or so closely spaced that precise alignment of the gates pushes the limits of current lithographic abilities.

SPM images of device D1 taken with varying back gate voltages are shown in figures 5.3 (A)-(C). As the back gate voltage is made more negative, the overall signal in the images is reduced and conductance becomes nonzero only at the intersections of rings, i.e. when a conductance peak is present on each quantum dot. This is the expected pattern for multiple series quantum dots with little or no coupling between them. The small black dots again denote quantum dot locations and the dashed ellipses in figure 5.3 (B)-(C) are the expected rings for the two outer dots. (The expected rings around the middle dot have not been overlayed with the images as they are so closely spaced that their inclusion would obfuscate the image.) In addition to tuning the electron number on each dot, the back gate tunes the tunnel barriers forming the dots, making them more

opaque with more negative voltage and thus reducing inter-dot coupling. In the limit of completely decoupled series dots, the condition for conductance through the whole series of dots is that conductance peaks are present on each of the quantum dots. In a spatial map of conductance vs. tip position, this condition manifests itself as spatially localized regions of peaked conductance at the intersections of rings from all the dots. This is clearly seen in figure 5.3 (C) taken with a back gate voltage of -2.13 V, very near pinch-off for the wire.

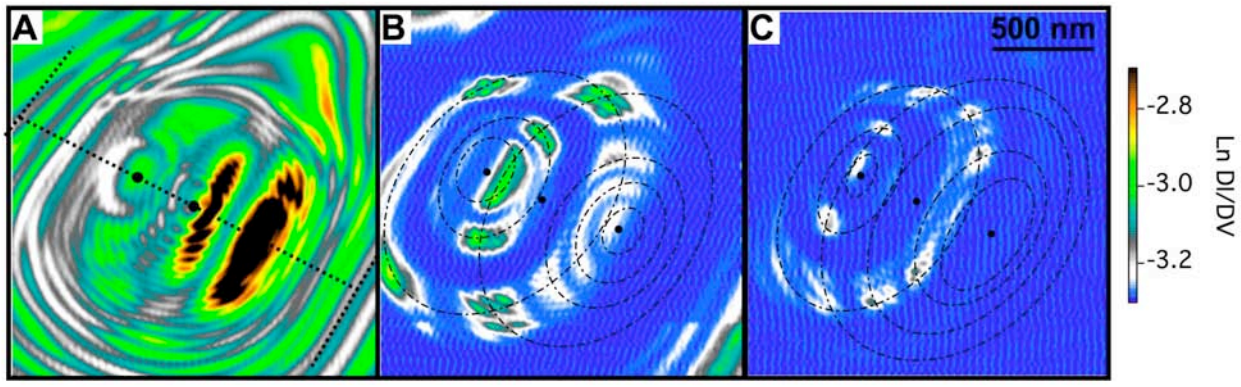

Figure 5.3 SPM images of nanowire conductance for device D1 showing interference of Coulomb blockade rings centered on multiple quantum dots in series along the nanowire. Black dots mark the quantum dot locations and the dashed lines in (A) show the outlines of the nanowire and leads. The images are taken with V_{tip} = 0 V, and V_{bg} = (A) -1.94 V, (B) -2.05 V, (C) -2.12 V. As V_{bg} is made more negative, the images show nonzero conductance only at the intersections of rings, i.e. only when the location of the tip is such that each dot is on a Coulomb blockade conductance peak. The elliptical rings are drawn in as guides to the eye and denote the expected concentric rings of Coulomb blockade peaks.

The SPM images of device D2 in Figures 5.4 (A)-(C) show the evolution of Coulomb blockade rings with tip voltage. Note the movement of the rings radially

outward with more positive tip voltage as well as the increasingly close spacing of the rings. The images are taken with V_{tip} = (A) 0.48, (B) 0.90, and (C) 1.44 V. In these images, there is one dominant set of rings centered on a nanowire quantum dot in the upper half of the image. The black triangle superimposed on each image tracks the same Coulomb ring, corresponding to the addition of the nth electron to the dot at the ring's center. In order to maintain the charge state of that quantum dot (exactly n electrons) as the tip voltage is increased, the tip must move further from the dot according to equation (1). Thus the location of the nth Coulomb ring moves outwards from the quantum dot. In addition to the ring radius increasing with increasing tip voltage, the rings become more closely spaced, also in accordance with equation (1). The change in tip to dot capacitance between two consecutive concentric rings located at distances r_1 and r_2 from the dot is $\Delta C = C_{t\text{-}d}(r_1) - C_{t\text{-}d}(r_2) = e/V_t$. As V_t increases, ΔC between peaks decreases and the tip does not have to move as far to get from one Coulomb peak to the next, thus decreasing the spacing between rings.

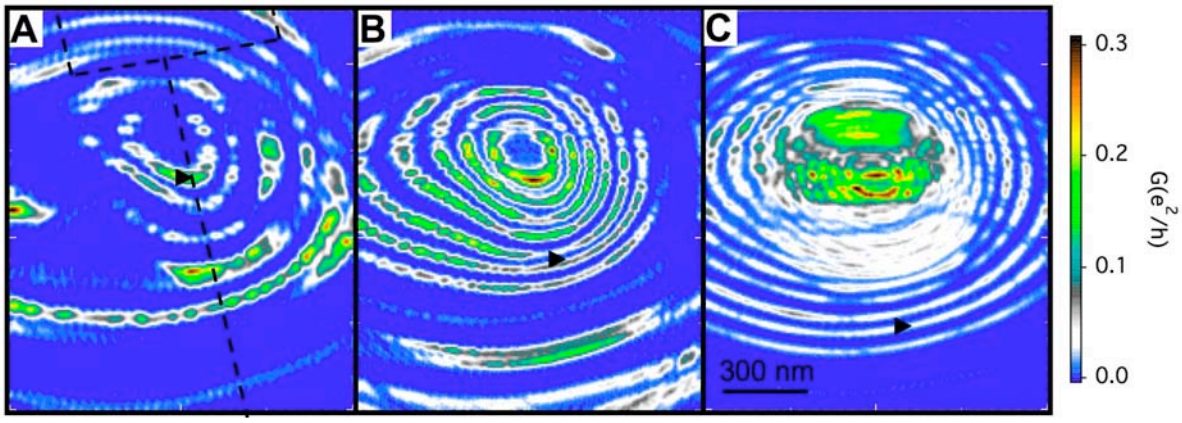

Figure 5.4 Evolution of SPM images with tip voltage: V_{tip} = (A) 0.48 V, (B) 0.90 V, (C) 1.44 V. The wire and top contact are denoted with dashed lines in A. Coulomb blockade rings surround a quantum dot in the upper half of the image. As the tip voltage increases, the rings expand outwards in size and become more closely spaced. The black triangle tracks one Coulomb peak, demonstrating the growing size of the rings with tip voltage.

5.4 Summary and Future Directions

The SPM has proven to be a powerful diagnostic tool. We have been able to locate quantum dots, tune their charge state, and vary the coupling between neighboring dots. In short, the SPM has provided us with a detailed picture of the potential landscape along the nanowire and the ability to modify it on a local scale. Understanding how electrons flow through these tiny channels will be useful for the development of future nano-electronic devices made of nanowires.

There are a lot of promising future directions for nanowires, both in basic physics and in more applied technologies. Scanning probe microscopy will be a valuable tool in both arenas. If quantum dots are placed controllably in a nanowire the SPM tip will be a useful way of tuning individual quantum dots in a multi-dot circuit. In the following chapter, we demonstrate the ability of our SPM tip to gate a single InAs dot defined in an InAs/InP nanowire heterostructure. Heterostructure defined quantum dots offer up many exciting possibilities that will be discussed in the next chapter.

We would like to use our SPM tip to form a quantum point contact in an InAs nanowire. The observation of quantized conductance through a narrow constriction in a nanowire has been elusive. The SPM tip has an advantage over static gating as there may be sections of the nanowire in which it is easier to form a QPC then others, for example if there are charges non-uniformly distributed in the wire from impurities or from the surface. To observe quantized conductance through a QPC, the mean free path for

electrons in the nanowire must be longer than the length of the one-dimensional channel forming the QPC. Measurements of the mean free path in nanowires are lacking and this is another area in which the SPM tip can be useful. It should be possible to form a variable length Fabry-Perot cavity with one end being defined by a static side gate and the other end defined by the SPM tip, free to move along the nanowire. Fabry-Perot interference fringes will be visible when the length of the cavity is smaller than the mean free path. It will most likely be necessary to have cleaner nanowires to perform the growth is continuously being improved as are the methods of fabrication.

Chapter 6

Imaging Quantum Dots in InAs/InP Nanowires

6.1 Introduction to Quantum Dots in Nanowires

We use a scanning probe microscope (SPM) as a movable gate to image single-electron transport through a few-electron quantum dot formed in an InAs/InP nanowire. The hockey puck shaped InAs quantum dot is formed between two InP barriers inside an InAs nanowire. The quantum dot is in the Coulomb blockade regime and measurements of conductance through the quantum dot reveal a discrete spectrum of atomic-like energy levels. The quantum dot can be operated in the few-electron regime or depleted of electrons completely. Its charge state can be tuned by sweeping the voltage on the back gate, a global gate, or by sweeping the voltage on the tip, a local gate. Additionally, by scanning the position of charged SPM tip, we can tune the number of electrons on the dot in a spatially dependent way. Rings of peaked conductance centered on the quantum dot correspond to Coulomb oscillations of the quantum dot. The nanowires, grown from metal catalyst particles using chemical beam epitaxy (CBE), have a diameter of 50 nm. The quantum dot is 18nm in length.

Heterostructure semiconducting nanowires provide an excellent system to make highly tunable and high quality ultra-small quantum dots [Bjork et al. 2004], thus opening up many exciting prospects for the fields of quantum information processing and single electronics. Such nanowire heterostructures have recently been demonstrated in a variety of semiconducting materials [Lieber 2003; Yang 2005; Samuelson et al. 2004]. Few-electron InAs quantum dots defined inside InAs/InP nanowires were measured in

the Lund group by Bjork et al (2004). Electrical transport measurements exhibit the shell structure of their quantum states as electrons are added to the dot, beginning with the very first electron on the dot [Bjork et al 2004]. Due to the bottom-up nature of their construction, the size and shape of these quantum dots are highly repeatable and controllable and interfaces are atomically sharp. A batch of many wires has a spread in diameters of about +/- 3nm but within a single nanowire, the diameter is uniform to less than a nanometer over its many microns of length. Such uniformity is possible because the bottom-up growth approach is not subject to the fluctuations inherent to top down lithography. Few electron nanowire quantum dots are thus attractive candidates for ultrasmall electronics and quantum information processing.

An SPM tip as a movable gate provides an ideal way to gate individual heterostructure nanowire quantum dots. Gating of quantum dots in nanowires and nanotubes is usually done with a back gate or lithographically defined side gates, both static gates. The dots are too small to individually gate with lithographically defined gates while a back gate indiscriminately gates the whole sample including the leads. A scanned gate overcomes both of these obstacles and can be use to locally probe and manipulate electrons on individual quantum dots. Additionally, an SPM will be a useful tool for gating electrons in a complex multi-dot circuit.

Semiconducting nanowires have already demonstrated their versatility as nano-LED's, lasers, biological/chemical sensors, field effect transistors and logic gates for computing [Huang et al. 2001; Duan et al. 2003; Duan et al. 2001; Xiang et al. 2006; De Franceschi et al. 2003, Bjork et al. 2004; Yang et al. 2005; Zhong et al. 2005]. They promise to have potential in quantum electronic devices and quantum computing devices.

6.1 InAs/InP Heterostructure Nanowire Growth

The nanowire quantum dots we have imaged were grown by Linus Froberg in Lars Samuelson's group at Lund University in Sweden. A transmission electron microscopy (TEM) photo of a 50nm diameter InAs/InP nanowire is shown in Figure 6.1(A). The composition of the nanowire varies along the growth direction; the dark sections are InAs and the light sections are InP. The short InAs section between the two InP barriers forms the quantum dot. The wires are grown via chemical beam epitaxy (CBE) in the following way [Bjork et al. 2001]. Small gold particles are deposited onto an InAs <111>B substrate and then the substrate is mounted onto a sample holder inside an ultra-high vacuum chamber and heated to 430° C, the growth temperature. The metal-organic precursors to In, P, and As (trimethyl indium, tertiarybutyl phosphine, and tertiarybutyl arsine) are stored in a water bath that is separated from the chamber by injection valves. To commence InAs nanowire growth, the injection valves to the In and As precursors are opened. The ultra low pressure of the growth chamber results in very long mean free paths for the atoms and the atoms arrive at the substrate in a beam (hence the name chemical beam epitaxy). Growth of the nanowires is nucleated at the sites of the gold particles and continues for as long as the valves to the metal-organic precursors are left open. The diameter of the nanowire is determined by the initial diameter of the gold particle. Note the presence of individual atomic layers in Figure 6.1 (A) indicating the high quality of the epitaxial growth. There is a ~ +/- 3nm spread in nanowire diameter between nanowires grown in the same batch, resulting predominantly from the

spread in diameter of the gold particles. However, the diameter of a single nanowire along its length is very uniform to within less than 1nm. This is made possible by suppressing radial growth through careful adjustment of the growth parameters, including pressure and temperature.

To form a heterostructure nanowire, the As and P precursors are alternated during growth to result nanowires such as the one shown in Figure 6.1(A). The short InAs section forms a quantum dot between the two InP barriers due to the conduction band offset between InAs and InP, as shown in Figure 6.1(C). Note the extremely abrupt interfaces forming a well-defined quantum dot volume. For a dot 18nm in length and 50nm in diameter, as the one we have studied in this experiment, the lowest energy state in a disc shaped quantum box is 65meV above the bottom of the conduction band and energy spacing between the ground state and first excited state is 24meV (see appendix A). In the InAs nanowire lead, the lowest energy state is 15meV above the conduction band bottom and the energy spacings between levels are less than 0.1 meV.

After growth, the nanowires are deposited onto a degenerately doped Si substrate capped with 100nm SiO_2 layer. This conducting substrate acts as a back gate that, through an applied voltage, can tune the Fermi level in the nanowire. Ti/Au electrodes, spaced by ~ 1-2 μm, are defined with electron beam lithography and subsequently deposited to contact individual nanowires as schematically shown in Figure 6.2(B). The width of the tunnel barriers and the quantum dot are tuned such that the few-electron Coulomb blockade regime can be reached at small back gate voltages.

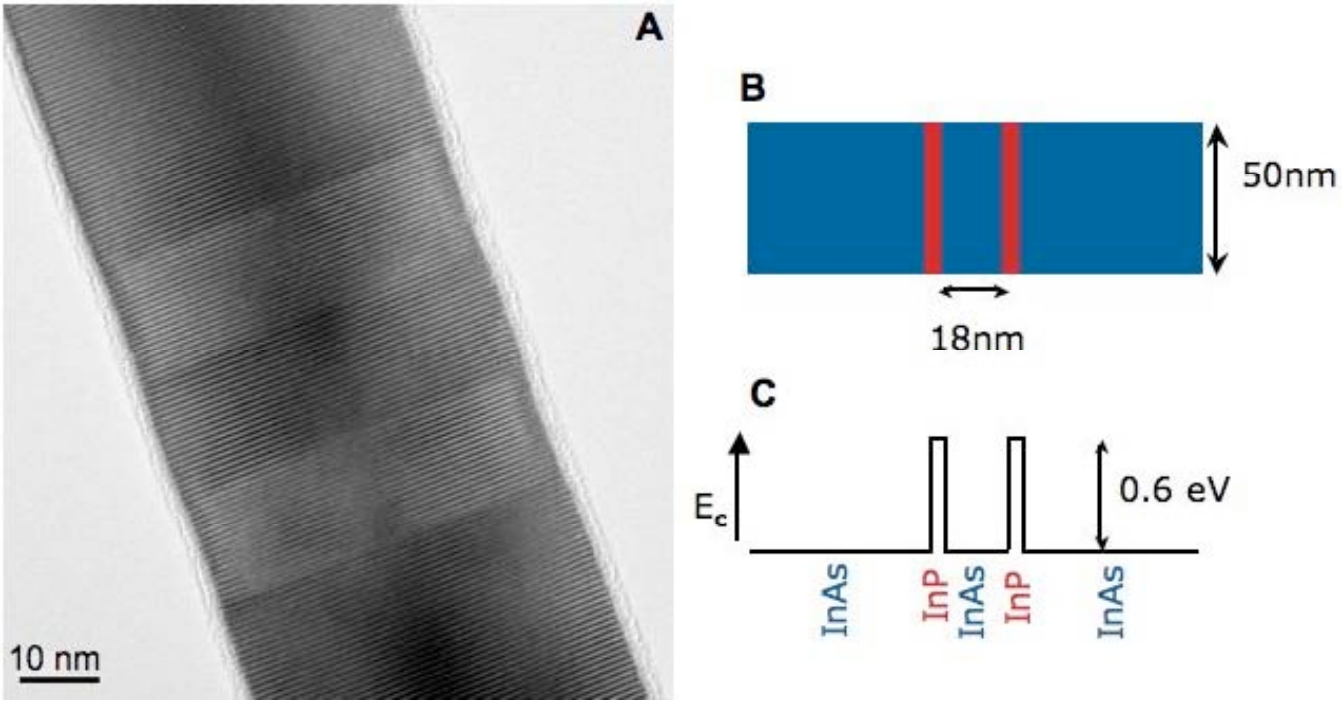

Figure 6.1 (A) TEM photo of an InAs/InP heterostructure nanowire similar to the ones used in this experiment. Individual atomic layers are clearly visible indicating the high quality of the epitaxial growth. The brighter sections of the wire are InP while the dark sections are InAs. The quantum dot is formed in the short InAs section between the two InP barriers and the sharp interfaces give it a well-defined disc-shaped geometry. (B) A schematic of the wire showing the material composition (InP is blue, InAs is red) and the dimensions of the wire. The dot we studied is 50nm in diameter and 18nm in length and the tunnel barriers are 8nm thick. (C) A plot of conduction band energy E_C as a function of axial position along the wire shows the 600meV conduction band discontinuity between InAs and InP that provides electron confinement inside the InAs quantum dot.

InAs nanowires are a particularly attractive system to study for several reasons. InAs has a large g-factor, making it useful for spintronics and quantum information processing (QIP) applications [Awschalom et al. 2002]. Furthermore, it has been shown recently that the g-factor of an InAs nanowire quantum dot can be varied from 2 to its bulk value of 14, through varying the size of an InAs nanowire quantum dot, an exciting prospect for QIP [Bjork et al. 2005]. Another property of InAs that makes it interesting to study is its large bulk exciton Bohr radius, a_B = 34nm. This produces quantum

confinement in the nanowires we study here. Quantum confinement occurs when one of the dimensions of the semiconducting structure approaches a_B and in this regime, the wave-like property of the electron becomes important. In fact the large variation of g-factors observed in InAs nanowire quantum dots is a consequence of quantum confinement [Kiselev et al. 1998; Hermann and Weisbuch 1977]. Lastly, whereas some semiconductors are known to have a surface depletion layer, the surface of InAs is known to have a charge accumulation layer (CAR) [Olsson et al. 1996]. This potentially allows for very small radius nanowires that are not depleted of electrons as well as Schottky-barrier-free contact to metallic leads. In the work done in Delft by Doh et al (2005), they used the Schottky barrier free nature of the contacts to make highly transparent contacts so that they could observe proximity induced superconductivity.

Imaging Nanowire Quantum Dots

In this research we use our scanning probe microscope (SPM) [Topinka 2002] to image electron flow through an InAs quantum dot formed between two InP barriers inside an InAs nanowire at T = 4.2 K. We use the SPM as local gate to locate the quantum dot and tune its charge state down to zero electrons. Figure 6.2(A) shows the SPM imaging setup. Using a Coulomb-blockade imaging technique [Fallahi et al. 2005; Woodside et al. 2002; Pioda et al] at T = 4.2K, the charged SPM tip is scanned at a fixed height above the nanowire and the resulting change in nanowire conductance is recorded to form a two-dimensional image. We adjust the back gate voltage so that the quantum dot is in the few-electron regime. At low temperatures and small source-drain bias V_{sd}

electron transport through quantum dots is blockaded except at the degeneracy point between n and n+1 electron occupation number [Kouwenhoven et al. 1997]. The electron occupation number refers to the number of electrons residing on the quantum dot. The control charge on the dot induced by the tip is given by $q_C(V_t, r_t) = C_{t-d}(r_t) * V_{t-d}$, where $C_{t-d}(r_t)$ is the capacitance between the tip and the dot when the tip is a distance r_t from the dot and V_{t-d} is the voltage difference between the tip and the dot. The discreteness of the electron charge forces the quantum dot to hold a discrete number of electrons, i.e. $q_{dot} = n * e$. Scanning the tip varies the induced charge and causes oscillations in quantum dot conductance each time another electron is allowed to enter or leave the dot. In the images, this behavior manifests itself as rings of peaked conductance surrounding the quantum dot with each ring corresponding to a Coulomb blockade peak. If the tip is scanned along one of these rings, the charge state of the dot at the ring's center remains constant and thus the rings can be thought of as contours of constant tip-dot coupling.

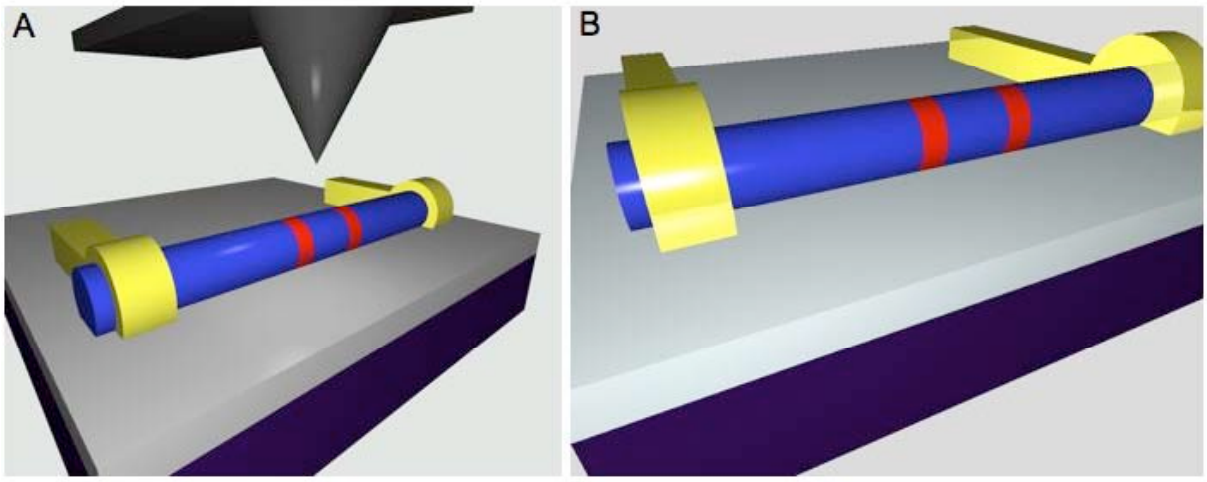

Figure 6.2 (A) Nanowire imaging schematic. A metallized SPM tip is scanned at a fixed height above the nanowire. Conductance between source and drain electrodes is recorded as a function of tip position to record the image. The height of the tip above the nanowire is typically 20nm to 100nm and typical tip voltages are -3V to 3V. (B) Metallic electrodes (110nm thick) were defined and evaporated 1-2 μm apart. The conducting

substrate forms the back gate (purple color) and is coupled capacitively to the nanowire across a 100nm thick insulating SiO_2 layer (grey color).

Experimental Results

The number of electrons on the dot and the energy of the first few electron states can be determined from the Coulomb blockade diamonds in plots of dot conductance vs. gate voltage and source to drain voltage, shown in Fig. 6.3. We can use either the back gate voltage or the tip voltage to reduce the quantum dot's electron occupation number to one or zero. The one-electron regime is important for applications in quantum information technology. In the absence of the tip, as shown in Figure 6.3(A), the dot is emptied of electrons for back gate voltages less than ~ 0.4 V due to quantum confinement in the growth direction [Bjork et al 2004]. This voltage is relatively small, because the energy of the electron ground state in the quantum dot is increased by the small dot size. The small back gate voltage at the zero to one electron transition is promising for QIP applications as it reduces the magnitude of the electric fields present in the one-electron regime. Differential conductance plotted as a function of source-drain voltage V_{sd} and back gate voltage V_{bg} displays regions of zero conductance, Coulomb diamonds, when the energy required to add another electron is smaller than V_{sd}. The addition energy $E_{add} = E_C + \Delta E(n)$ is seen to vary with electron number, revealing the electronic shell structure of the quantum dot. Using the constant-interaction model [Kouwenhoven et al. 2001], we can determine the charging energy of the quantum dot and the energy level spectrum. The constant-interaction model assumes a constant Coulomb interaction between electrons, regardless of the number of electrons on the quantum dot. We

determine the charging energy $E_C = \frac{e^2}{C}$, to be 8meV. We determine the energy level spacing between the lowest two quantum states to be 15meV, 3meV between the 2nd and 3rd lowest quantum states, 13meV between 3rd and 4th, and 12meV between 4th and 5th. Each of these levels can accommodate two electrons of opposite spin. At low V_{sd}, the spacing in gate voltage between Coulomb blockade peaks is given by $\Delta V_g = \frac{C}{C_g} * \frac{E_{add}}{e}$ where C_g is the capacitance of the dot to the back gate. C_g is inferred from the data to be 0.7aF for the first electron and then ~ 1aF for the rest of the electrons. The total capacitance *C* is found to be 9aF for the 1st electron and then increase gradually to 27aF for the 9th electron. These growing capacitances are an indication that either the CI model is not valid in the few-electron regime and/or the physical size of the wave function is increasing with increasingly positive back gate voltage. This will be discussed more in a later section in this chapter on simulations. Additionally, we can do simple geometric calculations to estimate the classical capacitances between a conducting disc and a plane (the dot and the back gate) and between two discs separated by a thin oxide layer (the dot and the leads). These yield $C_g = 1.9aF$, $C_S = 30aF$, and $C_D = 30aF$ yielding $C = C_g + C_S + C_D = 62aF$ where C_S and C_D are the capacitances of the dot to the nanowire source lead and the dot to the nanowire drain lead. These values are 2-3 times larger than our extracted values indicating that the orthodox theory of capacitances is not valid in the few electron regime.

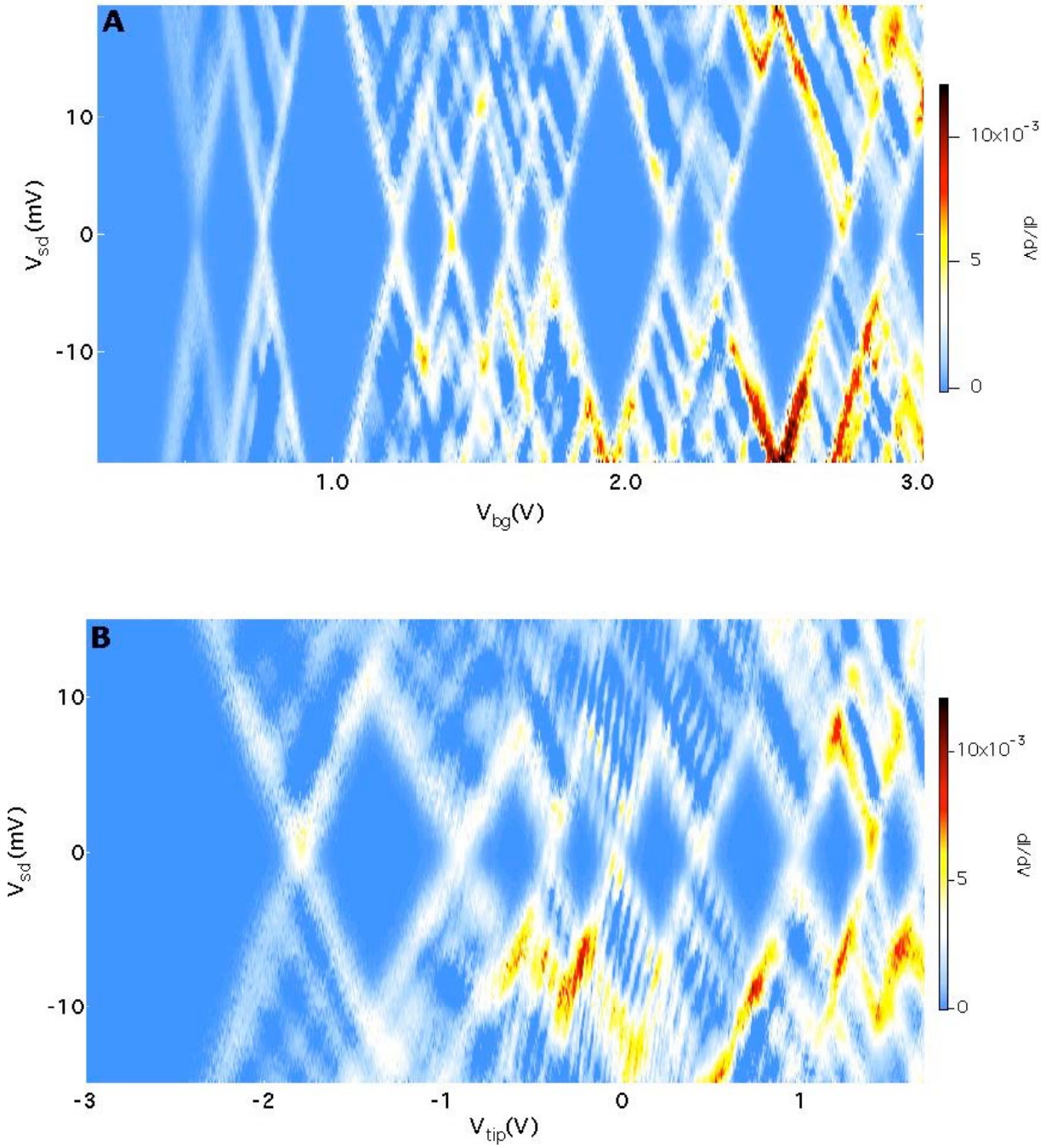

Figure 6.3 Coulomb blockade diamond plots for an InAs/InP nanowire quantum dot, plotting differential conductance as a function of V_{sd} and either (A) V_{bg} or (B) V_{tip}. These show that either the back gate or the SPM tip can tune the dot's charge state. The differing size of the diamonds indicates the atomic-like shell structure of the quantum dot. Both the tip and the back gate can reduce the number of electrons on the dot to zero or one as indicated by the large area of zero conductance that extends out to V_{sd} = 15 mV at the left of the two diamond plots.

We demonstrate the ability of the tip to function as a movable gate. The Coulomb diamond plot shown in Figure 6.3 (B) was obtained by fixing the position of the tip at a height of 70nm directly over the dot and sweeping V_{tip} and V_{sd} to tune the electron number on the dot. The back gate voltage is fixed at 1.2V and the dot is emptied of electrons for tip voltages less than ~ -2V at small V_{sd}. We determine $C_{tip-dot}$ to be ~ 0.4aF. It is reasonable that the dot's capacitance to the tip is ~2.5 times smaller than its capacitance to the back-gate because the SiO_2 separating the back gate from the dot has a dielectric constant ~3 times that of vacuum, which separates the tip from the dot. Both the tip and the back-gate are ~100nm away from the dot. The extracted 0.4aF value is slightly less than the value of 0.56aF obtained using a classical electrostatic simulation peformed in Comsol, a finite element solver. Again, this is an indication that the classical capacitance calculation is not valid in the few electron regime.

Like the back gate the tip is capable of tuning the dot's charge state to zero electrons. Unlike the back gate, the tip offers the extra advantage of movability: the tip's coupling to the dot can be varied through positioning. Additionally, if there is more than one dot in the wire, it will be possible to individually address one dot. We can move electrons between dots, pushing an electron off the target dot, or attracting an electron onto the target dot

SPM images of the quantum dot are shown in Figure 6.4. The images that plot quantum dot conductance as a function of tip position display rings of peaked conductance centered on the InAs quantum dot defined in the nanowire. Each ring corresponds to a Coulomb blockade conductance peak of the quantum dot. Starting at the quantum dot and moving radially outwards in an image, each successive ring encountered

corresponds to the addition of another electron to the dot. If we track the position of a single peak through multiple images, Figs 6.4(A)-(C), we see that radius of each ring shrinks as the back gate voltage is made more positive. The three images are taken with a tip voltage of -2V and back gate voltages of A) 2.5 V, B) 2.7 V, and C) 2.9 V. The red dot superimposed on each image tracks the Coulomb ring corresponding to the addition of the 11th electron.

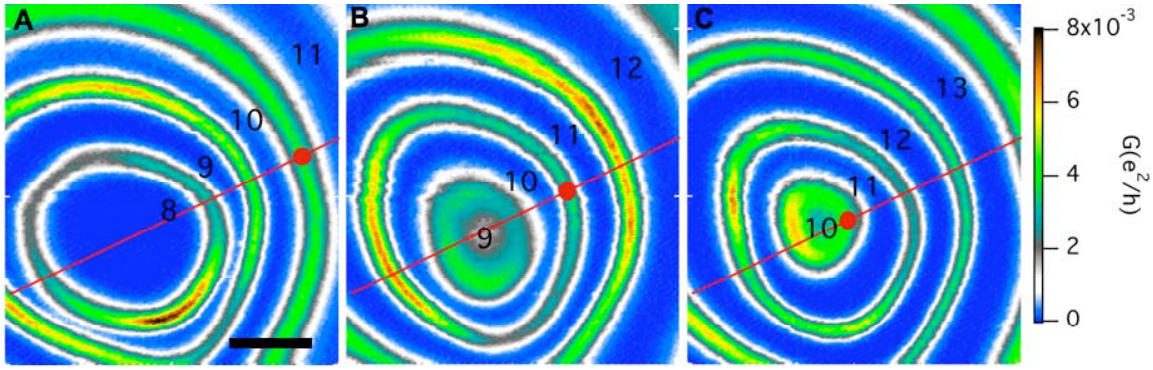

Figure 6.4 Coulomb blockade rings centered on an InAs quantum dot defined in an InAs/InP nanowire, whose location is schematically indicated by the red line. The images plot quantum dot conductance as a function of lateral position of a tip scanned 90nm above the wire with a tip voltage of -2V. In the valleys of zero conductance between successive peaked conductance rings, the dot holds N electrons, as denoted on the image. The red dot superimposed on each image tracks the position of the Coulomb blockade peak corresponding to the addition of the 11th electron. The three images are taken with Vbg = (A) 2.5 V, (B) 2.7 V, and (C) 2.9 V and red dot emphasizes the shrinking radius of each ring with increasing back gate voltage. Scale bar is 100 nm. The metallic contacts are defined 1.5 microns across.

To understand the shrinking of the rings, let us set the back gate voltage at 2.5V, as in Figure 6.4(A) and place the tip at the location of the red dot. The Fermi levels in the leads are then lined up with an energy level in the dot and it is equally energetically favorable for there to be 10 or 11 electrons on the dot, lifting the Coulomb blockade and allowing conductance through the dot. As V_{bg} increases positively to 2.6V, the total

energy of an electron in the quantum dot shifts downwards and the previously resonant energy level in the dot is no longer in resonance with the Fermi levels in the leads. In order to bring that energy level back into resonance, we need to raise the total energy of that 11th electron. We can do by bringing a negatively charged tip closer to the dot. At $V_{bg} = 2.6V$, the tip needs to be brought to the location of the red dot in Figure 6.4(B). As the back gate voltage is made even more positive, 2.7V, the negatively charged tip must be brought even closer to the dot, to the location of the red dot in Fig 6.4(C) In short, to stay on a Coulomb blockade peak and thus maintain the charge state of the dot while increasing V_{bg}, a negatively charged tip must be brought closer to the dot, resulting in the decreasing ring radius. The ring radius also shrinks with decreasing tip voltage as shown in Figure 6.5. The reasoning is similar to that presented above: as a negatively charged tip is made even more negative, the tip needs to be moved further away from the dot in order to keep a previously resonant energy level in resonance with the Fermi levels of the leads.

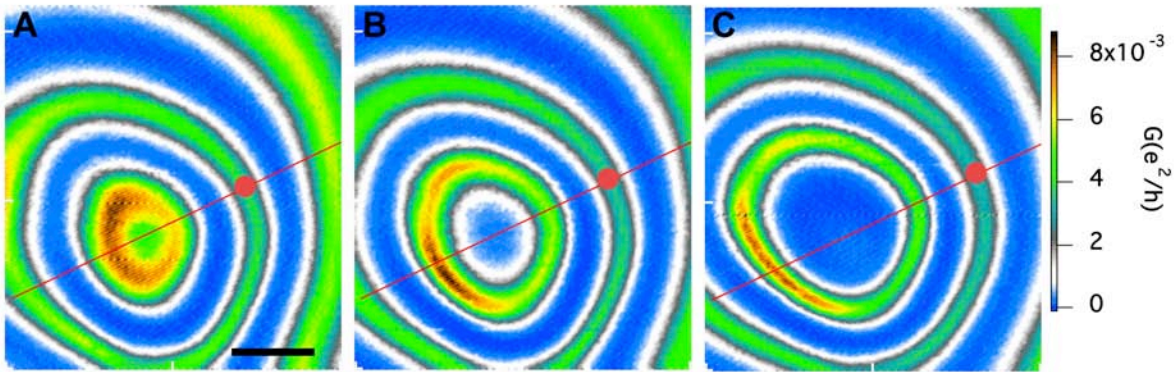

Figure 6.5 Series of SPM images showing the evolution of the Coulomb blockade rings with tip voltage. The images were taken with V_{tip} = (A) -1.0 V, (B) -1.2 V, and (C) -1.4 V. The rings are centered on an InAs quantum dot defined in an InAs/InP nanowire, whose location is schematically indicated by the red line. The images plot quantum dot conductance as a function of lateral position of a tip scanned 90nm above the wire. The red dot superimposed on each image tracks the position of the Coulomb blockade peak corresponding to the addition of the 13th electron. The red dot emphasizes the growing

radius of each ring with increasingly negative tip voltage. Scale bar is 100 nm. The metallic contacts are defined 1.5 microns across.

We present images of the last electron on the quantum dot in Figure 6.6. We adjust the back gate voltage and the tip voltage such that the quantum dot sits right around the zero-one electron transition with the tip nearby. Figure 6.6 shows three images in this regime. When the tip lies inside the ring in Figure 6.6(A), there are zero electrons on the dot and when the tip lies outside the ring, there is one electron on the dot. The quantum dot's occupation number is indicated on the image. The Coulomb blockade ring corresponding to the addition of the 2nd electron is just beginning to be visible at the corners of Figure 6.6(A). As the tip voltage is made less negative, the first Coulomb blockade ring shrinks to the feature seen in 6.6(C) and the ring corresponding to the addition of the 2nd electron also shrinks in size.

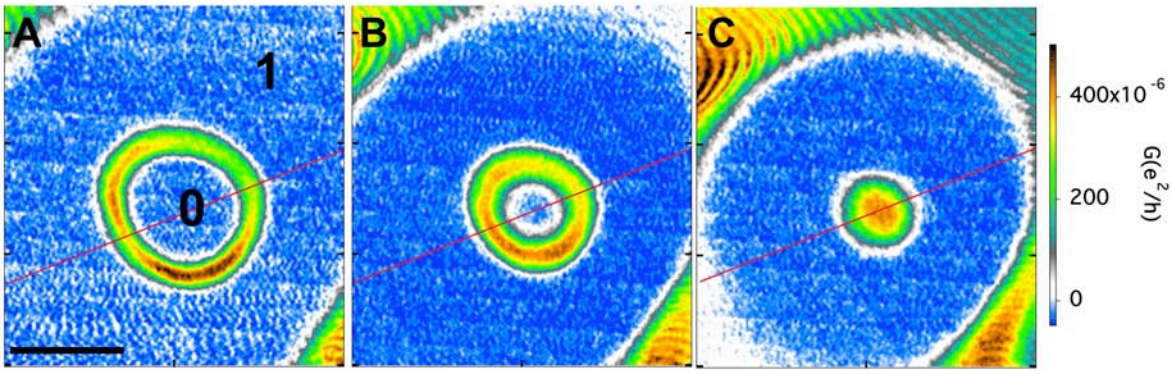

Figure 6.6 SPM images of the last electron on the InAs nanowire quantum dot. The numbers drawn on (A) indicate the number of electrons on the quantum dot when the tip lies inside the ring (0 electrons) and when it lies outside the ring (1 electron). The three images are taken at V_{tip} = (A) -2.5 V, (B) -2.0 V and (C) -1.5 V and the tip is scanned 100nm above the dot. The scale bar is 200nm.

We would like to use our imaging technique to infer spatial information about the electron on the quantum dot. From a series of images taken at different tip voltages, such as the series shown in Figure 6.5, it is possible to experimentally determine how the tip to dot capacitance $C_{tip-dot}$ varies as a function of tip position. In the limit of large electron occupation number, we expect $C_{tip-dot}$ to approach the classical value of capacitance between two metallic objects, a tip and a metal disc of the same dimensions as the InAs nanowire quantum dot. For smaller electron number, deviations from the orthodox theory will lend insight to the size of the wave function inside the quantum dot. We record the spatial Coulomb blockade peak position r_n as the tip voltage is varied (r_n is the lateral distance from the dot to a point on the Coulomb ring corresponding to the addition of the nth electron). For the tip positioned on a ring, we can write the charge induced by the tip on the dot as $q_{ind}(r_n) = q(r_\infty) - (n + \frac{1}{2})e = C_{t-d}(r_n)V_{t-d}$ where r_n is the lateral distance from the dot to the nth electron peak position taken along a line directly over the nanowire (like the red line in figure 6.6), $q(r_\infty)$ is the charge on the dot when the tip is very far away, and V_{t-d} is the voltage difference between the tip and the dot. Figure 6.7 plots C_{t-d} as a function of tip position taken along the red line in Figure 6.9. I have plotted C_{t-d} for n=7 and n=8 where n is the number of electrons on the quantum dot. For comparison, in Figure 6.8, I plot the results of a classical electrostatic simulation for $C_{tip-dot}$, calculated using Comsol, a finite element solver. Again, the magnitude of $C_{tip-dot}$ is overestimated in the simulation.

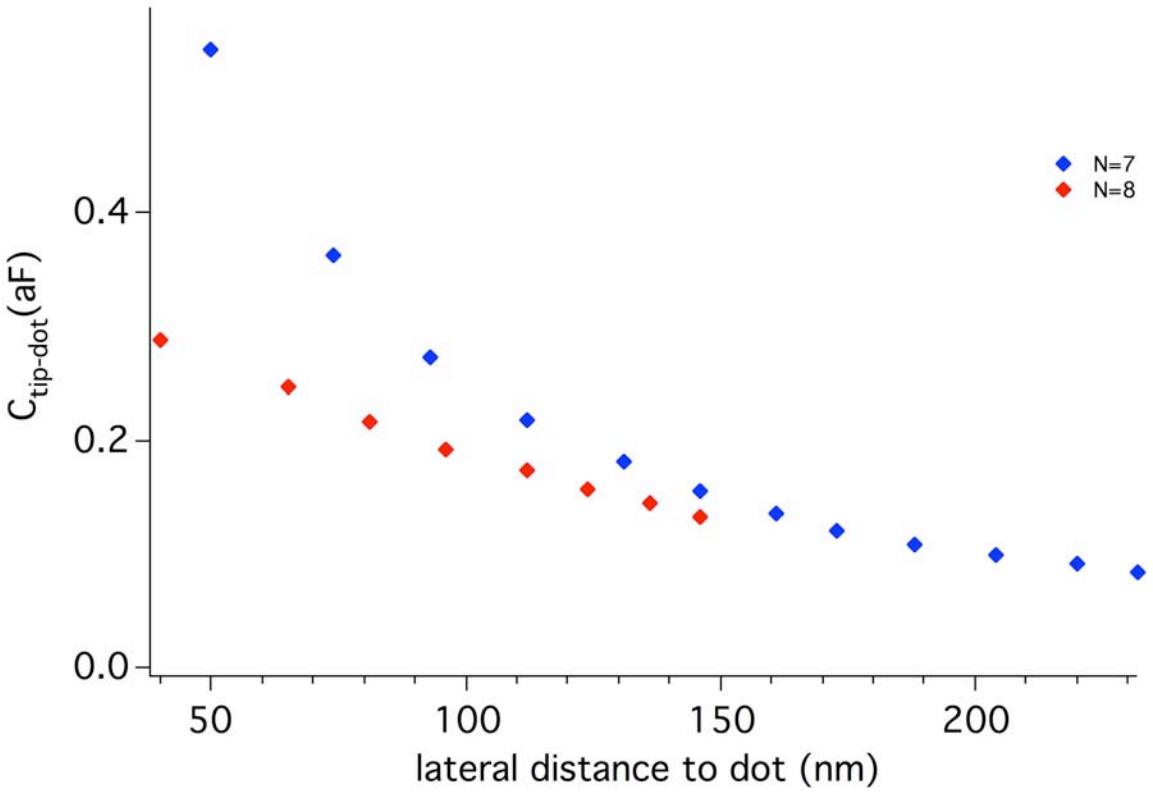

Figure 6.7 Experimentally determined SPM tip to dot capacitance $C_{t-d}(r)$ plotted as a function of lateral distance from the tip to the quantum dot. The tip is 100nm above the dot. The different color data points are labeled by n where n is the number of electrons on the quantum dot. The capacitances are extracted by tracking the position of the Coulomb blockade peak corresponding to the addition of the n^{th} electron.

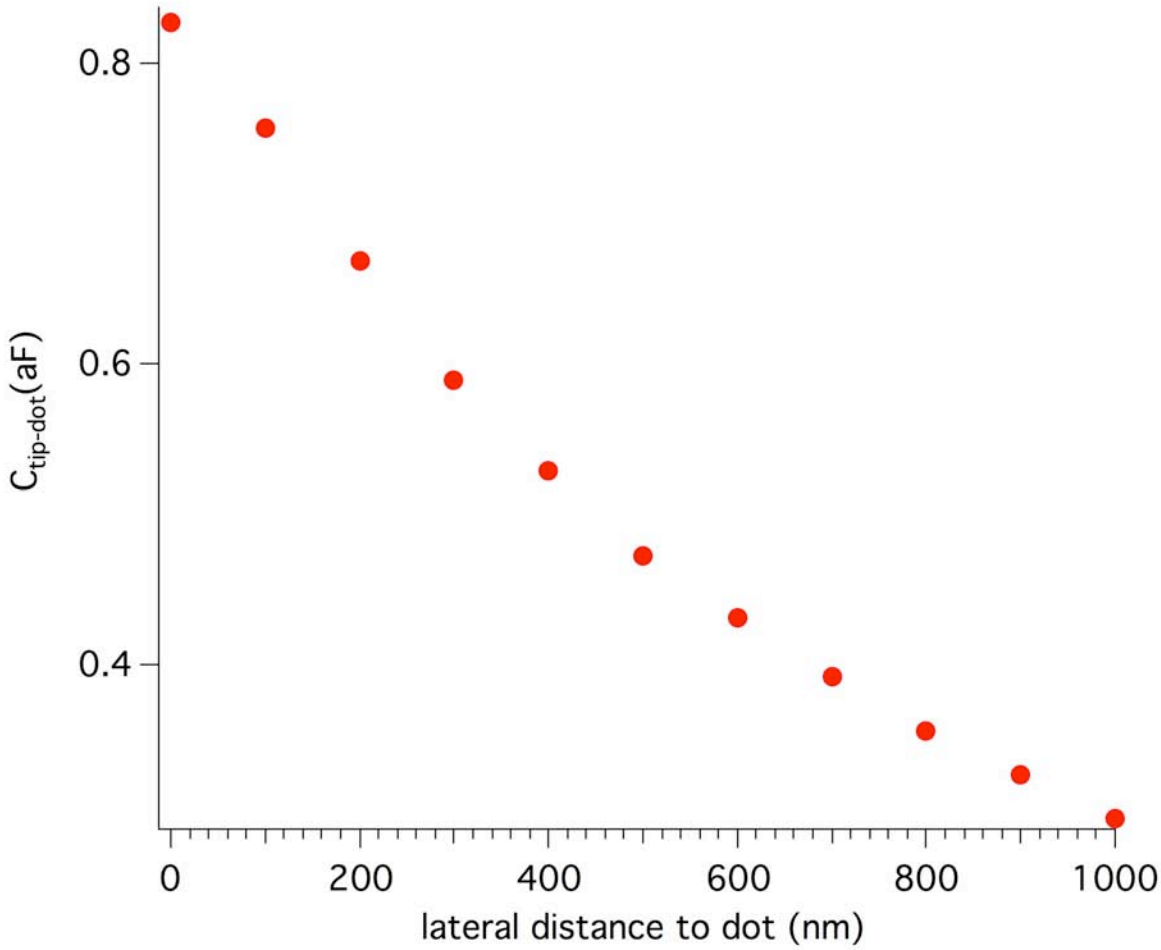

Figure 6.8 Electrostatic simulation of the SPM tip to quantum dot capacitance $C_{tip-dot}$ as a function of the tip's lateral distance from the quantum dot. The simulation was performed in Comsol with a conical tip with a 200 nm radius of curvature at a height of 100nm above the nanowire. The nanowire had a 25 nm radius and the length of the quantum dot was 20nm.

We would like to point out an additional set of features that appear in the Coulomb blockade diamond plot of Figure 6.3(B) in a range of tip voltages around V_{tip} = 0 V. There are is a pattern of sets of closely spaced lines of peaked conductance running parallel to each other. A zoom-in of Figure 6.3(B) highlighting these features is shown in Figure 6.9(A). The transport measurements themselves give little insight into the origin

of these features, but our SPM imaging technique has been valuable in identifying their source. Through imaging we can attribute these saw-tooth like features to the formation of another quantum dot, for a certain range of tip and back gate voltages, in another section of the wire. At a tip voltage of -3.25 V, the image in Figure 6.5(B) shows only two concentric peaked conductance rings centered on the 18nm long defined quantum dot, indicating the presence of only a single dot. However, for a tip voltage of 0.25V, there are two sets of concentric rings, one centered on the defined quantum dot and another set of closely spaced, elongated rings centered on the section of the wire to the left of the defined quantum dot, as shown in Figure 6.5(C). This section is forming another quantum dot between the left InP tunnel barrier and another barrier in the wire, possibly a poor contact. From the spacing of the rings, we can see that the dot is significantly longer than the defined quantum dot. The elliptical shape is also indicative of a quantum dot that is more extended in the axial direction than the defined quantum dot. The rings around the longer dot appear at the same tip voltages that the saw tooth pattern appears in the Coulomb blockade diamonds plot of Figure 6.3B. We are able to eliminate the second dot by adjusting either the tip voltage or the back gate voltage to a regime.

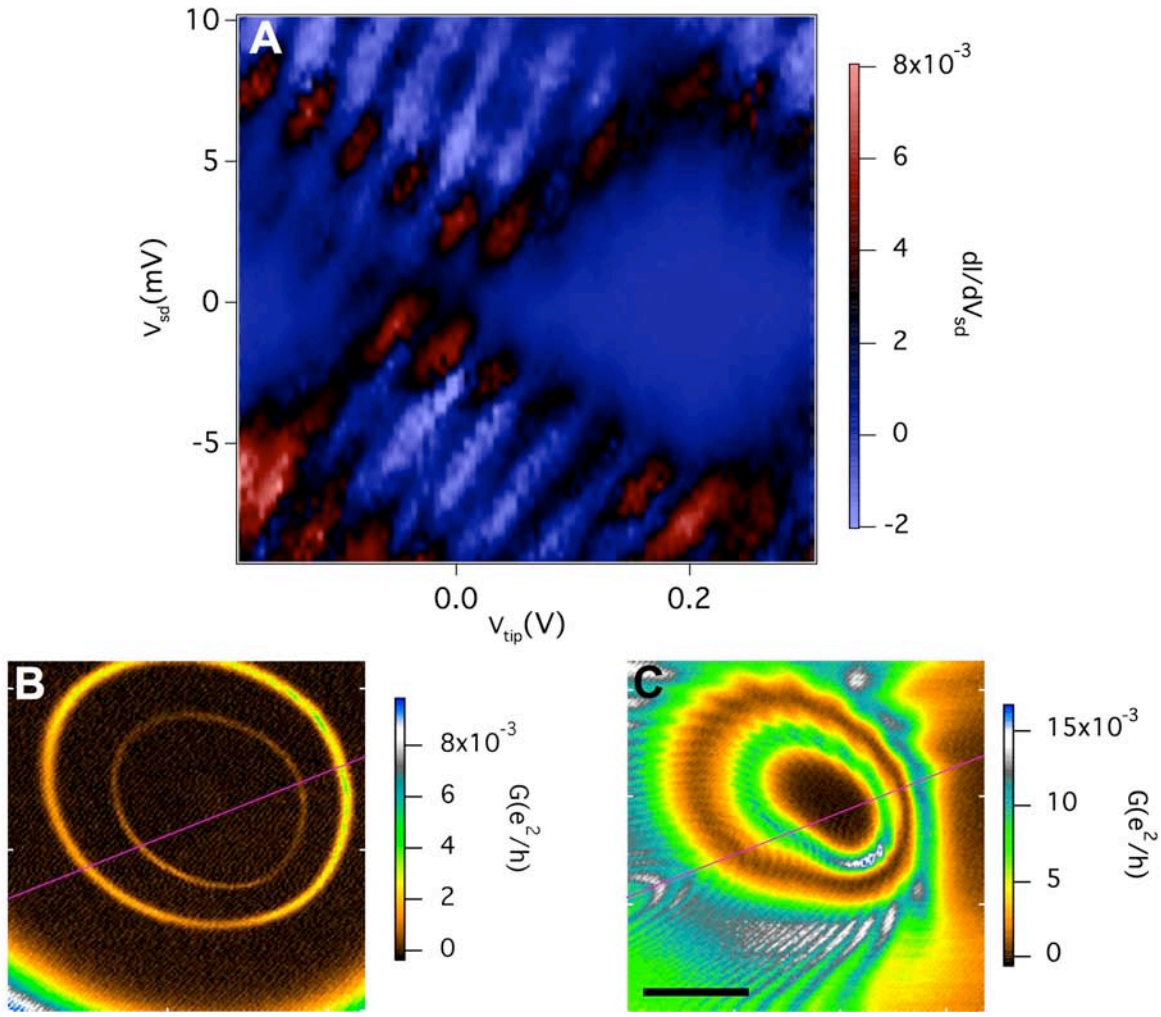

Figure 6.9 (A) A zoom-in of the Coulomb blockade diamond plot of Fig. 6.3(B) showing a pattern of sets of closely spaced lines running parallel to each other. These features are only present in the Coulomb blockade diamond in a range of tip voltages close to $V_{tip} = 0V$. The SPM images in (B) and (C) plot dot conductance as a function of tip position for a tip scanned 100nm above the wire with (B) $V_{tip} = -3.25V$ and (C) $V_{tip} = 0.25V$. The image in (B) displays peaked conductance rings centered on the defined quantum dot. The image in (C) displays rings centered on the defined quantum dot as well as rings centered on another quantum dot, revealing the origin of the saw-tooth features seen in (A).

SETE-Wire Simulations

For electrons inside a quantum dot, calculations of the eigenenergies and eigenfunctions of electron states provide information that is very useful for interpreting features shown in the images. As mentioned earlier in the chapter, InAs nanowire devices have many attractive qualities that give them much promise for future quantum information processing applications. These qualities include a large exciton Bohr radius (34nm) producing strong quantum confinement in reasonably sized structures, a charge accumulation layer at the InAs surface that makes it possible to make small structures without depletion, and a large g-factor (good for spintronics and QIP) that is tunable through tuning the size of the InAs structure. Development of practical devices made from InAs nanowires will require a good understanding of where the electrons reside inside the nanowire. Questions arise like: is it valid to assume the confining potential is hockey-puck shaped? How much do applied voltages on external gates deform the wave function? Are the electrons preferentially attracted to the surface of the InAs due to Fermi level pinning at the surface? Do charges on the surface or in the oxide affect the shape of the wavefunction? Imaging, together with simulations, may be able to provide answers to these questions, giving us new information about the effects of surface states, the quantum state energies, and perhaps some information about the wave function. We have collaborated with Mike Stopa on simulations and interpretations of our results in light of the simulations [Stopa 1996]. We have used his SETE-wire program to simulate the quantum dot wave functions and energy spectra, as well as the capacitances to the gate, tip, leads etc.

The SETE-wire program allows you to specify the material and the dimensions of the quantum dot, the tunnel barriers, the oxide layer, the tip, the nanowire leads, and the metallic leads. A schematic of the geometry is shown in Figure 6.10. The tip is assumed cylindrical with a hemisphere at the end whose radius of curvature is the radius of the cylinder. The quantum dot, tunnel barriers, and nanowire leads are shown: InAs is yellow and InP is red. The metallic leads do not cover the nanowire, as they do in reality, but instead abut the nanowire at its ends with a small gap in between. Although the metallic lead geometry is not completely accurate, the exact geomtery should have little effect on the area where the quantum dot and tip are. The wire rests atop a thin insulating layer (100nm in our case – only the top is shown in the figure). The program then self-consistently solves Poisson's equation and Schroedinger's equation to determine the number of electrons on the quantum dot and their wave functions. It also calculates the induced charge on the dot, the leads, the back gate, and the tip for a given set of voltages applied to the elements in the system. All the relevant capacitances to the dot (C_{tip},C_g,C_S,C_D.etc) can then be determined from the induced charges.

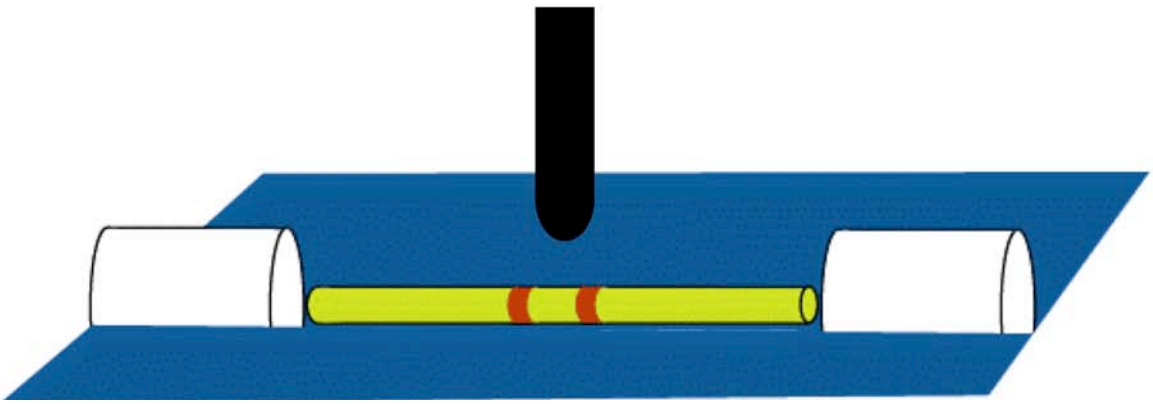

Figure 6.10 Schematic of the geometry inputted to the SETE-wire program. The black cylinder with the rounded end is the SPM tip and the white half cylinders at the ends of

the wire are the metallic leads. The red stripes are 8 nm thick InP tunnel barriers and the yellow wire is a 50 nm diameter InAs nanowire, with an 18 nm long quantum dot between the two tunnel barriers.

We have simulated the single particle wave functions for our nanowire quantum dot in the presence of applied voltages on the back gate and on the tip. In Figure 6.11 we plot the amplitude of the wave function squared $|\Psi(\rho,\varphi)|^2$ as a function of cylindrical coordinates, ρ the radial coordinate and φ the azimuthal angle. The simulated wave functions are plotted along a cut perpendicular to the axis of the wire taken at the center of the quantum dot, 9 nm away from each of the tunnel barriers. Figure 6.11(A)-(D) plot $|\Psi(\rho,\varphi)|^2$ for the lowest four eigenstates, solved with a negative voltage on the back gate and a negative voltage on the tip. Figure 6.11 (E)-(H) plot $|\Psi(\rho,\varphi)|^2$ for the lowest four eigenstates, solved in the presence of a positively charged back gate and a negatively charged tip. For a cylindrically symmetric confining potential, one would expect cylindrically symmetric wave functions. See Appendix A in which I solve for the eigenstates and eigenenergies for a uniform disk with hard walls. The symmetry is clearly broken in the plots of Fig. 6.11 due to voltages applied to the tip and back gate. Whereas the assumption of cylindrical symmetry explained the energy level structure of the experiments of Tarucha et al (1996) in which an InGaAs disc-shaped quantum dot was formed between two AlGaAs tunnel barriers inside a vertical pillar, it is not valid to assume cylindrical symmetries in our disc shaped nanowire quantum dots. The difference between the two experiments lies in the gating technique: the Tarucha group used a cylindrically symmetric wrap gate, thus preserving the symmetry.

A voltage on the back gate has a significant effect on the vertical position of the ground state wave function, as seen in Figure 6.11. A positive back gate voltage brings the electron towards the substrate while a negative back gate voltage pushes the electron away from the substrate. Another effect of switching the polarity of back gate voltage is to swap the shapes of the 1st and 2nd excited state wave functions. (B) and (G) have a similar form and (C) and (F) have a similar form (again they are mirrored vertically due to the back gate voltage pulling/pushing on the wave function). These level crossings induced by an external voltage are shown numerically in Figure 6.12.

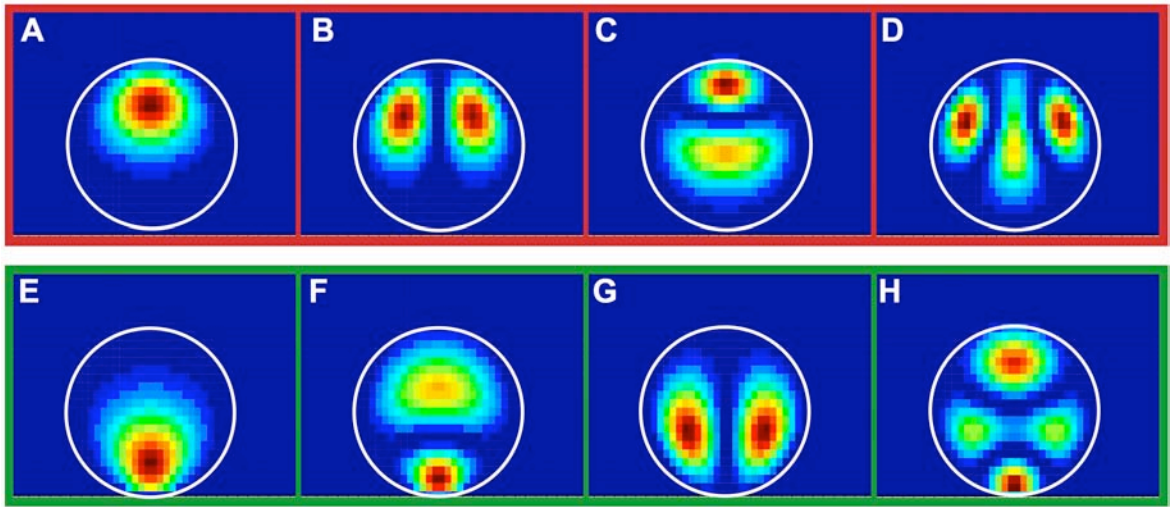

Figure 6.11 Simulations of $|\Psi(\rho,\varphi)|^2$ inside a nanowire quantum dot with the same geometry as the quantum dot studied in this research. The images are cuts taken at the center of the dot in a plane perpendicular to the nanowire axis. The white circle denotes the outline of the 50nm radius wire. In (A)-(D), V_{bg} = 1.5V and V_{tip} = -2V, whereas in (E)-(F), V_{bg} = -1.5V and V_{tip} = -3V. (A) plots the ground state wave function, (B) the 1st excited state, (C) the 2nd, and (D) the 3rd. (E)-(H) also plot the ground sate through the 3rd excited state but their shapes differ from (A)-(B) due to the different back gate and tip voltages. A negative V_{bg} pushes the wave function away from the substrate and a positive V_{bg} pulls the wave function towards the substrate. Additionally, the shapes of the 1st and 2nd excited state wave functions are swapped for the two different applied voltages.

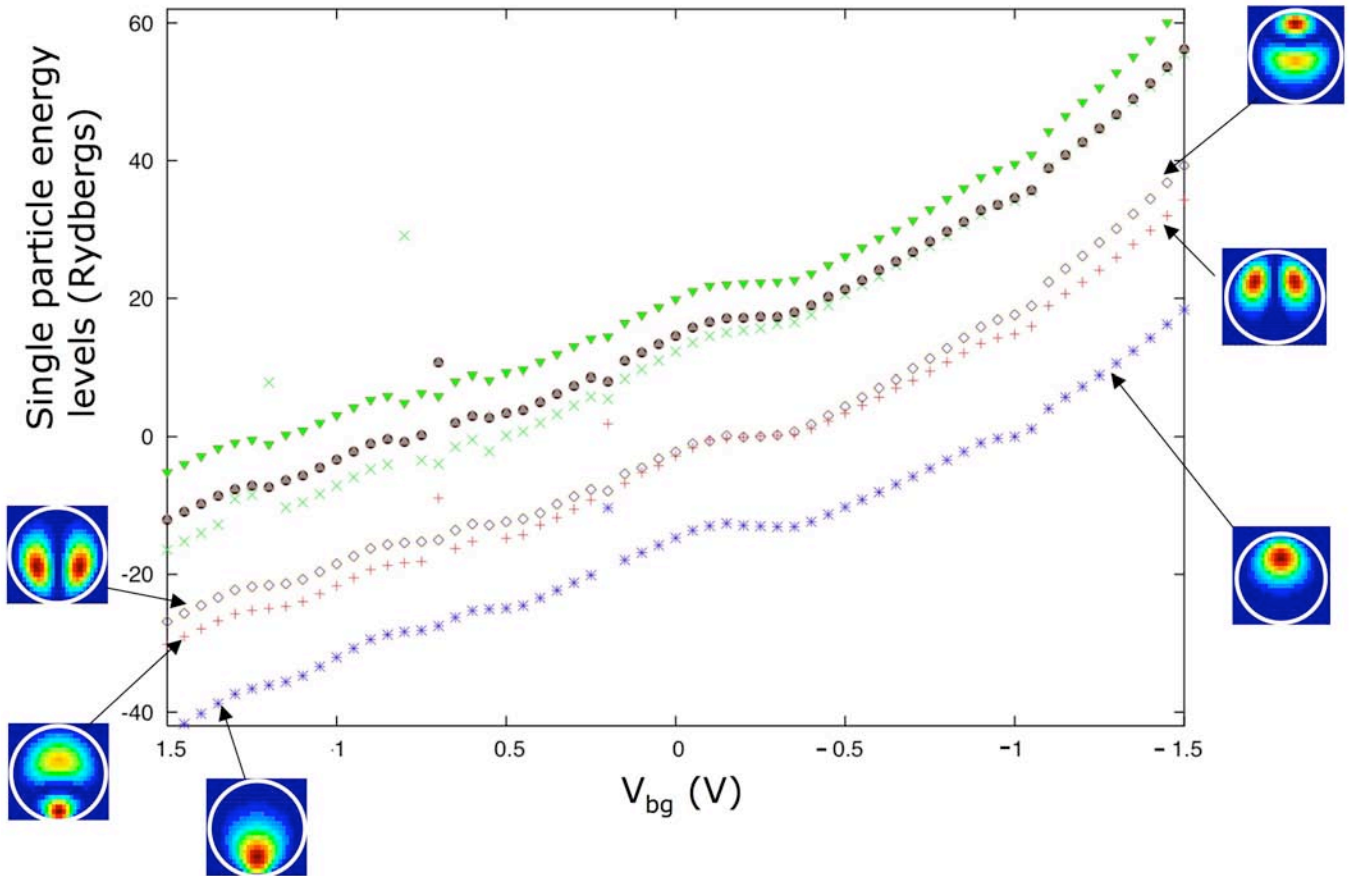

Figure 6.12 Evolution of the lowest six single particle energy levels inside a nanowire quantum dot with back gate voltage. An energy level crossing between the 1st and 2nd excited states occurs at V_{bg} ~ -0.25V and the 3rd and 4th excited state energy levels begin to cross at V_{bg} ~ -0.75 V.

This opens up the possibility of manipulating the shape of the wave function, while keeping the electron number constant, through modifying the confining potential now with two knobs – the back gate and the tip. For example, at one back gate voltage transport through the dot occurs through a certain quantum state. We can adjust the tip and back gate voltages appropriately so that we keep the dot's electron number constant, but change the state through which transport occurs. This might be useful if, for example, we wanted to change the coupling of the resonant state to the leads.

Bibliography

Ahn, Y., J. Dunning, and J. Park (2005). “Scanning photocurrent imaging and electronic band studies in silicon nanowire field effect transistors” *NanoLetters* **5**, 1367.

Ashoori (1996). “Electrons in artificial atoms” *Nature* **379**, 413.

Awschalom, D.D., D. Loss, N. Samarth (eds) (2002) “Semiconductor spintronics and quantum computation” Springer-Verlag, Berlin.

Bakkers, E.P.A.M., J.A. van Dam, S. De Franceschi, L.P. Kouwenhoven, M. Kaiser, M. Verheijen, H. Wondergem, and P. van der Sluis (2004) “Eptixial growth of InP nanowires on germanium” *Nature Materials* **3**, 769.

Beenakker, C.W.J., and H. van Houten (1991). “Quantum transport in semiconductor nanostructures,” *Solid State Physics* 44, H. Ehrenreich and D. Turnbull, (eds.), Academic Press, San Diego, CA.

Beenakker, C.W.J. (1991). “Theory of Coulomb-blockade oscillations in the conductance of a quantum dot” *Phys. Rev. B* **44**, 1646.

Bjork, M. T.; C. Thelander, A.E. Hansen, L.E. Jensen, M.W. Larsson, L.R. Wallenberg, and L. Samuelson (2004). “Few-electron quantum dots in nanowires” *NanoLetters* **4**, 1621.

Bjork, M.T., B.J. Ohlsson, T. Sass, A.I. Persson, C. Thelander, M.H. Magnusson, K. Deppert, L.R. Wallenberg, and L. Samuelson (2001). “One-dimensional steeplechase for electrons realized” *NanoLetters* **2**, 87.

Chan, I.H., P. Fallahi, A. Vidan, R.M. Westervelt, M. Hanson, and A.C. Gossard (2004). “Few-electron double quantum dots” *Nanotechnology* **15**, 609.

Cui, Y., Q. Wei, H. Park, and C.M. Lieber (2001). "Nanowire Nanosensors for Highly Sensitive and Selective Detection of Biological and Chemical Species" *Science* **293**, 1289.

Davies, John H. (1998). “The physics of low-dimensional semiconductors,” Cambridge University Press, New York, USA.

De Franceschi, S., J.A. van Dam, E.P.A.M. Bakkers, L.F. Feiner, L. Gurevich, and L.P. Kouwenhoven (2003). “Single-elecron tunneling in InP nanowires” *Appl. Phys. Lett.* **83**, 344.

Doh, Y., J.A. van Dam, A.L. Roest, E.P.A.M. Bakkers, L.P. Kouwenhoven, and S. De

Franceschi (2005). “Tunable supercurrent through semiconductor nanowires” *Science* **309**, 272.

Duan, X., Y. Huang, Y. Cui, J. Wang, and C.M. Lieber (2001). “Indium phosphide nanowires as building blocks for nanoscale electronic and optoelectronic devices” *Nature* **409**, 66.

Duan, X., Y. Huang, R. Agarwal, and C.M. Lieber (2003). “Single-Nanowire Electrically Driven Lasers" *Nature* **421**, 241.

Elzerman, J.M., R. Hanson, J.S. Greidanus, L.H. Willems van Beveren, S. De Franceschi, L.M. Vanderseypen, S. Tarucha, and L.P. Kouwenhoven (2003). “Few-electron quantum dot circuit with integrated charge read out” *Phys. Rev. B* **67**, 161308.

Bjork, M.T., A. Fuhrer, A.E. Hansen, M.W. Larsson, L.E. Froberg. L. Samuelson (2005). “Tunable effective *g* factor in InAs nanowire quantum dots” *Phys. Rev. B* **72**, 201307.

Fallahi, P.F., A.C. Bleszynski, R.M. Westervelt, J. Huang, J.D. Walls, E.J. Heller, M. Hanson, A.C. Gossard (2005) “Imaging a single-electron quantum dot” *NanoLetters* **5**, 223.

Giuliani, Gabriele F. and John J. Quinn (1982). “Lifetime of a quasiparticle in a two-dimensional electron gas,” *Phys. Rev. B* **26**, 4421.

Gu, Y. E.-S. Kwak, J.L. Lensch, J.E. Allen, T.W. Odom, and L.J. Lauhon (2005). “Near-field scanning photocurrent microscopy of a nanowire photodetector” *Appl. Phys. Lett.* **87**, 043111.

Hermann, Claudine and Claude Weisbuch (1977). “k•p perturbation theory in III-V compounds and alloys: a reexamination” *Phys. Rev. B* **15**, 823.

International Technology Roadmap for Semiconductors 2005 Edition. Available from: http://www.itrs.net/Common/2005ITRS/Home2005.htm

Jarillo-Herrero, P., J.A. van Dam, and L.P. Kouwenhoven (2006). “Quantum supercurrent transistors in carbon nanotubes” *Nature* **439**, 953.

Huang, M., S. Mao, H. Feick, Y. Yan, Y. Wu, H. Kind, E. Weber, R. Russo, and P. Yang (2001). “Room temperature ultraviolet nanowire nanolasers” *Science* **292**, 1897.

Kastner, M.A. (1993). “Artificial Atoms” *Physics Today* **46**, 24.

Kiselev, A.A., E.L. Ivchenko, U. Rossler (1998) “Electron g factor in one- and zero-dimensional semiconductor nanostructures” *Phys. Rev. B* **58**, 16353.

Kouwenhoven, L. P., D.G. Austing, and S. Tarucha (2001) “Few-electron quantum dots” *Rep. Prog. Phys.* **64**, 701.

Kouwenhoven, L.P., C.M. Marcus, P.L. McEeuen, S. Tarucha, R.M. Westervelt, and N.S. Wingreen (1997) “Electron transport in quantum dots” In: L.L. Sohn ,ed. “Mesoscopic Electron Transport”. Kluwer Academic, Boston, MA.

Lauhon, L.J., M.S. Gudiksen, D. Wang, and C.M. Lieber (2002). "Epitaxial core-shell and core-multi-shell nanowire heterostructures," *Nature* **420**, 57.

Lauhon, L.J., M. S. Gudiksen and C. M. Lieber (2004). "Semiconductor nanowire heterostructures," *Philosophical Transactions of the Royal Society of London Series A-Mathematical Physical and Engineering Sciences* **362**, 1247.

LeRoy, B.J. (2003). “Imaging coherent electron flow through semiconductor nanostructures” Ph.D. Thesis, Harvard University.

LeRoy, B.J., A.C. Bleszynski, K.E. Aidala, R.M. Westervelt, A. Kalben, E.J. Heller, S.E.J. Shaw, K.D. Maranowski, and A.C. Gossard (2005). “Imaging electron interferometer” *Phys. Rev. Lett.* **94**, 126801.

LeRoy, B.J., Topinka, M.A., Westervelt, R.M., Maranowski, K.D., Gossard, A.C. (2002). “Imaging electron density in a two-dimensional electron gas” *Appl. Phys. Lett.* **80**, 4431.

Lieber, C.M. (2003). “Nanoscale science and technology: building a big future from small things” *Materials Research Society Bulletin* **28**, 486.

Loss, D. and D.P. DiVincenzo (1998). “Quantum computation with quantum dots” *Phys. Rev. A* **57**, 120.

Olsson, L.O., C.B.M. Andersson, M.C. Håkansson, J. Kanski, L. Ilver, and U.O. Karlsson (1996). “Charge accumulation at InAs surfaces” *Phys. Rev. Lett.* **76**, 3626.

Potok, R. M., J.A. Folk, C.M. Marcus, V. Umansky, M. Hanson, and A.C. Gossard, (2003). “Spin and Polarized Current from Coulomb Blockaded Quantum Dots” *Phys. Rev. Lett.* **91**, 016802.

Pioda, A., S. Kicin, T. Ihn, M. Sigrist, A. Fuhrer, K. Ensslin, A. Weichselbaum, S.E. Ulloa, M. Reinwald, and W. Wegscheider (2004) “Spatially Resolved Manipulation of Single Electrons in Quantum Dots Using a Scanned Probe” *Phys. Rev. Lett.* **93**, 216801.

Ruzin, I.M., V. Chandrasekar, E.I. Levin, L.I. Glazman (1992). “Stochastic Coulomb blockade in a double-dot system” *Phys. Rev. B* **45**, 13469.

Samuelson, L., C. Thelander, M.T. Bjork, and M. Borgstrom (2004). “Semiconductor nanowires for 0D and 1D physics and applications” *Physica E (Amsterdam)* **25**, 313.

Shaw, S.E.J., R. Fleischmann, and E.J. Heller (2001). "Quantum coherence beyond the thermal length" *cond-mat*/0105354.

S.E.J. Shaw, Ph.D, Thesis, Harvard University, 2002.

Sohn, L.L., L.P. Kouwenhoven and G. Schön (eds) (1997). "Mesoscopic electron transport," Kluwer Academic, Boston MA.

Stopa, M. (1996). "Quantum dot self-consistent electronic structure and the Coulomb blockade" *Phys. Rev. B.* **54**, 13767.

Tarucha, S.; D.G. Austing, T. Honda, R.J. van der Hage, and L.P. Kouwenhoven (1996). "Shell filling in a few electron quantum dot" *Phys. Rev. Lett.* **77**, 3613.

Topinka, M.A., B.J. LeRoy, S.E.J. Shaw, E.J. Heller, R.M. Westervelt, K.D. Maranowski, and A.C. Gossard (2000). "Imaging coherent electron flow from a quantum point contact" *Science* **289**, 2323.

Topinka, M.A., B.J. LeRoy, R.M. Westervelt, S.E.J. Shaw, R. Fleischmann, E.J. Heller, K.D. Maranowski, and A.C. Gossard (2001). "Coherent branched flow in a two-dimensional electron gas" *Nature* **410**, 183.

Topinka, M. A. (2002). "Imaging coherent electron wave flow through 2-D electron gas nanostructures" Ph.D. Thesis, Harvard University.

Topinka, M.A., R.M. Westervelt, and E.J. Heller (2003). "Imaging electron flow" *Physics Today* **56**, 47 and references therein.

Tsui, D.C., H.L. Stormer, and A.C. Gossard (1982). "Two-dimensional magnetotransport in the extreme quantum limit" *Phys. Rev. Lett.* **48**, 1559.

van Wees, B.J., H. van Houten, C.W.J. Beenakker, J.G. Williamson, L.P. Kouwenhoven, D. van der Marel, and C.T. Foxon (1988). "Quantized conductance of point contacts in a two-dimensional electron gas" *Phys. Rev. Lett.* **60**, 848.

Von Klitzing, K., G. Dorda, and M. Pepper (1980). "New method for high-accuracy determination of the fine-structure constant based on quantized Hall resistance" *Phys. Rev. Lett.* **45**, 494.

Wagner, R.S. and W.C. Ellis (1964). "Vapor-liquid-solid mechanism for single crystal growth" Appl. Phys. Lett. **4**, 89.

Waugh, F. R., M.J. Berry, D.J. Mar, R.M. Westervelt, K.L. Campman, and A.C. Gossard (1995). "Single-electron charging in double and triple quantum dots with tunable coupling" *Phys. Rev. Lett.* **75**, 705.

Wharam, D.A., T.J. Thornton, R. Newbury, M. Pepper, H. Ahmed, J.E.F. Frost, D.G. Hasko, D.C. Peacock, D.A. Ritchie, and G.A.C. Jones (1988). “One-dimensional transport and the quantization of the ballistic resistance” *J. Phys. C: Solid State Phys.* **21**, L209-L214.

Woodside, Michael T. and Paul L. McEuen (2002) “Scanned probe imaging of single-electron charge states in nanotube quantum dots” *Science* **296** 1098.

Xiang, J., W. Lu, Y. Hu, Y. Wu, H. Yan and C.M. Lieber (2006). "Ge/Si nanowire heterostructures as high-performance field-effect transistors" *Nature* **441**, 489.

Yang, C., Z. Zhong, and C.M. Lieber (2005) "Encoding electronic properties by synthesis of axial modulation doped silicon nanowires," *Science* **310**, 1304.

Yang, P. (2005). “The chemistry and physics of semiconductor nanowires” *Materials Research Society Bulletin* **30**, 85.

Zheng, Lian and S. Das Sarma (1996) “Coulomb scattering lifetime of a two-dimensional electron gas” *Phys. Rev. B* **53**, 9964.

Zhong, Z., Y. Fang, W. Lu and C.M. Lieber (2005). “Coherent single charge transport in molecular-scale silicon nanowires," *Nano Letters* **5**, 1143.

Appendix A

Calculated Wave Functions for a Quantum Dot in a Cylindrical Nanowire

The InAs/InP nanowire quantum dots studied in Chapter 7 have an approximately cylindrical shape. Making the assumption that the nanowire cross section is in fact cylindrical and that the InP barriers are infinitely hard walls[2], the problem becomes a standard quantum mechanics "particle in a box" problem. I have solved for the expected wave functions and corresponding energies. I then used Mathematica to plot the first few electronic wave functions.

A schematic of the nanowire quantum dot is shown below. The nanowire has radius R and the InAs quantum dot (light blue) between the two InP barriers (red) has length L. For the nanowires we have studied in Chapter 7, R = 25nm and L = 18nm. We also did a few measurements on quantum dots with R = 25nm and L = 120nm.

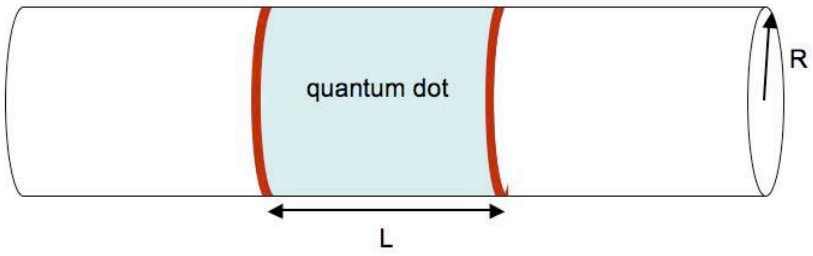

We start with the Schrodinger equation in cylindrical coordinates

[2] The infinitely hard wall assumption begins to break down when the electron energy becomes comparable to the depth of the potential well which is 600 meV.

$$\mathrm{H}\Psi = \frac{-\hbar^2}{2m^*}\left[\frac{1}{r}\frac{\partial}{\partial r}\left(r\frac{\partial \Psi}{\partial r}\right) + \frac{1}{r^2}\frac{\partial^2 \Psi}{\partial \varphi^2} + \frac{\partial^2 \Psi}{\partial z^2}\right]$$

Using separation of variables, we make an ansatz:

$$\Psi(r,\varphi,z) = u(r)e^{im\varphi}e^{ikz}$$

where m is the azimuthal quantum number and z is along the axial direction. Applying boundary conditions, we get:

$$\Psi(r,\varphi,z) \propto J_m\left(a_{mn}\frac{r}{R}\right)e^{im\varphi}\sin\left(\frac{N\pi z}{L}\right)$$

where N is the axial quantum number, n is the radial quantum number, J_m is the m^{th} order Bessel function and a_{mn} is the nth zero of J_m. The corresponding energies are:

$$E_{mnN} = \frac{\hbar^2}{2m^*}\left[\left(\frac{a_{mn}}{R}\right)^2 + \left(\frac{N\pi}{L}\right)^2\right]$$

For dots of short length, the lowest energy electrons occupy the lowest sub-band along the axial direction, i.e. they have axial quantum number N=1. For our dot of length 18nm and radius 25nm, the second sub-band is not occupied until the 25^{th} electron enters the dot. In order for the first excited state to have quantum number N=2, the dot length must exceed 45 nm.

Table A.1 below shows the ground state energy and first eight excited state energies and their corresponding quantum numbers and degeneracies for a quantum dot of length 18nm and radius 25nm.

Level	Energy (meV)	Axial quantum number (N)	Azimuthal quantum number (m)	Radial quantum number (n)	Degeneracy
1	65	1	0	1	2
2	89	1	1	1	4
3	120	1	2	1	4
4	130	1	0	2	2
5	157	1	3	1	4
6	180	1	1	2	4
7	202	1	4	1	4
8	216	2	0	1	2
9	237	1	2	2	4

Table A.1 Energies, quantum numbers, and degeneracies of ground state and first eight excited states for a disc shaped nanowire quantum dot of length 18nm and radius 25nm.

Figure A.2 plots the ground state wavefunction (A) and first four excited state wave-functions (B)-(E).

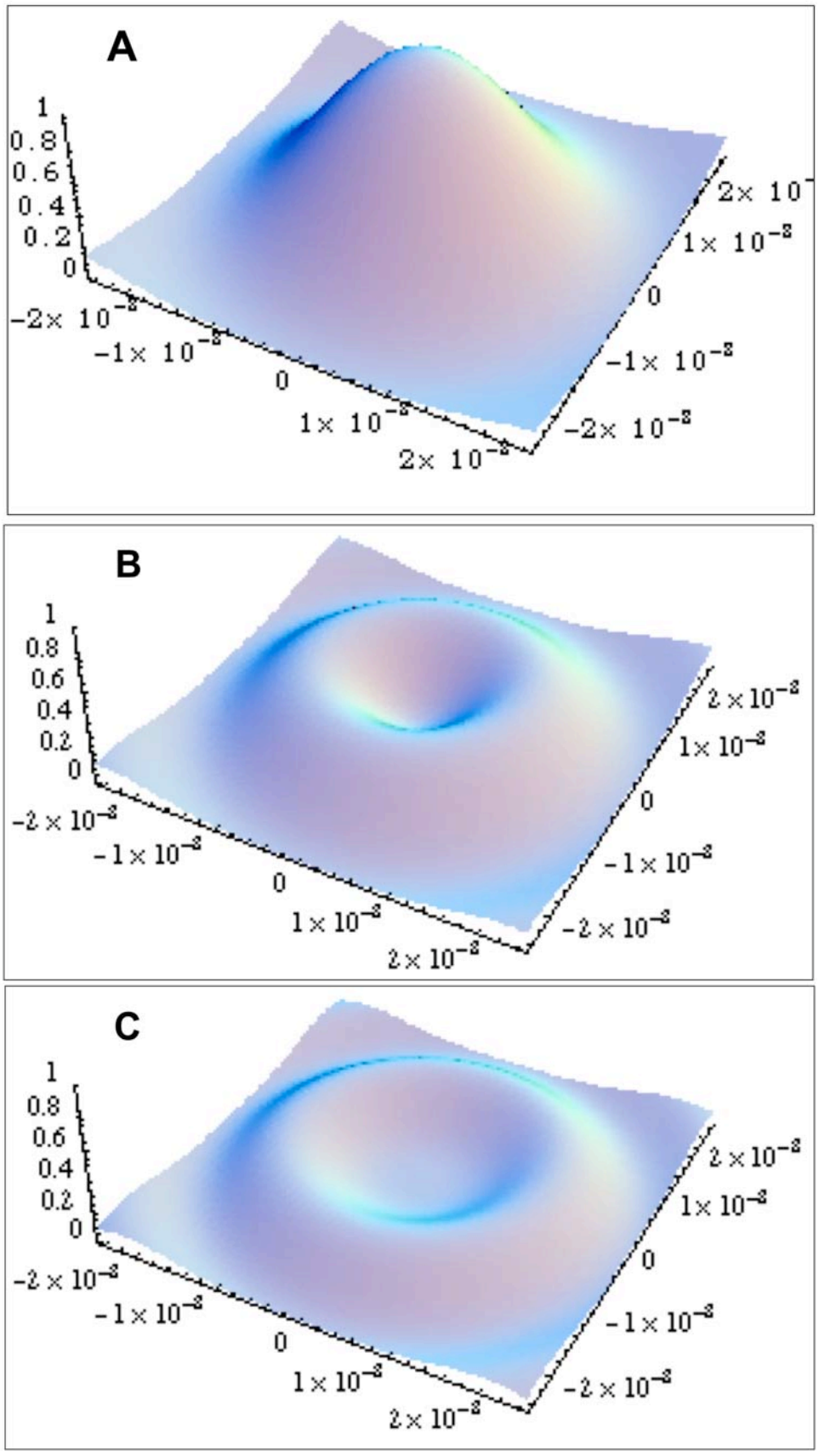
A
1
0.8
0.6
0.4
0.2
0
−2× 10⁻³
−1× 10⁻³
0
1× 10⁻³
2× 10⁻³
2× 10⁻³
1× 10⁻³
0
−1× 10⁻³
−2× 10⁻³
B
1
0.8
0.6
0.4
0.2
0
−2 × 10⁻³
−1 × 10⁻³
0
1 × 10⁻³
2 × 10⁻³
2 × 10⁻³
1 × 10⁻³
0
−1 × 10⁻³
−2 × 10⁻³
C
1
0.8
0.6
0.4
0.2
0
−2 × 10⁻³
−1 × 10⁻³
0
1 × 10⁻³
2 × 10⁻³
2 × 10⁻³
1 × 10⁻³
0
−1 × 10⁻³
−2 × 10⁻³

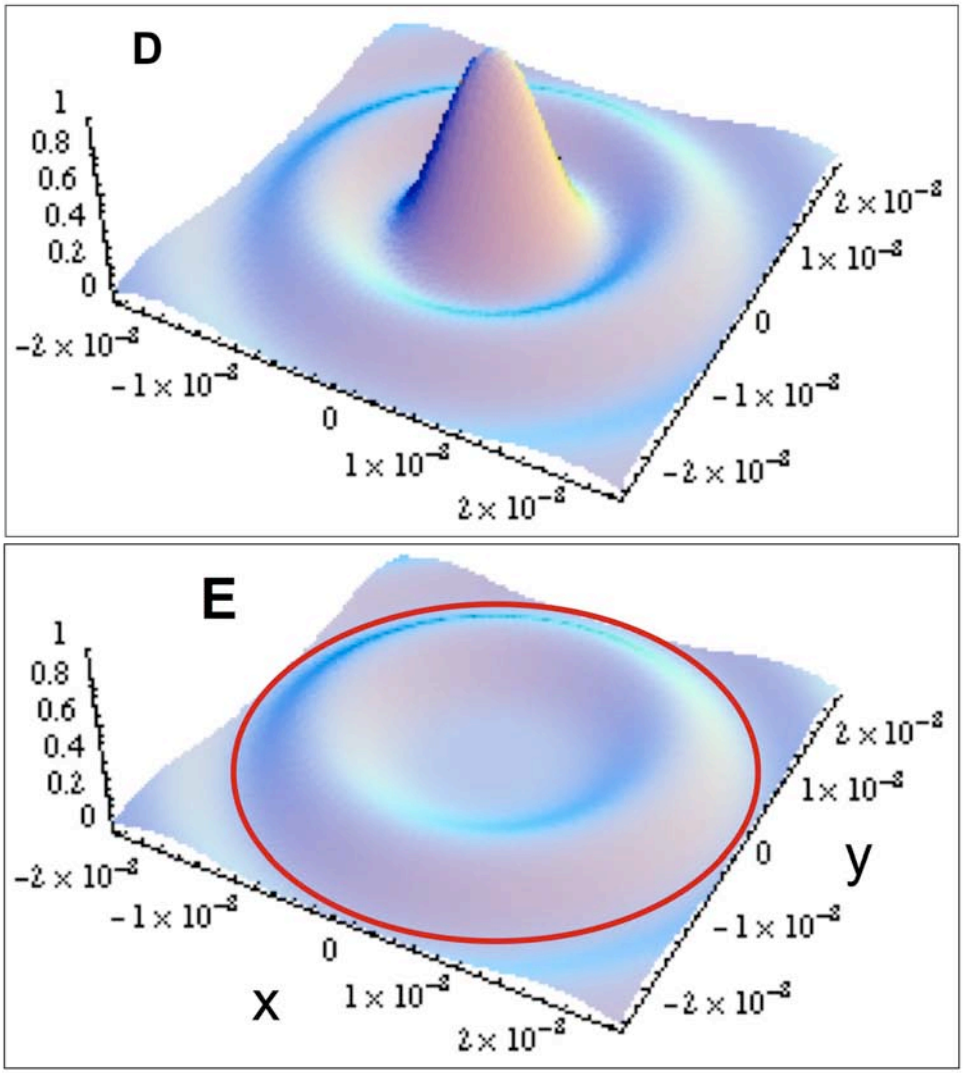

Figure A.2 Plots of $|\Psi(r,\varphi)|^2$ for the lowest five single particle energy states taken along a cut perpendicular to the axial direction of the nanowire. A cylindrical confining potential with infinitely hard walls is assumed. The outline of the nanowire is shown in red in (E). The quantum numbers in the various plots are (A) m = 0, n = 1 (B) m = 1, n = 1, (C) m = 2, n = 1, (D) m = 0, n = 2, (E) m = 1, n = 3. The axial quantum number N is 1 for all five plots.

Through Coulomb blockade spectroscopy, it is possible to experimentally determine the energies of the first few eigenstates. The theoretically expected values give a good first order estimate to the experimental results, but they are far enough off that the assumptions we have made have to be modified. We have used Mike Stopa's fully self-consistent and quantum mechanical SETE program to more accurately model the system. Some important factors that SETE considers are the shape change of the confining potential due to external voltages on the back gate or the tip, electron-electron interactions inside the dot, and a background charge density in the wire. Results from simulating the nanowire quantum dots using SETE are presented in Chapter 8.

Abstract

Imaging Electrons in Semiconductor Nanostructures

by

Ania Claire Bleszynski

Doctor of Philosophy in Physics, 2006

Harvard University

Advisor: Professor Robert M. Westervelt

Scanning probe microscopy (SPM) is a powerful tool that allows us to probe and manipulate electrons at the nanoscale. We have used a liquid helium cooled SPM with a conducting tip to image electrons in three types of semiconducting nanostructures: two-dimensional electron gases (2DEG's), quantum dots, and nanowires. Our images are obtained by scanning a charged tip over the sample and recording changes in device conductance as a function of tip position. We have directly imaged coherent electron wave flow from a quantum point contact (QPC) defined in a GaAs/AlGaAs 2DEG. The phase coherence of electron waves makes it possible to form an imaging electron interferometer. We have used our cooled SPM to image a one-electron GaAs quantum dot formed in a 2DEG by surface gates. Few electron quantum dots are promising candidates for single electronics, spintronics, and quantum information processing. Imaging and manipulating electrons in quantum dots promises to be useful in understanding and building circuits for these purposes. I present images of electron

motion through InAs nanowires with diameters of ~50nm, grown catalytically from Au nanoparticles. Semiconducting nanowires, assembled in a bottom-up approach, have recently seen an immense amount of research activity. Our images provide a detailed understanding of where the electrons are in the wire and how they flow through it. Heterostructure InAs/InP nanowires can be used to make an InAs quantum dot defined by two InP barriers. I demonstrate the ability of the cooled SPM tip to locate the InAs dot and tune the number of electrons down to one, and then zero, in a spatially dependent way.

Table of Contents

Acknowledgements

I would first and foremost like to thank my advisor Bob Westervelt who has been a wonderful advisor, scientifically and personally. I am very glad to have worked in his group throughout my six years at Harvard. I also want to thank the other two members of my committee: Rick Heller and Federico Capasso. It has always been a pleasure discussing physics with them, especially ideas for new projects.

Throughout the course of this project, I have also had the privilege to work closely with Leo Kouwenhoven's group in Delft and Lars Samuelson's group in Lund. I learned an immense amount of new physics in both collaborations and I am grateful to them and their groups for their hospitality while I worked there. Thank you Floris Zwanenburg, Linus Froberg, Jorden van Dam, Silvano De Franceschi, and Mikael Bjork!

I would like to thank all the imaging members of the Westervelt group with whom it has been a pleasure to work with, learn from, and teach. Thanks to Mark Topinka, Brian LeRoy, Kathy Aidala, Parisa Fallahi, and the newbies: Halvar Trodahl, Erin Boyd, and Melaku Muluneh. It has also been a pleasure to work with Tom Hunt and Jonathan Aguilar on the AFM – dielectrophoresis project. Also, many thanks to the other members of the group: Hak-ho Lee, Dave Issadore, Andy Vidan, Ian Chan, and Chungsok Lee.

A big thank you to the clean room staff here at Harvard, especially Steve Shepard, who provided us with state-of-the-art and (working!) equipment.

And of course, my family and friends. You know who you are…